
Electronic Thesis and Dissertation Repository

10-23-2020 1:45 PM

Evaluation of Warpage for Composite Automotive Components

Eric J. Martin, *The University of Western Ontario*

Supervisor: Tutunea-Fatan, Remus, *The University of Western Ontario*

A thesis submitted in partial fulfillment of the requirements for the Master of Engineering Science degree in Mechanical and Materials Engineering

© Eric J. Martin 2020

Follow this and additional works at: <https://ir.lib.uwo.ca/etd>



Part of the [Computer-Aided Engineering and Design Commons](#), and the [Other Materials Science and Engineering Commons](#)

Recommended Citation

Martin, Eric J., "Evaluation of Warpage for Composite Automotive Components" (2020). *Electronic Thesis and Dissertation Repository*. 7409.

<https://ir.lib.uwo.ca/etd/7409>

This Dissertation/Thesis is brought to you for free and open access by Scholarship@Western. It has been accepted for inclusion in Electronic Thesis and Dissertation Repository by an authorized administrator of Scholarship@Western. For more information, please contact wlsadmin@uwo.ca.

Abstract

Thermoplastic composite parts are manufactured using compression molding for the purposes of assembly in a car seat sub-assembly. Concerns about the dimensional accuracy of the parts prompted an investigation into the part warpage. The warpage of the parts needs to be evaluated for the purposes of determining processing conditions which are linked to part warpage, in order to reduce part warpage.

Laser line probes (LLP) are becoming a more attractive tool for the purposes of part inspection. LLPs quickly acquire point cloud data from complex surfaces and are a non-contact method of measurement; these qualities make LLPs the best tool for the inspection of warped composite parts. Currently there are no guidelines for inspecting this class of parts which require special scanning conditions (no rigid fixtures). There exists no evaluation of the repeatability or accuracy of LLP scans under these specific scanning conditions. To address this knowledge gap, research was conducted comparing several methods of scanning to outline a scanning procedure which would provide reliable results.

Similarly there are no guidelines for warpage measurement in general. The method of measuring warpage is typically informed by part geometry and warpage behavior, and thus can be different for each case. To address this issue several warpage metrics are proposed and applied to discover the effectiveness of each method. Finally the investigation of processing parameters can be accomplished. In this thesis several experiments are conducted to understand the impacts of mold temperature, charge placement, material, and geometry on the final part warpage.

Keywords

Laser line scanning (LLP), laser scanning, warpage, warpage measurement, composite, thermoplastic composite, compression molding, automotive, seat structure, design of experiments (DoE), ANOVA, t-test, Long fiber thermoplastic composite (LFT), Glass mat thermoplastic composite (GMT)

Summary for Lay Audience

Composite parts are made from a plastic matrix which is embedded with fibers (common fibers include glass and carbon fibers). Composites are useful materials for the automotive industry because they are both light and strong. Compression molding is a method of mass production which can be used to produce composite parts. Unfortunately parts made of composite materials which are manufactured using compression molding do not come out perfectly. The geometry is slightly different than what it was intended to be, this is commonly known as warpage. A method of quantifying warpage is needed to investigate potential causes of warpage.

Laser line probes (LLP) are an advanced tool which is used for gathering measurements on objects. This is achieved by using lasers to scan the object and replicate the object on a computer. Using the replicate of the object on the computer measurements can be obtained from the object. The use of LLPs to evaluate the warpage on composite parts is not well documented in literature. There is no assessment reporting the expected accuracy of the measurements obtained using this tool on a part made of composite materials. To address this gap in knowledge a study was conducted which compared many methods of applying the LLP to scan a composite part. The aim of the study was to outline the most accurate way of using an LLP to scan a composite part and what the accuracy of this method is.

Collecting the warpage measurement is the next step required to evaluate the composite parts. There is no set standard for collecting warpage measurements. Methods of measuring warpage used in previous work are very simple and are not necessarily the best methods of measuring warpage for the specific work carried out in this thesis. To deal with this problem several methods of measuring warpage are proposed and investigated. Finally a study is conducted to find out how some manufacturing conditions impact the warpage of the composite parts.

Acknowledgements

I'm glad to have found myself fortunate enough to be surrounded by amazing people who have driven me to thrive and help me better myself. There is no way I could have completed my graduate studies without the support I have received, and so I will try to express my thanks to all of you even though I know these words will fall short of conveying my gratitude.

First I would like to thank my supervisor, Dr. Remus Tutunea-Fatan, who provided me the opportunity to work on my master's degree, and made all of this possible. I could never put a price on the knowledge and experience I have gained under your guidance. I know it is no trivial feat to be a supervisor who is so quick to respond to questions and lend a hand; I truly appreciate all the time you have dedicated helping me, it did not go unnoticed. I will always remember your 'stories' which held little kernels of wisdom. Your dedication as a professor, researcher, and to the graduate students under your care is nothing short of inspirational. I could not have hoped for a better supervisor, thank you.

Next I would like to thank Ryan Gergely, Dave Okonski, and Stanislav Ivanov. Ryan and Dave I would like to thank you for the time you dedicated to helping me with writing, technical analysis, and so many other tasks. Stan, thank you for sharing your valuable technical knowledge and giving me the opportunity to get hands on experience. The mentorship all of you have provided gives me something to aspire to in the workplace.

Finally, I would like to thank my research colleagues, family, and friends. To the guys in the office, who provided not only technical support but also personal support; I'm glad to call you all friends and grateful I had the opportunity to work with all of you. To my family and friends, your unconditional love and support provides me the strong foundation on which I stand. Thank you.

Tables of Contents

Abstract	ii
Keywords.....	iii
Acknowledgements.....	v
Tables of Contents	vi
List of Tables	xi
List of Figures.....	xii
List of Abbreviations.....	xvii
Chapter 1: Introduction	1
1.1 Overview	2
1.2 State of the Art/Literature Review.....	2
1.2.1 Thermoplastic Composite Materials LFT and GMT.....	2
1.2.2 Compression Molding	4
1.2.3 Measurement Systems	5
1.2.4 Accuracy and Repeatability of Laser Scanning	7
1.2.5 Measuring Warpage	7
1.3 Motivation	9
1.5 Research Objectives.....	11
1.6 Contributions.....	12
1.7 Thesis Overview	13

Chapter 2: Repeatability and Accuracy of Laser Scans of Composite Parts.....	15
2.1 Overview	16
2.2 Background	16
2.3 Repeatability Assessment.....	17
2.3.1 Fixtured Scanning	19
2.3.2 Free-state scanning on a low-quality flat surface.....	20
2.3.3 Free-state on a high-quality flat surface	21
2.3.4 Antireflective Coating	22
2.3.5 Discussion.....	22
2.4 Accuracy Assessment	23
2.4.1 Physical Measurements	24
2.4.2 Virtual Measurements	25
2.4.3 Discussion.....	26
2.5 Case Study: Simple Geometry	27
2.5.1 Repeatability Assessment	28
2.5.2 Accuracy Assessment.....	28
2.5.3 Effect of Mesh Artifacts	30
2.6 Chapter Summary	34
Chapter 3: Investigation of Different Warpage Metrics.....	36
3.1 Overview	37

3.2 Background	37
3.3 Mesh Alignment	38
3.4 Global Global Warpage Metric	40
3.5 Global Local Warpage Metric	41
3.6 Local Global Warpage Metric	43
3.7 Local Local Warpage Metric.....	44
3.8 Vector Deviation Warpage Metric.....	45
3.9 Comparison of Warpage Metrics.....	47
3.8 Chapter Summary	57
Chapter 4: Application: Simple Experiments	58
4.1 Overview	59
4.2 Background	59
4.3 Mold Temperature Experiment	59
4.3.1 Selection of Warpage Metric	60
4.3.2 Data and Analysis.....	61
4.3.3 Discussion.....	64
4.4 Charge Placement Experiment	65
4.4.1 Selection of Warpage Metric	66
4.4.2 Data and Analysis.....	66
4.4.3 Discussion.....	69

4.5 Chapter Summary	70
Chapter 5: Application: Impact of Geometry and Material on Part Warpage	71
5.1 Overview	72
5.2 Background	72
5.3 SBI Mesh Alignment and Warpage Metrics	73
5.4 Details of DoE	75
5.5 Selection of Warpage Metric	76
5.6 Data and Analysis	79
5.6.1 Global Global Evaluation of DoE	79
5.6.2 Global Local Evaluation of DoE	82
5.6.3 Local Global Evaluation of DoE	84
5.6.4 Local Local Evaluation of DoE	87
5.6.5 Vector Resultant Evaluation of DoE	89
5.7 Discussion	92
5.7.1 Warpage Metrics Focused on Data at the Flanges	92
5.7.2 Data at the Flanges ('local') vs Data across the Entire Part ('global')	94
5.7.3 Interaction Effects	96
5.8 Chapter Summary	97
5.8.1 Measurements at the Flanges ('local global', 'local local', and 'vector resultant')	97
5.8.2 Measurements across the Whole Part ('global global' and 'global local')	98

5.8.3 Summary.....	102
Chapter 6: Conclusion and Future Work.....	103
6.1 General Comments	104
6.2 Future Directions	106
References	108

List of Tables

Table 2.1: Summary of repeatability results for different scenarios.	22
Table 2.2: Distance to the reference surface in the physical setup.	24
Table 2.3: Distance to the physical reference plane in the virtual setup.	26
Table 2.4: Complex geometry: comparison of physical and virtual accuracy.	26
Table 2.5: Simple geometry: comparison of physical and virtual accuracy (error bars represent one standard deviation).	30
Table 2.6: Distances to the virtually-generated reference plane.	33
Table 2.7: Effect of outlier rejection amount on virtual measurements.	33
Table 3.1: ‘Global global’ metric results.	41
Table 3.2: ‘Global local’ metric results.	41
Table 3.3: ‘Local global’ metric results.	44
Table 3.4: ‘Local local’ metric results.	45
Table 3.5: ‘Vector resultant’ metric results.	47
Table 5.1: Shows the four conditions of the material and geometry DoE, and the number of replicates for each condition.	76

List of Figures

Figure 1.1: Illustrates a typical compression molding process a) shows charge in mold (charge can be a lump of LFT or sheets of GMT) with the top half of the mold preparing to close on the charge b) shows top half of the mold lifting and the finished product of the molding.	4
Figure 2.1: Error assessment plan.	17
Figure 2.2: Repeatability evaluation in the “fixtured” scenario: (a) overview of the fixturing setup, (b) sample deviation map between two replicate scans (mm).	20
Figure 2.3: Sample paired comparisons between replicate scans (mm): (a) unclamped on low quality flat surface, (b) unclamped on high quality surface, (c) scenario (b) covered with antireflective coating.	21
Figure 2.4: Direct comparison of replicate scans acquired through different scanning techniques (mm): (a) fixtured, (b) free-state on low quality flat table, (c) unclamped on high quality flat table, (d) scenario (c) covered with antireflective coating.	23
Figure 2.5: RE validation protocol for SBO: (a) inspection points, (b) validation distance examples.	24
Figure 2.6: Deviation map between two replicate scans (mm).	28
Figure 2.7: Physical measurements of the cube geometry (mean values in mm).	29
Figure 2.8: Virtual measurements of the cube geometry (mean values in mm): (a) X axis, (b) Y axis, and (c) Z axis.	29
Figure 2.9: Mesh artifacts present around the edges of the cube geometry.	31
Figure 2.10: Scan of SBO backside.	32
Figure 2.11: Virtual measurements involving SBO backside: (a) reject no outliers, (b) reject 0.01% outliers, (c) reject 0.1% outliers.	32

Figure 2.12: Road map of scanning procedure to produce scans with reasonable repeatability ($\sigma = 0.047\text{mm}$) and accuracy (0.8%).	35
Figure 3.1: Example SBO scan with selected elements (red elements) used for best fit alignment procedure.	39
Figure 3.2: Example of separated positive a) and negative b) warpage color maps for ‘global global’ evaluation (SBO part).	40
Figure 3.3: Example of ‘global local’ measurement points.	42
Figure 3.4: Cross section view of inspection of the top left of SBO flange. Circled section shows CAD that is not mapped to the scan. CAD has two layers and scan has one layer.	43
Figure 3.5: Example of separated positive a) and negative b) warpage colour maps for ‘local global’ evaluation (SBO part).	44
Figure 3.6: Example of ‘local local’ measurement points (SBO part).	45
Figure 3.7: Example of mapped points on CAD a) and scan b) used for ‘vector resultant’ metric (SBO part).	47
Figure 3.8: Graph of results from several potential warpage metrics. Measurements are made on five SBO parts from series 1.	48
Figure 3.9 Graph of results from several potential warpage metrics. Measurements are made on five SBO parts from series 2.	48
Figure 3.10: Average deviation colour map for series 1 SBO parts.	49
Figure 3.11: Section view of SBO evaluation. Circled area shows where results for ‘local local’ warpage metric are gathered.	50
Figure 3.12: Section view of SBO evaluation. Circled area shows where results for ‘local global’ warpage metric are gathered.	51

Figure 3.13: Section view of SBO evaluation. Arrows show point to point mapping used for ‘vector resultant’ metric.52

Figure 3.14: Average standard deviation colour map for series 1 SBO parts.53

Figure 3.15: Average deviation colour map for series 2 SBO parts.54

Figure 3.16: Average standard deviation colour map for series 2 SBO parts.55

Figure 4.1: Measured warpage (mm) of each part in ‘Mold Temperature Experiment’ using ‘global global’ metric.62

Figure 4.2: Bar chart shows average deviation for each mold temperature and error bars show one standard deviation for that series. Data is gathered using ‘global global’ metric.62

Figure 4.3: Measured warpage of each part in ‘Mold Temperature Experiment’ using ‘local local’ metric.63

Figure 4.4: Bar chart shows average deviation for each mold temperature and error bars show one standard deviation for that series. Data is gathered using ‘local local’ metric.64

Figure 4.5: Charge placement location visualization: a) Center charge placement, b) Left charge placement, c) Right charge placement.66

Figure 4.6: Measured warpage of each part in ‘Charge Placement Experiment’ using ‘global global’ metric.67

Figure 4.7: Bar chart shows average warpage for each charge placement and error bars show one standard deviation for that series. Data is gathered using ‘global global’ metric.67

Figure 4.8: Measured warpage of each part in ‘Charge Placement Experiment’ using ‘local local’ metric.68

Figure 4.9: Bar chart shows average warpage for each charge placement and error bars show one standard deviation for that series. Data is gathered using ‘local local’ metric.69

Figure 5.1: a) SBI CAD model b) Assembly of SBI (gray) and SBO (green) CAD models.73

Figure 5.2: SBI scan with selected elements for the purposes of best fit alignment.74

Figure 5.3: CAD geometries with respective reference planes (black grid) a) SBI and b) SBO. Reference plane demonstrates area to be targeted for best-fit alignment.75

Figure 5.4: GMT a) SBI and b) SBO part scans (green) overlaid on their respective CAD models (gray). View looks down at X Y plane. Circles highlight differences in warpage for SBI and SBO parts (ie: Warpage in y-direction is much larger for SBO parts).....77

Figure 5.5: LFT a) SBI and b) SBO part scans (green) overlaid on their respective CAD models (gray). View looks down at X Y plane. Circles highlight differences in warpage for SBI and SBO parts (ie: Warpage in y-direction is much larger for SBO parts).....77

Figure 5.6: Section view of measurements conducted on: a) SBI and b) SBO parts which are aligned to their respective CAD models. Coloured lines show how warpage measurements are acquired. Circled sections show better point to point mapping for SBI scan. In image a) the scan was difficult to see so it was outlined using orange lines.78

Figure 5.7: Measured warpage for each part in DoE using ‘global global’ metric.80

Figure 5.8: Average warpage for each set of parts in DoE using ‘global global’ metric. Error bars represent one standard deviation.....81

Figure 5.9: Pareto chart showing impact of input variables according to DoE assessment using the ‘global global’ results.....82

Figure 5.10: Measured warpage for each part in DoE using ‘global local’ metric.....83

Figure 5.11: Average warpage for each set of parts in DoE using ‘global local’ metric. Error bars represent one standard deviation.....83

Figure 5.12: Pareto chart showing impact of input variables according to DoE assessment using the ‘global local’ results deviation.	84
Figure 5.13: Measured warpage for each part in DoE using ‘local global’ results.	85
Figure 5.14: Average warpage for each set of parts in DoE using ‘local global’ metric. Error bars represent one standard deviation.	86
Figure 5.15: Pareto chart showing impact of input variables according to DoE assessment using the ‘local global’ results deviation.	86
Figure 5.16: Measured warpage for each part in DoE using ‘local local’ results.	88
Figure 5.17: Average warpage for each set of parts in DoE using ‘local local’ metric. Error bars represent one standard deviation.	88
Figure 5.18: Average warpage for each set of parts in DoE using ‘local local’ metric. Error bars represent one standard deviation.	89
Figure 5.19: Measured warpage for each part in DoE using ‘vector resultant’ metric.	90
Figure 5.20: Average warpage for each set of parts in DoE using ‘vector resultant’ metric. Error bars represent one standard deviation.	91
Figure 5.21 Average warpage for each set of parts in DoE using ‘vector resultant’ metric. Error bars represent one standard deviation.	92
Figure 6.1: Road map to select appropriate warpage metric for a specific application.	104

List of Abbreviations

ANOVA	Analysis of Variance
CAD	Computer Aided Design
CAFE	Corporate Average Fuel Economy
CI	Confidence Interval
CMM	Coordinate Measurement Machine
DoE	Design of Experiments
FRP	Fiber Reinforced Polymer
GHG	Green House Gases
GMT	Glass Mat Thermoplastic
LFT	Long Fiber Thermoplastic Composite
LFT-D	Long Fiber Thermoplastic Composite - Direct
LLP	Laser line probe
RE	Reverse Engineering
SBI	Seat Back Inner
SBO	Seat Back Outer
StDev	Standard Deviation

Chapter 1 : Introduction

1.1 Overview

This chapter provides a brief introduction and literature review for many of the topics related to this thesis. The topics discussed (in order of appearance) are: composite materials, compression molding, measuring systems for part inspection, and measuring warpage. The literature review will be followed by a thorough explanation of the thesis: motivation, objectives, and contributions. The final section of the introduction will provide an overview of each chapter in the thesis.

1.2 State of the Art/Literature Review

This section will briefly introduce the topics related to the thesis. The structure of the section follows the typical part inspection workflow, from manufacturing, to the acquisition of data, and evaluation of the part.

1.2.1 Thermoplastic Composite Materials LFT and GMT

Composite materials are made by combining two (or more) discrete materials to create a material which has different properties than the individual component materials. The components materials remain discrete within the composite; this is important to take note of because it delineates what is a composite and what is a mixture or solid solution. Although composites are thought of as ‘new materials’, this broad definition of composite fits many materials going back many thousands of years. An ancient example of a composite material are bricks made with mud and straw. The ‘new composites’ which are constantly researched today (and what this paper is focused on) are fibre-reinforced polymers (FRP). Using the mud brick example, in the case of FRP, the plastic matrix is the mud and the fibers (glass, carbon, aramid, etc.) are the straw. The matrix holds the fibers together and the fibers strengthen the matrix.

To further reduce the broad category of FRP, this project is specifically concerned with thermoplastic composites. A thermoplastic composite is defined as a FRP with a thermoplastic matrix. There are two categories of thermoplastic composites used in this project: long fiber thermoplastic composite (LFT), and glass mat thermoplastic composite (GMT). Both LFT and GMT are classified as thermoplastic 'prepreg' composites. Meaning the matrix is pre-impregnated with fibers. There is a wide variety of potential automotive applications for LFT materials including: body structures, floor panels, bumper, seat structures, and dashboard carrier; just to name a few [18]. Components made using LFT materials are being mechanically tested for a number of automotive applications including side impact beam and seat structure [5],[20]. GMT type thermoplastics have a similar applicability to automotive systems [18]. Both materials use randomly oriented discontinuous long fibers. The randomly oriented discontinuous fibers typically make the material isotropic, however material flow during molding can cause some anisotropy in the finished product [11]. Both materials have similar advantages which are: good strength/stiffness to weight ratio, good impact properties, and high toughness and ductility [18]. In this study the LFT and GMT have the same matrix and fiber materials, which are, polyamide 6 (PA6) and glass fibers respectively. Aside from the fact that these are two different types of thermoplastic prepregs, one very important difference to note is the % wt of fibers for each material. The LFT material has 40% wt fibers and the GMT is 65% wt fibers.

One of the key benefits of LFT is the ability to utilize the LFT-D system. The letter 'D' in LTF-D stands for 'direct'. This process is direct in the sense that the prepreg LFT is directly made at the manufacturing site from the matrix and fiber raw materials (i.e.: PA6 pellets and glass fiber rovings). This allows a cost reduction because there is no need for expensive prepreg production by a material supplier [18]. The process results in an LFT charge extruded at high temperature,

ready for compression molding. GMT on the other hand is produced by a material supplier in sheets which are cut, stacked, and heated in preparation for compression molding. The result of the differences in compression molding procedure allows LFT-D to have a significantly lower cycle time compared to GMT.

1.2.2 Compression Molding

Compression molding uses a heated charge (typically made of plastic or composite) which is placed into an open and heated mold, and then the top of the mold is then pressed down. The application of force and heat enables the charge fill the mold. The result of the process is the charge taking the shape of the mold cavity. An illustration of a typical compression molding process can be seen in Figure 1.1.

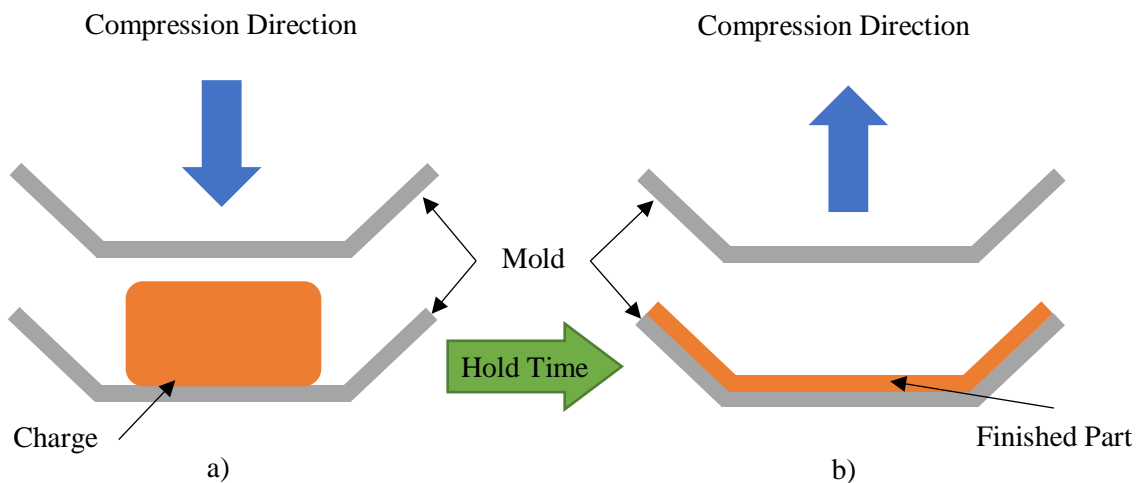


Figure 1.1: Illustrates a typical compression molding process a) shows charge in mold (charge can be a lump of LFT or sheets of GMT) with the top half of the mold preparing to close on the charge b) shows top half of the mold lifting and the finished product of the molding.

In this study all parts are manufactured using compression molding. Compression molding process is a mass production method of manufacturing suitable for the automotive industry [18]. Meaning that the process can produce many parts quickly. This ability comes at a very large initial

investment cost, the equipment (press and tooling) to compression mold parts is very costly and therefore is only worthwhile if a massive number of parts are produced.

1.2.3 Measurement Systems

Contact measurements acquired using a coordinate measurement machine (CMM) are the gold standard for the application of part inspection. CMMs are characterized by their high accuracy and repeatability. CMMs are well established tools in industry and errors/inaccuracies from these machines are well understood and can be mitigated. A CMMs probe must make physical contact on the part; therefore CMMs are an intrusive measurement tool. In typical industrial applications CMMs are used on metal components with low warpage, and these metal components are held secured to ensure the component doesn't move while measurements are conducted. Using a CMM to measure an entire geometry can be very time consuming and the process gets more time consuming as the complexity of the geometry is increased.

The use of laser line probes (LLP) is a more recent method of collecting geometry data. Laser scanners can collect data extraordinarily quickly, even on complex geometries [19],[31]. The speed of laser scanners have made them an attractive tool which can replace a CMM in many circumstances. Laser scanners have been applied to many different problems, including restoration of cultural artifacts and various medical applications [17],[30]. Laser scanners have also been used in an industrial setting, as a tool to investigate part-mold dimensional accuracy [30]. Innovation in laser scanning technology has allow for the improvement of their accuracy, however they are still not as accurate as CMMs. However, CMMs are limited in what objects they can measure due to the nature of intrusive measurements (physical contact with measurand). A sponge, for example, would deform under the application of force by a CMM in its attempts to generate measurements. Although a sponge is an extreme example these concerns generated from intrusive measurement

devices are present in the measuring of composite components. Work by Polini et al [28] showed that attempts to measure flexible composite components were impacted by the contact forces from the use of a CMM to measure the surface. The study found that measurements made using the CMM and the laser scanner were comparable, however on the keys to the success of the CMM measurements was the ‘over-constraining the part using clamps’ [28]. Similarly, in work by Ascione et al [2] a CMM was used to inspect a nonrigid part, however the part in question had fixed datums necessary for assembly, and so these datums were used to design fixturing equipment used during CMM scanning. Both of these studies show CMM inspections can obtain accurate measurements on nonrigid parts as long as they are well constrained and precautions are taken to mitigate the impact of the force imparted by the CMM probe.

Components measured by CMMs must be somehow fixed, if not then the object to be measured could be moved during the measurement collection procedure which would create significant errors in measurement. Placing several warped composite components in fixtures without impacting the results of the measurements is a very challenging task. Rigid fixtures clamps or other devices will force the geometry into fixed datums, given that the areas and magnitude of warpage in composite components will vary part to part, it is very likely that the parts will be bent in order to reach those fixed datums. The goal of this study is assess the warpage of the part as it is manufactured. The purpose is not to assess the part geometry once it is forced into a fixture. The inability to use rigid fixtures with fixed datums to evaluate the warpage of thermoplastic composite components presents a challenging problem for any measurement system. However this issue impacts contact measurement systems disproportionately because they must physically touch the unconstrained part while conducting measurements; this would ensure the part moves while measurements are collected and result in unusable data. Laser line scanners do not have this issue

because they do not require contact with the part. The non-contact nature of laser line scanners and the ability to quickly collect data on complex surfaces make it the ideal measurement tool for the purposes of the work conducted in this thesis.

1.2.4 Accuracy and Repeatability of Laser Scanning

The accuracy of laser scanners remains relatively low compared to their physical contact counterparts [1],[7],[12],[25-27],[29] In many studies, CMM was used as the primary validation tool, a route enabled by the high rigidity of the validation sample, typically made of metal. Similarly, Besic et al [4] attempted to improve the accuracy of the line scanning process by using advanced filtering operations in order to obtain a better agreement between the non-contact and contact (CMM) results.

Other experiments using laser scanners simply rely on the manufacturers recorded accuracy and repeatability for the individual device [32]. Typically manufacturers supplied accuracy and repeatability assumes ideal conditions for measurement gathering. However, due to the nature of the material to be scanned, typical ideal conditions cannot be applied. Ideal conditions would include fixing the component during the scanning process to ensure no movement of the object while the scan is collected. Unfortunately, as of right now there is no recorded repeatability or accuracy for parts scanned under these conditions. Due to this lack of knowledge it is important that these errors are determined for this application, in order to make informed decisions about measurements obtained under these conditions.

1.2.5 Measuring Warpage

Warpage is a constant problem for both plastic and composite materials. Efforts to reduce the warpage for composite materials are common [14],[16]. Warpage can cause many problems for

manufacturing, the largest of these problems manifests itself in the assembly stage, where the warped geometry must be bent into proper shape to fit into the designated fixture points in an assembly. The geometry will experience pre-stresses as it is forced into shape during the assembly process. This is not much of a problem for most plastic components because of their typically lower stiffness and common applications are not structural. Pre-stresses, become a much larger problem for composite components with typically higher stiffness and structural/semi-structural applications.

Warpage measurements acquired using scan data can manifest in many forms, though it is typically a colour map depicting deviations from a nominal part (CAD model). Although this method is generally used because it provides a good visual to engineers and highlights problem areas on the part, the primarily qualitative nature of the measurements is not particularly useful for a number of important applications. There are a large number of ways to obtain quantitative warpage measurements, but no generally accepted method; it changes from application to application [14]. Typically the largest warpage along one axial direction is used as the warpage measurement [14],[16].

Work by Song et al used a FARO laser scanner to evaluate warpage of a compression molded LFT part. The evaluation was used to compare experimental results to molding simulation results [32]. The parameters of this work are very similar to the work carried out in this thesis, however, there is very little amount of information on the procedure, and evaluation method. Therefore there is a need to investigate this problem and develop an outline for evaluating the warpage of this class of part. Once this has been established the procedure can be used to gather reliable warpage data. The warpage data has a multitude of potential uses. It can be used as the output for a 'design of experiment' (DoE) which can be used to understand what processing

parameters impact the warpage. It can also be used as a way to validate molding simulations. It may also be possible to use the warpage data to predict assembly issues.

1.3 Motivation

The looming threat of climate change has heightened the attention of government regulators in regard to CO₂ emissions produced due to the automotive industry. Many nations across the globe have imposed emissions regulations. These regulations have magnified the importance for automotive manufacturers to realize even more fuel-efficient vehicles. The fuel-efficiency of automobiles was targeted primarily because the bulk of the environmental damage caused over a vehicle's life cycle occurs while the vehicle is in use [21]. In the United States, the new 'corporate average fuel economy (CAFE) standards' and 'greenhouse gas (GHG) emission' standards were implemented with the purpose of encouraging automakers to focus on innovation in the realm: of fuel efficiency (through lightweighting and increasing powertrain efficiency) [8],[34], and alternative fuel systems [23]. Although these are not the only ways automotive companies respond to these regulations [33].

Vehicle lightweighting can become a strong contributor in attaining the goal of increasing an automobile's fuel efficiency [36]. Reduction in the mass of any vehicle will cause a reduction in the amount of energy required to operate it, thus reducing emissions. The benefits of lightweighting do not stop at better fuel efficiency; it can also improve vehicle handling and reduce the magnitude of force exerted in automobile collisions. Exploiting the properties of composite materials presents a promising path to achieve vehicle lightweighting [18]. Composite materials are characterized by their impressive strength to weight ratio. Some composite materials possess sufficient strength and stiffness to replace heavier metal components. The process of replacing

metal components with a composite counterpart is a common method of achieving vehicle lightweighting.

Even though technical requirements can be met using composite materials, there are economic requirements which must also be met [3]. High volume manufacturing is a necessity to make any automobile affordable. The cost of the materials will also decide whether or not utilizing composites provides a realistic solution. Assembly of composite parts is another issue of paramount importance. Welding is an incredibly important joining operation in the automotive industry, however any composite made using a thermoset matrix cannot be welded together [9]. Due to advancements in manufacturing technology in recent decades all three conditions can be met in almost all aspects. Compression molding of thermoplastic composites has a low cycle time, allowing for high volume production. Material cost for these composites are relatively low. Thermoplastic composite parts can be welded together by an ultrasonic welding machine [9]. All of these factors makes compression molding thermoplastic composite parts an incredibly attractive option for automobile manufacturers. Although on the surface, the process of replacing traditionally metal components with components made of composite materials seems simple; in reality there are still many challenges.

One of the largest problems with thermoplastic composite production is the dimensional accuracy of the produced parts [13]. Thermoplastic composites parts are characterized by large amounts of warpage. Meaning that the geometry of the produced part will vary from the geometry of the designed part by a considerably large margin. Warpage of composite parts generally can be attributed to many factors including the shrinkage of two different materials within the same part. The fibers and the matrix will have different thermal expansions and contractions creating thermal stresses within the component as it cools and thus warping the part [13]. Part warpage can create

a number of production issues, especially in assembly. If the warped part is to be included in an assembly it will become pre-stressed when it is forced into the required shape for assembly. As previously stated an important benefit to producing thermoplastic composites is their ability to be welded together. Assembly complications stemming from large amounts of warpage are further magnified if two thermoplastic composite parts need to be welded together. Addressing these problems is necessary to realize the full potential of these materials in the automotive industry. To do this the warpage of compression molded thermoplastic composite parts must be studied.

1.4 Research Objectives

The goal of this work is to provide a methodology for measuring the free-state warpage of highly warped composite parts using a laser line probe (LLP) scanner. The methodology will then be applied to evaluate the impact of specific processing conditions on the warpage of compression molded automotive seat back parts. Based on the final goal of the project four research objectives have been outlined:

- Investigate the repeatability and accuracy of different scanning procedures for the purposes of collecting scans of free-state seat back parts.
- Investigate different methods of measuring warpage to provide useful results for statistical analysis of the impact of processing conditions on the resulting warpage of the part.
- Apply scanning procedure and warpage metrics to evaluate the results of simple experiments in which one variable is altered. The variables of interest are mold temperature and charge placement.

- Apply scanning procedure and warpage metrics to evaluate the results of a more complex DoE style experiment in which multiple variables are investigated at the same time. In this experiment the variables of interest are material and geometry.

1.5 Contributions

Closely related to the research objectives, the contributions of this work are fourfold:

- The creation of a clear scanning procedure to accurately and repeatably scan highly warped composite parts using an LLP. In this investigation the problems associated with fixing the object while collecting scans are highlighted.
- The creation of five warpage metrics which can be applied to LLP generated mesh data. The data from the warpage metrics can be used to evaluate the relative warpage of several parts, and be used in statistical analysis. With the creation of the warpage metrics guidelines have been created to ensure their appropriate application.
- In the investigation of the warpage metrics it was discovered that depending on how warpage is measured, the results can be significantly different and great care should be taken while applying warpage metrics.
- Finally, the results of the statistical analysis on processing conditions such as: mold temperature, charge placement, material, and geometry. The results showed that mold temperature and charge placement appear to have no significant (based on t-test & ANOVA with 95% confidence interval) impact on the resulting warpage. In the investigation of material and geometry it showed that both had significant impacts on the warpage. Material has a more significant impact than geometry. The interaction between the material and geometry has the smallest impact.

1.6 Thesis Overview

This section will provide a brief summary of the contents in each chapter of this thesis. The summaries here will also be placed in the ‘overview’ section of each chapter.

Chapter 2 goes into details about laser scanning repeatability and accuracy. Details about point cloud filtering and meshing are discussed. Different methods of laser scanning the parts are explained and performed. The first half of the chapter focuses on an analysis of the repeatability of each of these methods, which is used to determine which scanning strategy produces scans with the highest repeatability (lowest random error). The accuracy of the scan measurements is evaluated by comparing measurements collected from scans to complementary physical measurements obtained from the part.

Chapter 3 explores the concept of warpage measurement. Previously applied methods of measuring warpage are explained. For the purposes of comparing the resulting warpage from multiple methods of manufacturing the parts, it was determined that different warpage metrics could provide more insightful results than previously employed methods. In total there are five different warpage metrics proposed in chapter 3. The mesh alignment procedure is explained and used for all warpage metrics. The concept of each warpage metric is explained and two sets of five SBO parts are used to test the warpage metrics. Finally, the results obtained from the different warpage metrics are compared which is followed by a summary of the chapter.

Chapter 4 shows the application of two of the warpage metrics applied to two simple experiments. The first experiment investigates the impact of altering the mold temperature from 100°C to 150°C. The results obtained using the two metrics are shown and a t-test is used to determine if altering the mold temperature had a statistically significant impact on the measured warpage. In the second

experiment, the impact of charge placement is investigated. In this experiment there were three different charge placements tested. Since there are three sets of data (one for each condition) an ANOVA was used to determine if changing the charge placement yielded statistically different warpage for any of the sets.

Chapter 5 details the construction of a DoE used for the purposes of evaluating the factors of material and geometry. The materials used are the LFT material and GMT material discussed in section 1.2.1. The geometries used are the seat back outer (SBO) (Figure 5.3 b)) and SBI (Figure 5.3 a)) geometries. For the evaluation of this DoE all five of the warpage metrics proposed in chapter 3 are used. Pareto charts generated from analyzing the DoE (using each metric) highlight the impact of the two factors (material and geometry). A discussion about the results obtained using each of the metrics highlights important factors to consider while measuring warpage. Finally the relative impacts of each factor are clarified.

Chapter 6 includes the conclusion of the thesis. Final comments on the five warpage metrics and their applications are delineated. A summary of the entire thesis, which outlines the advancements made in each chapter solidifies the important work detailed in this thesis. Finally, potential future work building off the achievements of this thesis are proposed.

Chapter 2 : Repeatability and Accuracy of Laser Scans of Composite Parts

2.1 Overview

Chapter 2 goes into details about laser scanning repeatability and accuracy. Details about point cloud filtering and meshing are discussed. Different methods of laser scanning the parts are explained and performed. The first half of the chapter focuses on an analysis of the repeatability of each of these methods, which is used to determine which scanning strategy produces scans with the highest repeatability (lowest random error). The accuracy of the scan measurements is evaluated by comparing measurements collected from scans to complementary physical measurements obtained from the part.

2.2 Background

Measurement tools such as the 'FARO Edge' LLP used in this study will have its accuracy and repeatability supplied by the manufacturer. However, these parameters are calculated in idealized scenarios. A different scanning procedure will be developed for collecting data on non-fixtured warped thermoplastic composite parts. Since these parts present an added challenge to scanning it would be unrealistic to assume the factory accuracy/repeatability will be achieved while operating in this unideal (no proper fixture) scenario. Therefore it is necessary to carry out experiments to understand the accuracy and repeatability that can be achieved for this specific application. The resulting repeatability and accuracy can be used to evaluate different methods of collecting the data. The method which produces results with the best repeatability and highest accuracy will be selected as the measurement gathering procedure. The structure of the error assessment plan is shown in Figure 2.1.

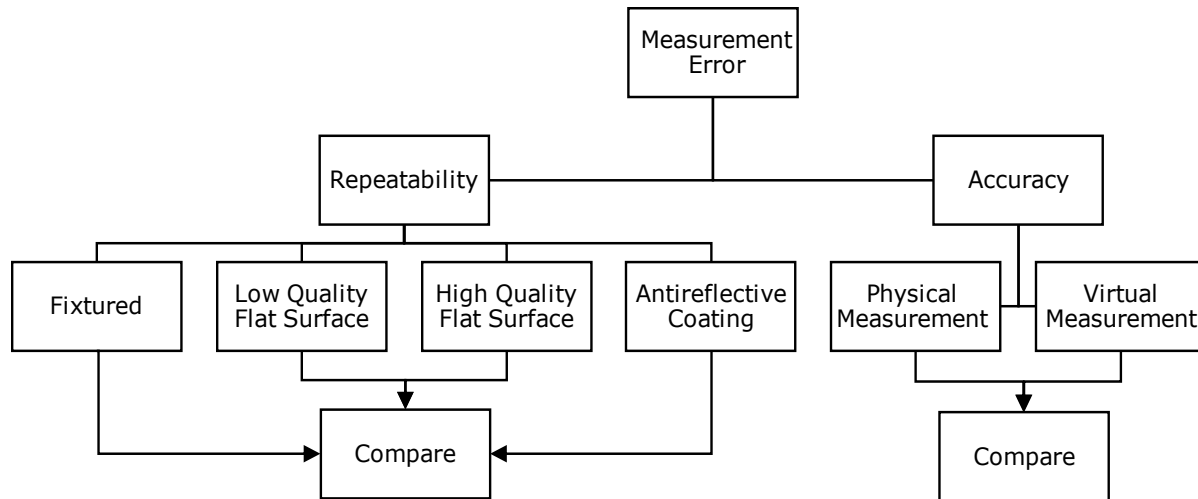


Figure 2.1: Error assessment plan.

2.3 Repeatability Assessment

First the repeatability of the measurements was investigated. In this work the measurement gathering procedure evolved in four different steps, each step providing an incremental improvement in repeatability. Since the FARO LLP was manually operated there is natural variation in scan passes (distance from scanner to object, number of scan passes, and angle of laser scanner to the surface being scanned), which would impact the repeatability of measurements. These variables will exist in an industrial setting and it is up to a trained laser scanning operator to mitigate these issues to the best of their abilities. Although this natural variability exists in the collection of scan data it must not be eliminated because the purpose of this study is to provide practical results for realistic situations.

In each of these measurement scenarios point cloud data filtering and meshing remained constant. Overlapping scan passes are merged automatically by the reverse engineering software. For the data acquired in these experiments, the maximum allowable merging distance was set to 2 mm and the number of iterative blending steps was set to 15. These settings were used to achieve

smooth transitions between overlapping scanning passes, which minimize the inherent deviations associated with adjacent scanning passes. The data points are then filtered by the software by means of a user-set standard deviation (0.025 mm) that was determined heuristically. This value removes outlier points which are outside of the threshold of $(\pm 3\sigma)$. Evidently the lower the σ is set the more points will be filtered out, if this goes too far then the resulting mesh will have a very large number of holes. Conversely, if σ is set too high, then many outliers will be retained and therefore too much ‘noise’ will be introduced in the data. According to the trial-and-error tests performed on the analyzed geometries/parts, the chosen value (0.025 mm) – while subjective – appeared to strike a good balance between the completeness and smoothness of the post-filtering data.

Once scanning was completed the result was a filtered point cloud data set. The next step is to convert the point cloud into a triangular mesh. User-set mesh generation controls were applied to further improve the quality of the mesh. One of them was a mesh smoothing operation which used a small rolling ball of 0.5 mm radius. The other operation was a mesh reduction operation that was set to a low reduction rate (2%). Mesh reduction is applied in order to improve the flatness of the small near-planar areas that were visible in the data, this operation also has the added benefit of making the data file smaller. Larger ball radii could alter the innate fillets/curved regions of the geometry whereas larger decimation rates could inadequately flatten non-planar areas. Same as in the prior step, both parameters were determined through heuristic searches and therefore they are likely only applicable to the geometry analyzed in the present context.

After the completion of the data post-processing phases, two scans of the same part were aligned to each other by employing a conventional best-fit technique. According to the known principles, the best-fit alignment technique aims to minimize all distances between the two

geometries to be compared. Owing to the previously mentioned post-processing parameters that were kept consistent for all reconstructed geometries, the best-fit alignment method yielded repeatable results. More specifically, the minor post-processing artifacts that were still present in the geometry did not affect the quality of the relative positioning/alignment between the pair of geometries to be compared. This could also be regarded as a consequence of the global - rather than local - nature of the comparison involved in the best-fitting approaches that essentially allowed elimination of the possible perturbations to be introduced by small data artifacts/defects. The robustness and stability of the best fitting technique was also warranted by the large density of scanned points that were originally acquired: approximately 2M points for Seat Back Outer (SBO).

Once the alignment was completed, then differences (termed deviations) between these two scans were measured and exported as tabulated numerical values. Finally, the standard deviation and range of these values were calculated and used to assess the match between pairs of scans. The following sections present several different techniques used to investigate the repeatability.

2.3.1 Fixtured Scanning

Initial attempts to obtain scanned data made use of an adaptable fixture (or stand) whose purpose was to hold the part steady while giving the scanner access to both sides of the part. The stand was designed to be adaptable so that the part is not forced into any fixed datums which would bend the part and give inaccurate warpage measurement. The fixture was designed with telescopic arms to accommodate the scanning of parts of various dimensions and at different laser scanner heights. While conducting the repeatability study the part was removed and replaced in the fixture. The resulting standard deviation was ± 0.560 mm. As suggested by Figure 2.2 (b), the consistency of

the acquired scan data is relatively low with error in both positive and negative directions. The deviations ranged from a maximum of +1.514 mm and a minimum of -1.992 mm.

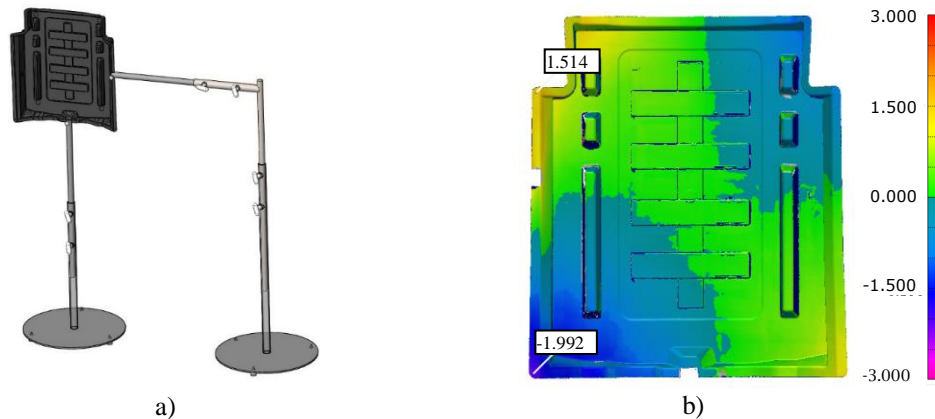


Figure 2.2: Repeatability evaluation in the “fixtured” scenario: (a) overview of the fixturing setup, (b) sample deviation map between two replicate scans (mm).

2.3.2 Free-state scanning on a low-quality flat surface

In an effort to improve RE repeatability, alternative scanning and part fixturing schemes were investigated. First, one side of the test part was scanned while at rest on the ‘flat’ surface of a common stainless-steel laboratory table. Since no fixturing was used, the part was in its free, but warped post-compression molding state. The resulting standard deviation was reduced to ± 0.087 mm compared to the previous setup. The deviations ranged from a maximum of +0.216 mm and a minimum of -0.279 mm.

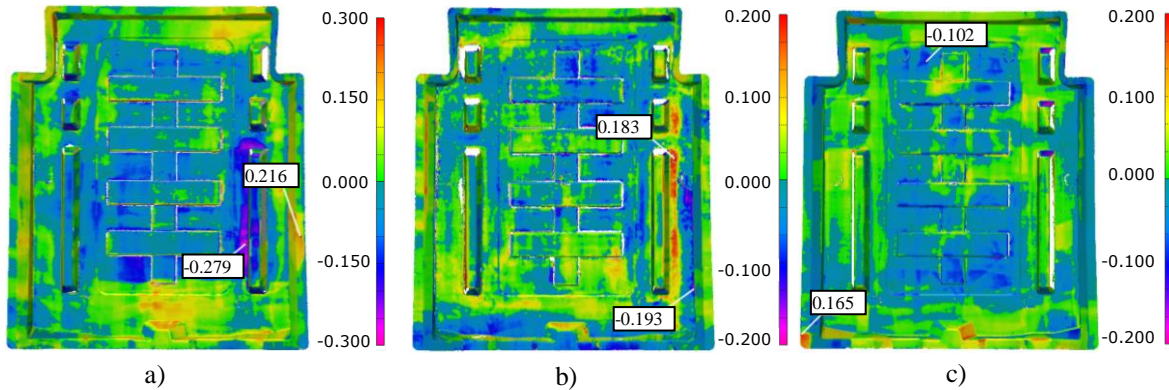


Figure 2.3: Sample paired comparisons between replicate scans (mm):
 (a) unclamped on low quality flat surface, (b) unclamped on high quality surface,
 (c) scenario (b) covered with antireflective coating.

It is believed this massive improvement in repeatability is due to the removal of the fixture. If the fixture forced the part into a fixed datum the repeatability of the part would be much higher for the fixture case than reported. The collection of geometry data from parts forced into fixed datums is not particularly useful for evaluating the post molded geometry of the parts. This is because the part is being bent out of shape to be fixed at those datums. Using the adaptable fixture presented similar but different issues. Despite the best efforts of the operator the fixture will most likely be applied to fix the part at a location it does not naturally rest. Since placing the part in the fixture is a manual operation there is undoubtedly differences in how the fixture is applied even on the exact same part. This means that for the exact same geometry the fixture will be applied at two distinctly different pairs of points in 3-D space. The difference between the locations of the fixture points and also the difference between where that point lies on the geometry can lead to two different warpings induced by the fixture.

2.3.3 Free-state on a high-quality flat surface

Since both the stability and the flatness of the laboratory table were questionable, the prior laser scanning experiments were repeated on a high-quality laboratory table whose principal component

was a granite slab. The resulting standard deviation was further reduced to ± 0.059 mm. The deviations ranged from a maximum of $+0.183$ mm and a minimum of -0.193 mm (Figure 2.3 (b)).

2.3.4 Antireflective Coating

To evaluate the possibility of further enhancing the repeatability of the scanning operation, an opaque white powder was applied in order to reduce/eliminate the artifacts introduced by the black and reflective surface of the composite parts. Reflective parts can introduce outliers which would impact accuracy; additionally, the outlier formation is dependent on the angle of the scanner compared to the surface [35]. This random distribution of outlier points could also have a negative impact on repeatability. After a new set of scans were performed in the free-state on the granite table, the resulting standard deviation was again further reduced to ± 0.047 mm. The deviations ranged from a maximum of $+0.165$ mm and a minimum of -0.102 mm (Figure 2.3 (c)).

2.3.5 Discussion

A summary of the discrepancies measured between pairs of replicate scans is presented in Table 2.1. Here, “StDev” is one standard deviation (σ) of the measured deviations between two replicate scans. This data suggests that repeatability is best ensured by coating parts with an antireflective coating and scanning in a free-state while resting on a high quality granite table.

Fixtured	Free-state		
	Low Quality Flat Surface	High Quality Flat Surface	Coated on High Quality Flat Surface
StDev [mm]	StDev [mm]	StDev [mm]	StDev [mm]
0.560	0.087	0.059	0.047

Table 2.1: Summary of repeatability results for different scenarios.

Similarly, the overlays between replicate scans depicted in Figure 2.4 suggest that the percentage of points outside of the preset range of the deviation map (± 0.100 mm) – presented in gray color - decreases as the repeatability of the scanning technique increases.

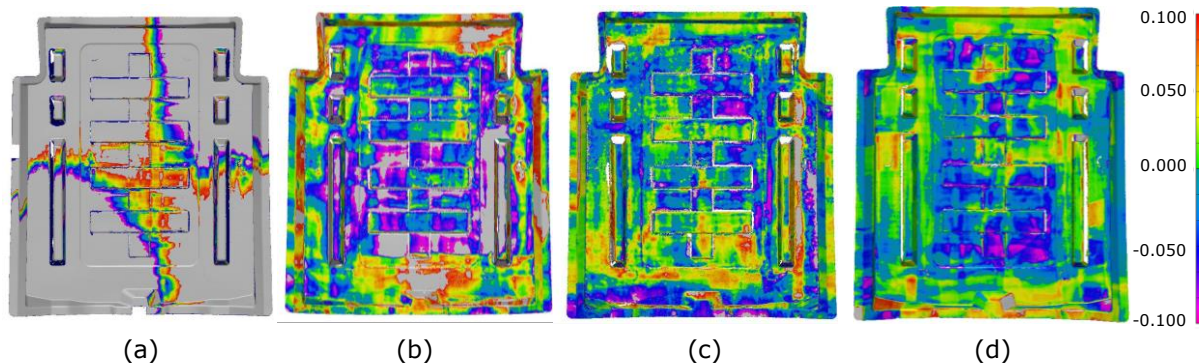


Figure 2.4: Direct comparison of replicate scans acquired through different scanning techniques (mm): (a) fixtured, (b) free-state on low quality flat table, (c) unclamped on high quality flat table, (d) scenario (c) covered with antireflective coating.

2.4 Accuracy Assessment

Once the repeatability of the process was brought within acceptable limits, the accuracy of the RE process was assessed by means of a reverse engineering validation scheme. The physical part was placed with the larger central flat zone in contact with the high-quality table and the distance between six different flange points (Figure 2.5(a)) and the flat surface table were measured by means of a touch trigger height measurement gage (accuracy = ± 0.03 mm, repeatability = 0.01 mm). Complementary virtual measurements were determined in a similar manner, but this time by means of the digital model obtained through RE.

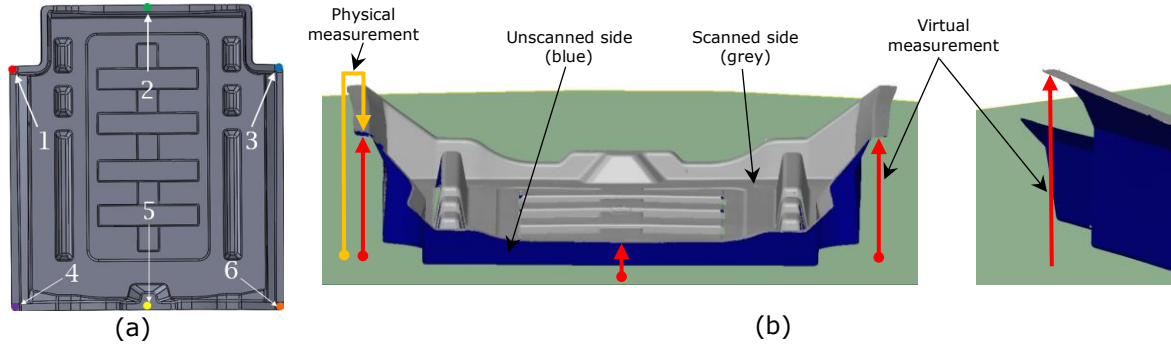


Figure 2.5: RE validation protocol for SBO: (a) inspection points, (b) validation distance examples.

2.4.1 Physical Measurements

The distance between the upper/scanned surface of the SBO and flat surface of the table was measured by means of the aforementioned height gauge. For this purpose, SBO was laid on the granite table and the height gauge was moved around the part in order to capture the distances depicted in Figure 2.5 (a). Triplicate measurements were taken at each of the six locations (Table 2.2).

Point Location	Top Left (Point 1)	Top Center (Point 2)	Top Right (Point 3)	Bottom Left (Point 4)	Bottom Center (Point 5)	Bottom Right (Point 6)
Test 1 [mm]	103.39	27.14	103.27	83.25	26.27	83.94
Test 2 [mm]	103.38	27.16	103.33	83.22	26.29	83.89
Test 3 [mm]	103.34	27.17	103.28	83.30	26.28	84.00
Mean [mm]	103.37	27.15	103.29	83.25	26.28	83.94
StDev [mm]	0.03	0.02	0.03	0.04	0.01	0.06

Table 2.2: Distance to the reference surface in the physical setup.

As the results suggest, data collected was characterized by a high level of consistency.

2.4.2 Virtual Measurements

It is important to note here that after extensive efforts were made to determine a flat reference plane exclusively by means of the scanned SBO model, this approach was eventually abandoned. Two factors contributed to this outcome. First, there are numerous RE artifacts in the final SBO mesh that effect the best fitting of the virtual reference plane. Second, the natural position where the part settles is affected by gravity, and not just the local conformation of the surface in contact with the table. When attempting to establish a virtual reference plane it was found that the actual position and orientation was extremely sensitive to the region of the mesh being included in the planar best-fitting. For these reasons, the initial comparisons between virtual and physical measurements were largely discrepant as a consequence of the incorrect positioning of the virtual reference plane. However, the issue of inconsistent virtual reference planes was solved by including a region of the physical table in the original scan of the part and using it to create the virtual reference plane. This enabled consistent and repeatable determinations of the virtual reference plane. More details on this topic will be presented in the upcoming Section 2.5.3.

The second observation to be made with respect to the virtual part model is that only its upper/visible/A side was scanned (Figure 2.5 (a)). This decision was prompted both by the large number of parts to be reverse engineered (in the hundreds range) as well as the fact that only this side was necessary for the downstream assembly/clamping simulations. While specific registration procedures could have been devised in order to align scans of both sides of the part (both acquired while having the part laying down on the table/flat surface), they were deemed both outside of the scope of the current study and time consuming. Mesh vertices located in the area targeted by the physical measurements were selected for the purpose of distance evaluations. Same as in the physical scenario, triplicate assessments - performed by means of repeated part scans - were used

to determine the gaps at the predetermined inspection points. Same as in case of physical measurements a high-level of consistency was observed in the acquired data (Table 2.3).

Point Location	Top Left (Point 1)	Top Center (Point 2)	Top Right (Point 3)	Bottom Left (Point 4)	Bottom Center (Point 5)	Bottom Right (Point 6)
Scan 1 [mm]	102.975	27.158	103.109	83.315	26.150	83.258
Scan 2 [mm]	103.075	27.183	103.177	83.545	26.202	83.285
Scan 3 [mm]	103.058	27.131	103.263	83.346	26.327	83.320
Mean [mm]	103.036	27.157	103.183	83.402	26.226	83.288
StDev [mm]	0.054	0.026	0.077	0.125	0.091	0.031

Table 2.3: Distance to the physical reference plane in the virtual setup.

2.4.3 Discussion

Student t-test was used to investigate the level of correlation between physical and virtual inspection metrics. In this context, t-test was used to verify whether the virtual measurements match their physical counterparts. While a larger number of measurement samples (i.e., $n = 21$) would have strengthened the accuracy findings, it is believed that the size of the set used was sufficient to assess the trends existent in the acquired data. As Table 2.4 suggests, point 1 (top left) and point 6 (bottom right) seem to exhibit statistically different means between physical and virtual measurements ($p < 0.05$). For the remainder of four points, no statistically significant difference could be identified.

Point Location	Top Left (Point 1)	Top Center (Point 2)	Top Right (Point 3)	Bottom Left (Point 4)	Bottom Center (Point 5)	Bottom Right (Point 6)
Physical Mean [mm]	103.370	27.150	103.290	83.250	26.280	83.940
Virtual Mean [mm]	103.036	27.157	103.183	83.402	26.226	83.288
Difference [mm]	0.334	-0.007	0.107	-0.152	0.054	0.652
p-value	0.003	0.972	0.117	0.173	0.415	0.000

Table 2.4: Complex geometry: comparison of physical and virtual accuracy.

The largest contributor to this discrepancy is believed to be movement of the part due to the light contact force induced by the touch-trigger jaw of the height gage. This is evidenced by inspecting the points that are located in the vicinity of the physical contact between the composite part and the reference plane (close to the projection of Top Center/Point 2 and Bottom Center/Point 5 onto the reference plane) that seem to yield measurements that are relatively close between physical and virtual measurement scenarios. This observation underscores the challenges associated with obtaining free-state measurements of warped composite components.

Theoretically, the physical contact points between the part and the flat reference plane/surface should be easy to determine. However, part inaccuracies caused by the manufacturing process combined with the artifacts introduced during by the mesh generation process (typically around sharp edges) translate into a difficult task that can only be solved – at least for the time being – through visual and tactile inspection of the physical setup. Nonetheless, the biggest drawback of this approach is that it cannot be automated in the digital environment; whereas, physical observations tend to be confined to the part/surface interface located around the periphery of the part, where a direct line of sight is present. That being said, an overview of all differences that were measured between physical and virtual setup indicates that the largest error found remains under 0.65 mm or 0.8%, assuming the physical measurement as the baseline value.

2.5 Case Study: Simple Geometry

Since the validation results (Table 2.4) at points 1 and 6 showed that the differences between physical and virtual measurements were statistically significant ($p < 0.05$) a secondary study was conducted by means of a simple quasi-cuboid geometry. This investigation was meant to eliminate or at least reduce the confounding effects caused by part geometry on scanning accuracy/repeatability. This supplementary evaluation was partly inspired by a study of

Campanelli, et al[6]. The same optimized reverse engineering techniques described in Sections 2.3 and 2.4 were used in this case.

2.5.1 Repeatability Assessment

The results of repeatability evaluation are depicted in Figure 2.6. According to the repeatability study, the resulting standard deviation was ± 0.041 , while deviations ranged from a maximum of $+0.154$ mm to a minimum of -0.152 mm. These results are quite similar to those achieved in the case of the more complex geometry.

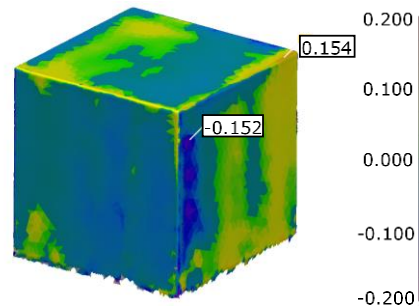


Figure 2.6: Deviation map between two replicate scans (mm).

2.5.2 Accuracy Assessment

To validate the scan accuracy, triplicate ($n = 3$) physical caliper-based measurements were conducted for each principal dimension of the cube (Figure 2.6). Nonetheless, a different measurement strategy had to be employed for the two virtual measurements located in the horizontal plane. In this new approach, the opposite side of the face to be measured was used to generate the virtual reference plane. This plane was then used to calculate the distance between itself and the opposite face of the cube. The plane was generated by best fitting it to scanned data by means of a method similar to the one used to generate the virtual reference plane based on the granite slab (Section 2.3.3). To avoid the errors introduced by the mesh artifacts associated with the edges of the geometry (to be detailed in the upcoming Section 2.5.3), near-edge regions of the

faces were excluded from the planar best fitting procedure. In contrast with X and Y dimensions, the vertical Z dimension was measured with respect to the high-quality surface/table in a manner similar to the one described in Section 2.4.1. The results of the virtual measurements are shown in Figure 2.7 (n = 3).

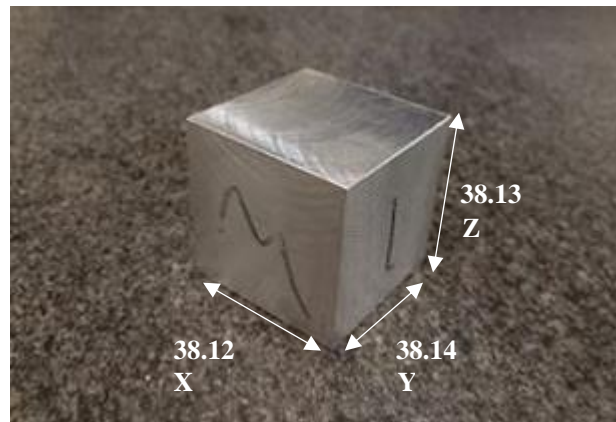


Figure 2.7: Physical measurements of the cube geometry (mean values in mm).

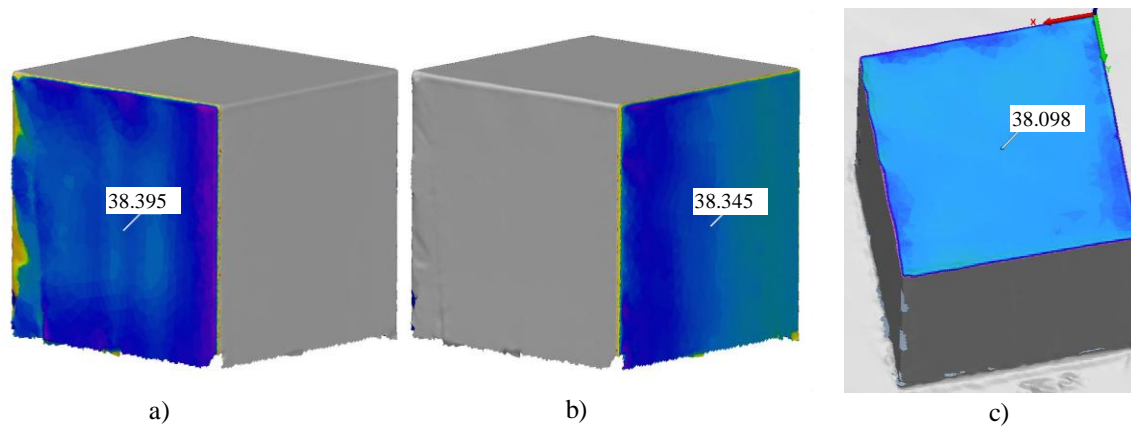


Figure 2.8: Virtual measurements of the cube geometry (mean values in mm):
(a) X axis, (b) Y axis, and (c) Z axis.

Same as in Table 2.4, the results in Table 2.5 seem to suggest that it is relatively difficult to obtain a match between virtual and physical measurements, essentially implying that the complexity of the geometry is not the only major cause of RE error. By corroborating the data in Tables 2.4 and 2.5, it can be speculated that the statistically significant discrepancy obtained at points 1 and 6

(Table 2.4) could be in fact a consequence of the unintentional movement of the part by the action of the light load exerted by the contact-based measuring device.

On the other hand, the results in Table 2.5 imply that the accuracy X and Y axes is lower (lower p values, and higher difference between physical and virtual measurement). This is suspected to be a consequence of the relative angle between the laser beam and the scanned surface [10],[24]. For the scanning of the surfaces used to create the X and Y virtual measurements, the angle of incidence between the laser beam and side surfaces was close to 45° , which was required to avoid hitting the granite surface. As such, with a scanning angle nearer 90° , as in the Z direction, the accuracy is improved (Table 2.5). Referring to the SBO geometry in Section 2.4.2, a near 90° scanning angle was also used at points 2 and 5 and resulted in a similar level of accuracy to the Z direction measurement on the block (Table 2.4).

Measurement	X	Y	Z
Physical Mean [mm]	38.12	38.14	38.13
Virtual Mean [mm]	38.345	38.395	38.098
Difference [mm]	0.225	0.255	0.032
p-value	0.00	0.04	0.11

Table 2.5: Simple geometry: comparison of physical and virtual accuracy (error bars represent one standard deviation).

2.5.3 Effect of Mesh Artifacts

In addition to the angle of incidence between the laser beam and the scanned surface, it was suspected that certain mesh artifacts introduced by the tessellation process itself could also introduce errors in the RE process. Unlike some of the previously described error types that affect the quality of the point cloud acquired (part stability/rigidity, surface reflectivity, beam incidence angle), this category of errors tend to be more concealed and thereby overlooked more often,

especially since the mesh generation process is usually based on robust and well-tested routines. However – as mentioned at the beginning of Section 2.4.2 – mesh artifacts tend to prevent definition of reliable references that are derived from the scanned geometry.

Unlike the physical object (Figure 2.6), its virtual replica was characterized by a relatively visible ‘filleting’ of its edges (Figure 2.9). This phenomenon was further aggravated by a certain amount of ‘pre-fillet’ that seemed to depart significantly from the innate planar nature of the cube faces. Various mesh generation settings were tested in order to further reduce this type of artifact, but they were largely unsuccessful.

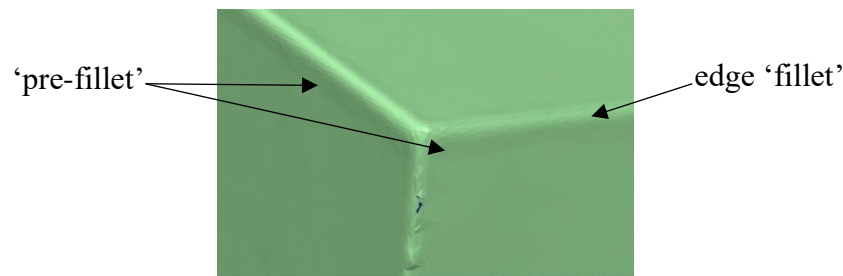


Figure 2.9: Mesh artifacts present around the edges of the cube geometry.

While it is possible to anticipate that advanced mesh generation algorithms could be developed to mitigate this issue, it is also important to note here that many of the commercial software on the market are unable to do it at this time. Moreover, while alternate solutions could be envisioned for simpler geometries (such as the cube), it is unlikely that robust edge meshing solutions can be developed for complex geometries.

To investigate the effect of mesh artifacts (i.e., ‘edge rounding’) on the accuracy assessment for a complex part, the B-side of the SBO was scanned (Figure 2.10). This geometry was required to facilitate the positioning of the virtual reference plane to be derived from it.

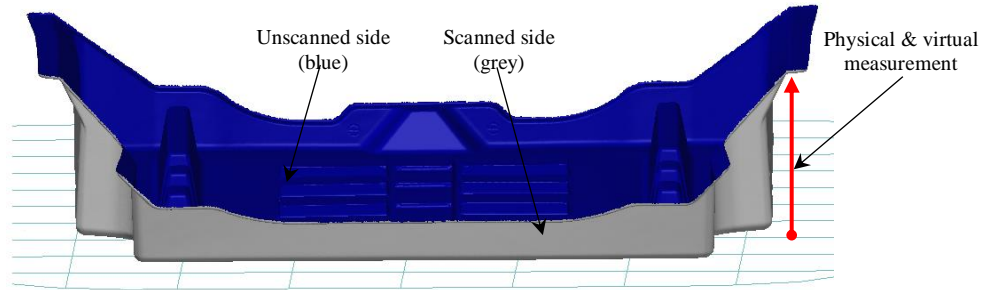


Figure 2.10: Scan of SBO backside.

The relative position of the plane with respect to the SBO backside is primarily controlled by the percentage of ‘outlier points’ to be ignored (rejection percentage). More specifically, while a nonzero rejection percentage implies that certain mesh artifacts will be adequately ignored, this also means that the plane will interfere with the reconstructed mesh. Alterations of the rejection percentage will also change the orientation of virtual reference plane, thus changing the virtual measurements. To illustrate this, Figure 2.11 shows the measurements at the same six measurement points for three distinct outlier rejection percentages. The six analyzed measurement points are the same used in Section 2.4.

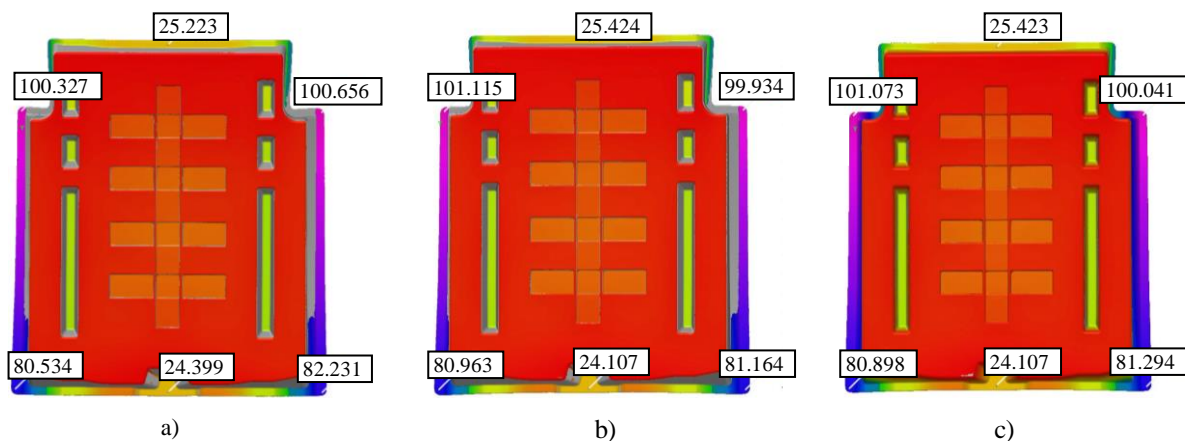


Figure 2.11: Virtual measurements involving SBO backside: (a) reject no outliers, (b) reject 0.01% outliers, (c) reject 0.1% outliers.

Both virtual and physical measurements were performed according to the schematic in Figure 2.10 and the summary of the results is shown in Table 2.6. The comparison of these measurements in Table 2.7 suggests that this method can produce results that are similar to the ones generated by involving a physical reference plane (Table 2.3). The difference in the absolute values recorded in the two tables is represented by the part thickness that was either excluded (Table 2.7) or included (Table 2.3) in the evaluation.

Point Location	Top Left (Point 1)	Top Center (Point 2)	Top Right (Point 3)	Bottom Left (Point 4)	Bottom Center (Point 5)	Bottom Right (Point 6)
“reject no outliers” [mm]	100.327	25.223	100.656	80.534	24.399	83.231
“reject outliers (0.01% of mesh)” [mm]	101.115	25.424	99.934	80.963	24.107	81.164
“reject outliers (0.1% of mesh)” [mm]	101.073	25.423	100.041	80.898	24.107	81.294

Table 2.6: Distances to the virtually-generated reference plane.

Nonetheless, the biggest drawback of this approach is that cannot be known *a priori* what is the most appropriate outlier rejection percentage since the ‘best’ value will largely depends on the (unknown) number of mesh artifacts that were introduced during the RE process.

Point Location	Top Left (Point 1)	Top Center (Point 2)	Top Right (Point 3)	Bottom Left (Point 4)	Bottom Center (Point 5)	Bottom Right (Point 6)
Physical Mean [mm]	100.57	25.24	99.90	80.67	23.98	80.98
Difference “reject no outliers” [mm]	-0.24	-0.01	0.75	-0.14	0.42	1.25
Difference “reject outliers (0.01% of mesh)” [mm]	0.55	0.19	0.03	0.29	0.12	0.19
Difference “reject outliers (0.1% of mesh)” [mm]	0.51	0.19	0.14	0.22	0.12	0.32
Difference [mm]	0.334	-0.007	0.107	-0.152	0.054	0.652

Table 2.7: Effect of outlier rejection amount on virtual measurements.

Beyond that, variability of the measurements is inherent - caused by the simultaneous modifications of both position and orientation of the virtual reference plane resulting from changing the rejection ratio. Therefore, this approach is less consistent than the approach using the granite table to create the virtual reference plane. Hence, the virtual reference plane method is not applicable to accuracy evaluations.

2.6 Chapter Summary

Work completed in this chapter has shown incremental improvements in repeatability of the tested scanning procedures. The most repeatable scanning procedure produced two scans of identical parts whose points have one standard deviation of 0.047mm. Next an assessment of the accuracy of the most repeatable scanning procedure was performed. The worst result from the accuracy test was 0.8% off of the physical measurement. With these results the chapter outlines a scanning procedure which can produce scans of reasonable repeatability and accuracy (Figure 2.12).

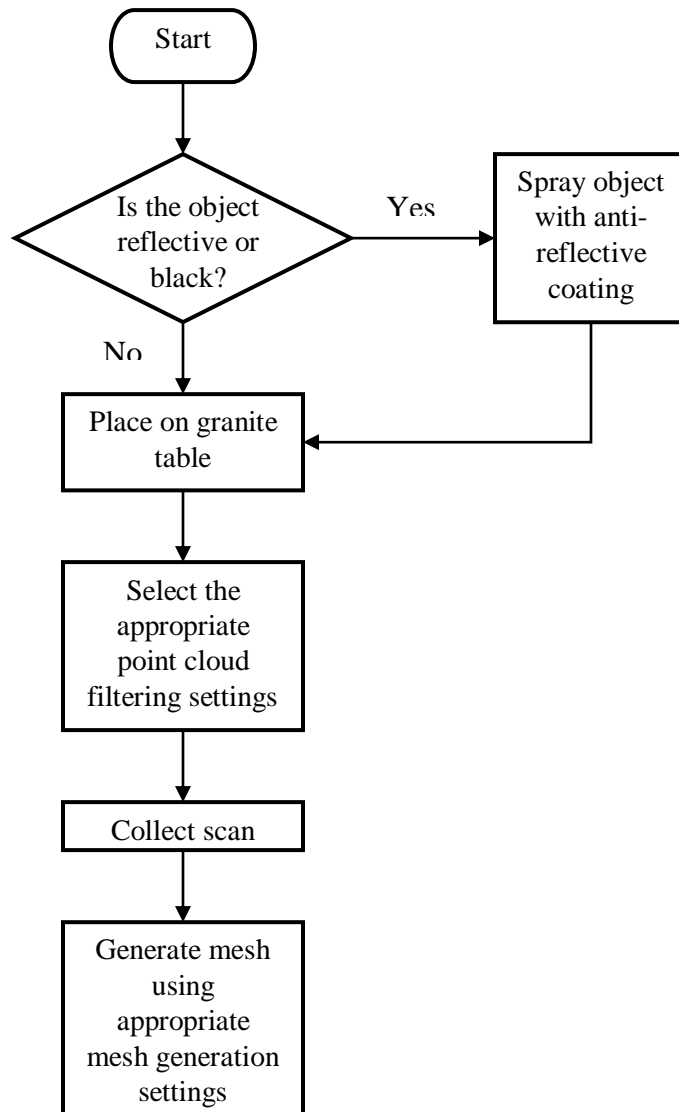


Figure 2.12: Road map of scanning procedure to produce scans with reasonable repeatability ($\sigma = 0.047\text{mm}$) and accuracy (0.8%).

Chapter 3 : Investigation of Different Warpage Metrics

3.1 Overview

Chapter 3 explores the concept of warpage measurement. Previously applied methods of measuring warpage are explained. For the purposes of comparing the resulting warpage from multiple methods of manufacturing the parts, it was determined that different warpage metrics could provide more insightful results. In total there are five different warpage metrics proposed in chapter 3. The mesh alignment procedure is explained and used for all warpage metrics. The concept of each warpage metric is explained and two sets of five SBO parts are used to test the warpage metrics. Finally there is a comparison of the results obtained from the different warpage metrics and then a summary of the chapter.

3.2 Background

There are many possible ways to generate a warpage measurement. In a typical reverse engineering workflow the warpage measurement is usually depicted as a ‘warpage (or deviation) colour map’ in which the CAD model and the scan of the part are aligned and then the distances between the scan and CAD model are calculated across the entire surface of the mesh at each node. A colour bar is shown and each facet of the mesh is coloured to correspond with the magnitude of warpage at that facet. Examples of these colour maps can be found in Section 2.3 (Figures 2.2, 2.3, and 2.4). Colour maps are primarily used as a qualitative measurement, essentially they are used to highlight problem areas on the part. While the colour bars help assign magnitudes of warpage to specific areas it is difficult to obtain a single number to represent that warpage. Without a consistent method of quantifying warpage of individual parts it is difficult to appropriately apply statistical tools such as: t-test, ANOVA, or DoE which can be used to understand the impact some variables have on the warpage.

An example of another potential warpage metric is presented in the work by Song et al [32]. In this paper a similar LLP is used to generate meshes of a compression molded composite part. The purpose of the scanning is to provide experimental validation for molding simulation results. The warpage metric used to perform this comparison between experimental and simulation results is a single measurement of warpage at a location which typically yields the maximum warpage of the part. Using the maximum warpage to represent the warpage of a part is a common method for evaluating the warpage of parts [14],[16].

Song et al also employed a more detailed comparison of the physical part to simulation results, measurements at multiple points were collected in one corner of the part, and at each location the measurement would be compared to measurements gathered from simulation results [32]. While these strategies seemed to work well for the application of simulation validation, a different method of warpage measurement was sought out for the purposes of applying statistical tools to assess the impact of specific processing conditions.

3.3 Mesh Alignment

All warpage metrics use the same scans of parts, the same CAD models for comparison, and the same alignment techniques. Therefore the differences between the results from each metric can only be due to the warpage metrics themselves. The purpose of the alignment procedure is to align the scan to the CAD model so that deviations can be calculated. Due to the vast number of methods of aligning scans to CAD models, measurements derived from this process should not be used in the 'absolute', but only for comparative purposes. If there is a deviation of 7 mm at a specific location, this deviation could very likely have a different magnitude if the part is aligned using a different method, this means the measurement is not absolute. If multiple parts are aligned using the same method, they can then be compared against one another.

The alignment procedure applied is a best fit alignment to selected elements on the scan. First the scan mesh and CAD model are imported. Using user selected point pairs, the scan is pre-aligned to the CAD. This point pair technique requires the user to select complimentary points on both the scan and CAD which are used to roughly align the parts. This technique saves computational time and is recommended for highly warped parts because automatic pre-alignments might have difficulty due to the large magnitude of warpage. After pre-alignment all elements in the center area of the scan are selected (see Figure 3.1).

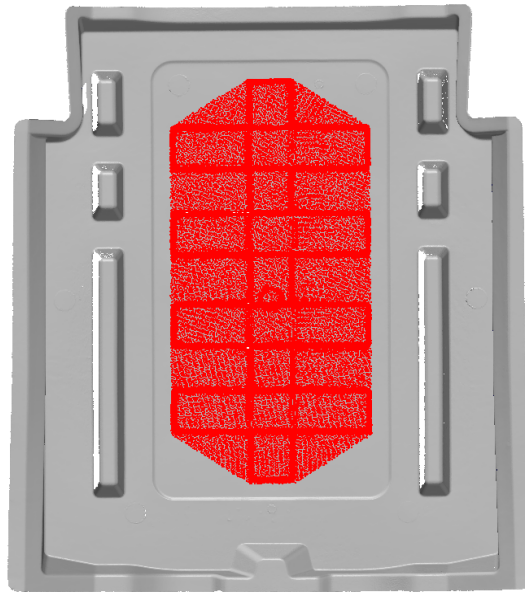


Figure 3.1: Example SBO scan with selected elements (red elements) used for best fit alignment procedure.

These elements will be used as a target for the best-fit alignment procedure. The best-fit alignment procedure seeks to minimize the distances between the selected elements and the CAD model. To achieve this the solver constantly varies the position of the scanned geometry and calculates the distance between the elements and the CAD model and changes the position of the CAD model until these distances are minimized. Essentially the RE software uses an ‘iterative closest point’ (ICP) algorithm to minimize the distances between the scan and CAD model [22].

3.4 Global Global Warpage Metric

The ‘global global’ warpage metric measures warpage across the entire part (global warpage) and calculates an average warpage by utilizing all vertices (global average). This data can be extracted from typical deviation colour maps used in RE inspection software. It is important to note that a simple average from a deviation colour map should not be used. This is because warpage in the negative direction will counteract warpage in the positive direction, resulting in an average warpage of roughly zero. Instead positive and negative warpings must be separated (see Figure 3.2), and the absolute value of the negative warpings must be used to calculate the average.

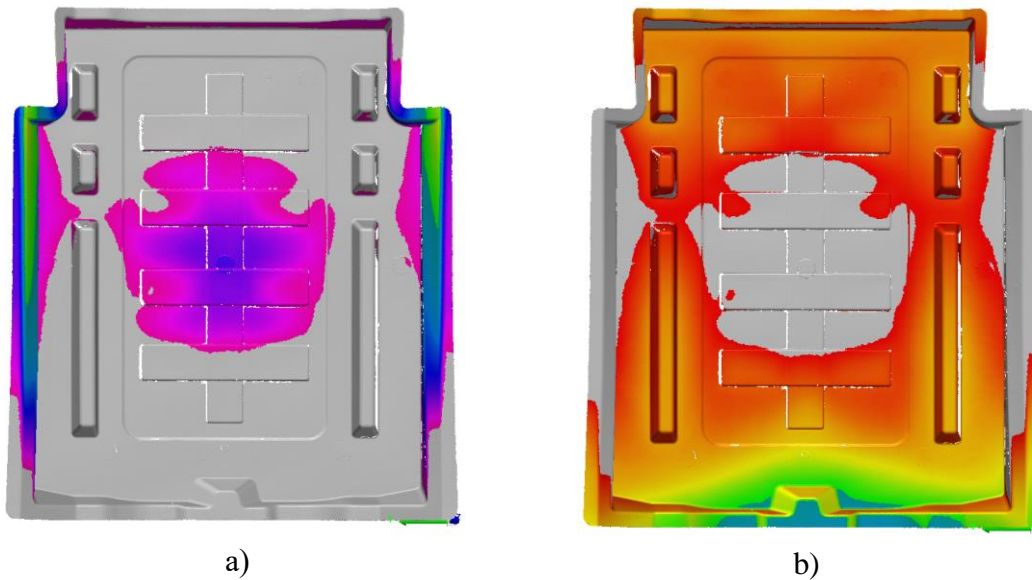


Figure 3.2: Example of separated positive a) and negative b) warpage color maps for ‘global global’ evaluation (SBO part).

A weighted average should be calculated using the number of points included in the positive and negative colour maps to designate the weights of the positive and negative warpings. The equation used for calculating average warpage for the ‘global global’ metric is shown below:

$$Average = [(MPD * NPP) + (MND * NNP)] / (NPP + NNP) \quad (3.1)$$

Where MPD is the mean positive deviation, NPP is the number of positive points, MND is the mean negative deviation (absolute value), and NNP is the number of negative points. From this metric the following results were extracted from the first five sample pieces (Table 3.1).

Part ID	Weighted Average Deviation (mm)
191002-1-1	1.712
191002-1-2	1.755
191002-1-3	1.978
191002-1-4	1.750
191002-1-5	1.826

Table 3.1: ‘Global global’ metric results.

3.5 Global Local Warpage Metric

Similar to the ‘global global’ metric, the ‘global local’ warpage metric evaluates the warpage of the entire part. The ‘global local’ metric differs from the ‘global global’ metric in the method of extracting the measurements. Instead of gathering measurements from all vertices, 26 specific points are selected (see Figure 3.3). Vertices in a 1mm radius surrounding the selected points will be averaged to give a single measurement at each point. For a single part, the absolute value is taken for all the deviations and then averaged. Using this metric the following measurements were obtained from the same five sample parts (sample parts evaluated in Table 3.1).

Part ID	Weighted Average Deviation (mm)
191002-1-1	2.912
191002-1-2	2.952
191002-1-3	3.265
191002-1-4	3.038
191002-1-5	2.928

Table 3.2: ‘Global local’ metric results.

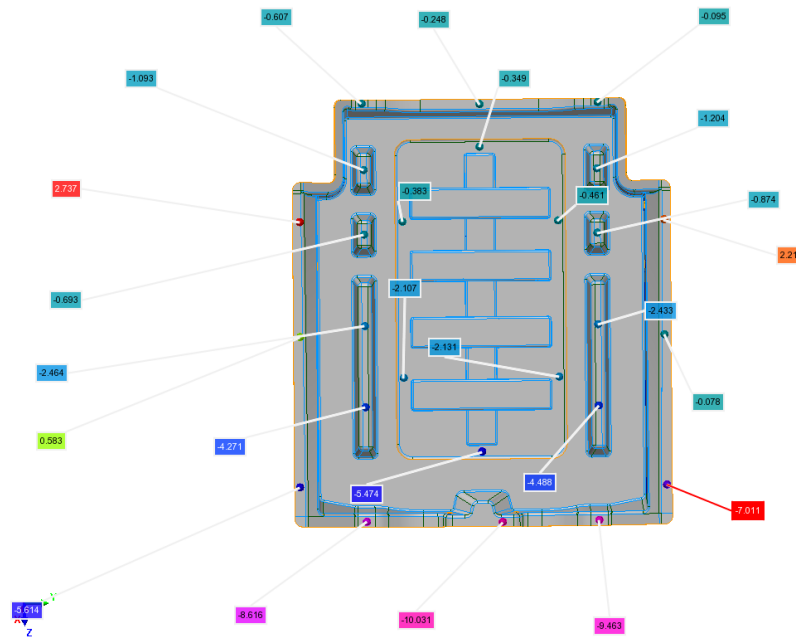


Figure 3.3: Example of ‘global local’ measurement points (image shows measurement callouts).

Unfortunately, due to the nature of the measurement gathering method (specific points of comparison) the measurements are actually collected from the CAD model and not the scan. The measurements are collected by essentially attempting to find the shortest distance between the CAD and scan. However there are some sections of the CAD geometry which cannot ‘find’ the complementary points on the scan. There is poor point to point mapping at this location, the points from CAD and scan generating the distance measurements are not from the same locations on their respective geometries. This is unfortunately a limitation of the software. The problem is displayed in Figure 3.4, which is a section view of the top corner of the left flange. The circled area shows where there is no measurement completed on the CAD geometry. In this area ‘local’ measurements (point measurements) cannot be collected because that surface of the CAD model has no warpage

measurement attached to it. Due to this problem ‘local’ measurements cannot be collected in the area around the top of the left and right flanges.

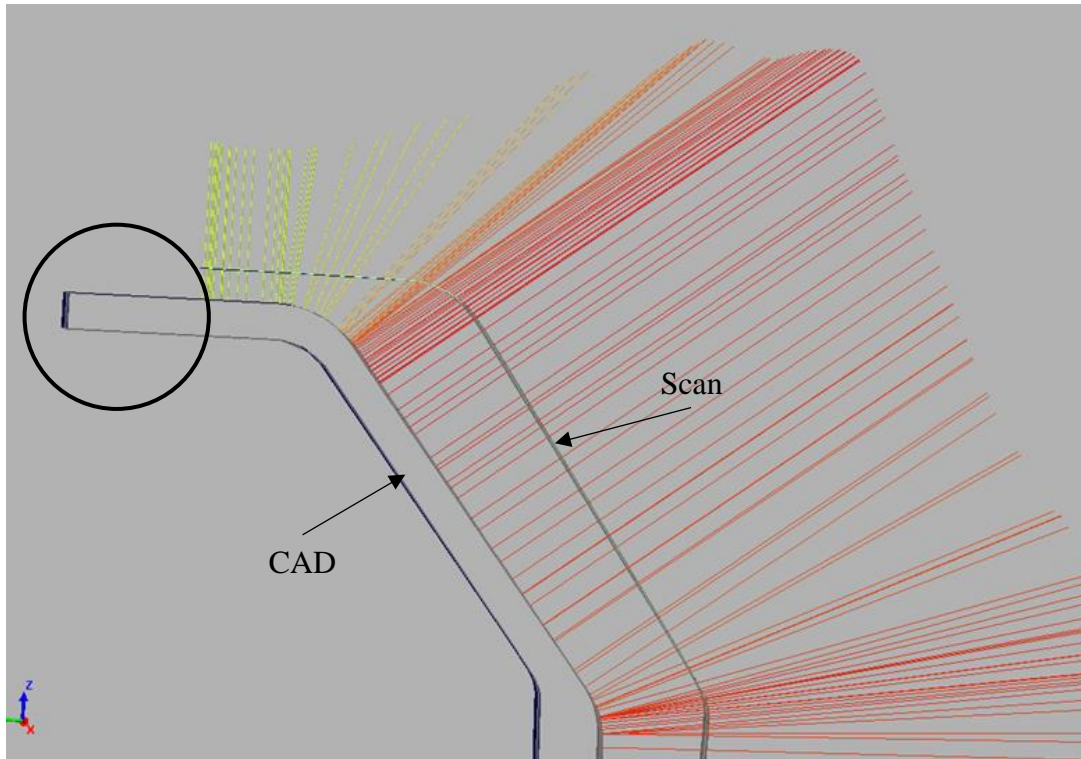


Figure 3.4: Cross section view of inspection of the top left of SBO flange. Circled section shows CAD that is not mapped to the scan. CAD has two layers and scan has one layer.

3.6 Local Global Warpage Metric

The ‘local global’ warpage metric is used to focus measurements on specific areas of interest. In the case of this geometry; the left and right flanges are areas of interest because they are typically the most warped and are weld areas necessary for assembly. Measurements on these flanges are acquired ‘globally’ (that is, all vertices on the flanges are averaged into a single measurement). This process is very similar to the ‘global global’ measurement process described before, the only difference being that data is exclusively collected from the flanges (see Figure 3.5).

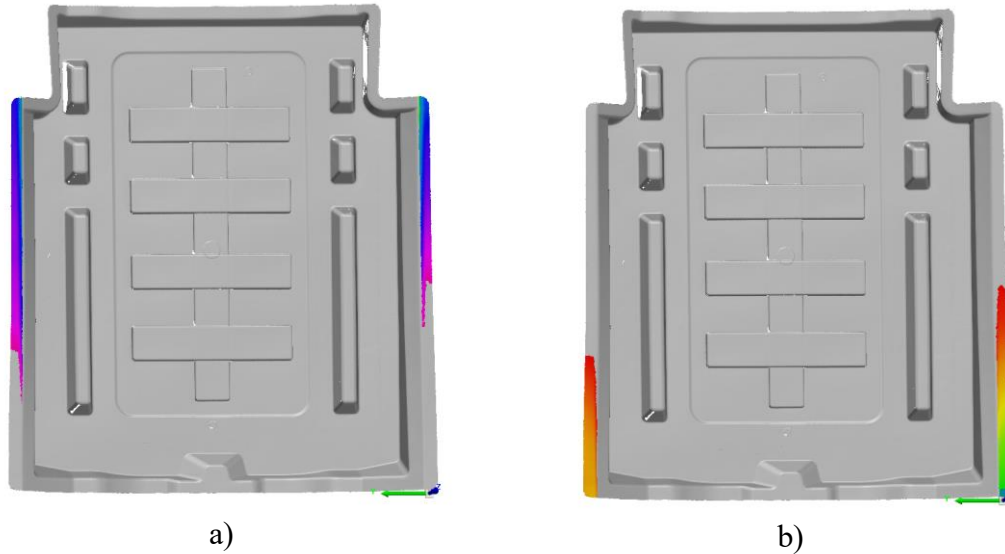


Figure 3.5: Example of separated positive a) and negative b) warpage colour maps for ‘local global’ evaluation (SBO part).

Once again positive and negative warpages must be separated to acquire the absolute value of negative deviations before averaging (see equation 3.1 in Section 3.4). The following results were extracted on the same five sample parts using the ‘global local’ metric (Table 3.3).

Part ID	Weighted Average Deviation (mm)
191002-1-1	4.276
191002-1-2	5.263
191002-1-3	5.815
191002-1-4	4.563
191002-1-5	5.763

Table 3.3: ‘Local global’ metric results.

3.7 Local Local Warpage Metric

Similar to the ‘local global’ warpage metric, the ‘local local’ metric is used to acquire data from specific areas of interest (left and right flanges). However, unlike the ‘local global’ metric only a small number of vertices at specific locations will be used to gather measurement data. There are six measurement locations for each flange (12 points total). As with previous ‘local’

measurements, data cannot be collected from the top of each flange which is why there are no measurements collected at those locations (see Figure 3.6). Warpage measurement extracted using this metric on the same five sample parts are shown in Table 3.4.

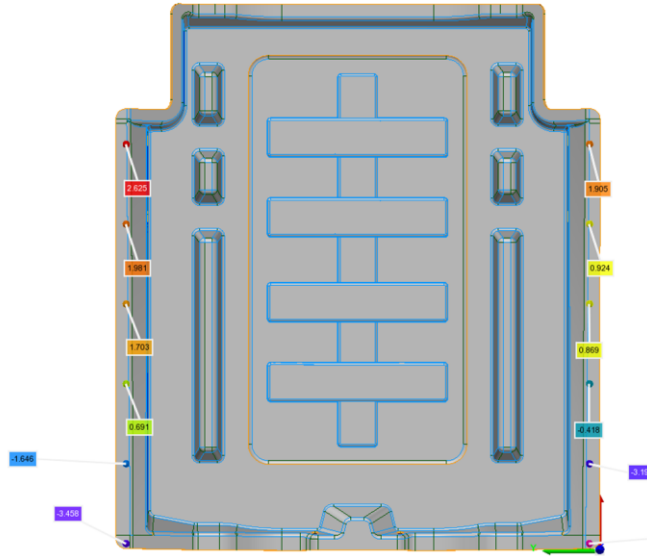


Figure 3.6: Example of ‘local local’ measurement points (SBO part).

Part ID	Weighted Average Deviation (mm)
191002-1-1	2.977
191002-1-2	2.979
191002-1-3	3.578
191002-1-4	1.170
191002-1-5	3.185

Table 3.4: ‘Local local’ metric results.

3.8 Vector Deviation Warpage Metric

The vector deviation metric is a very time-consuming methodology designed to correct problems with automatic point to point mapping that’s experienced by the RE software. This method is mostly manual and thus it should be noted there will be additional random error associated with the measurements. Despite this additional random error, the measurements from this method are

significantly more accurate along the entire flange. In order to accurately map points from CAD to scan features on the flange are used as references to place points at proper locations. The boundaries of the flange and the tangent of the fillet curve are used as features for more consistent point placement. Reverse engineering software can generate a curve which is tangent to a fillet, this curve can be exported as an IGES file. In CAD software the IGES file along with the scan (with the best fit orientation applied) are imported. Using the scan, two additional curves are made. One at the boundary of the flange, and another between the boundary and the tangent fillet curve. Along each of these curves three points are placed equal distance from each other. This process must be carried out for each scan. This will generate the 'mapped points' on the scan geometry (see Figure 3.7 b)).

On the CAD geometry generating the mapped points is much simpler and only needs to be carried out once. On the CAD model existing curves are used to generate the mapped points for the curve at the boundary and the curve at the tangent to fillet. The curve between those two is generated manually using the two curves as references. Similarly, 3 points are placed on each curve at equal distance from each other (see Figure 3.7 a)). Using the 'mapped points' on both the CAD and scan, distances from one point to another can be calculated; this represents the warpage. This entire process is carried out for both flanges, 9 points are used on each flange making for a total of 18 points. Using this point to point measurement style, component vectors along each axial direction can be extracted. The additional information that these component vectors provide could be used to better understand the warpage and to make better informed judgement calls about which part might be easier to assemble. In order for direct comparison with the other metrics, the resultant of each of the 18 vectors are calculated and then an average resultant vector is used to represent the warpage of each part (see Table 3.5).

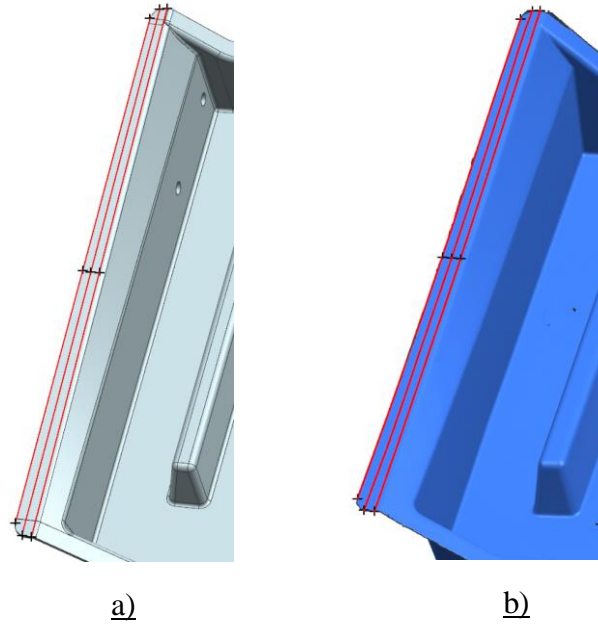


Figure 3.7: Example of mapped points on CAD a) and scan b) used for ‘vector resultant’ metric (SBO part).

Part ID	Weighted Average Deviation (mm)
191002-1-1	7.009
191002-1-2	7.509
191002-1-3	8.201
191002-1-4	7.031
191002-1-5	7.793

Table 3.5: ‘Vector resultant’ metric results.

3.9 Comparison of Warpage Metrics

To compare all of the different warpage metrics, five parts were evaluated from each of two sets of processing conditions (Series 1 & 2). The difference between the two processing conditions was mold temperature, however this is not the focus of this section. In this section the results produced by the warpage metrics will be compared within the sets, not between the two sets. The purpose of this comparison is to assess the results from the different warpage metrics (similarities/differences and the causes). The results from this study are shown in Figures 3.8 &

3.9 below, Figure 3.8 showing the results from five parts from series 1 and Figure 3.9 showing the results from five parts in series 2.

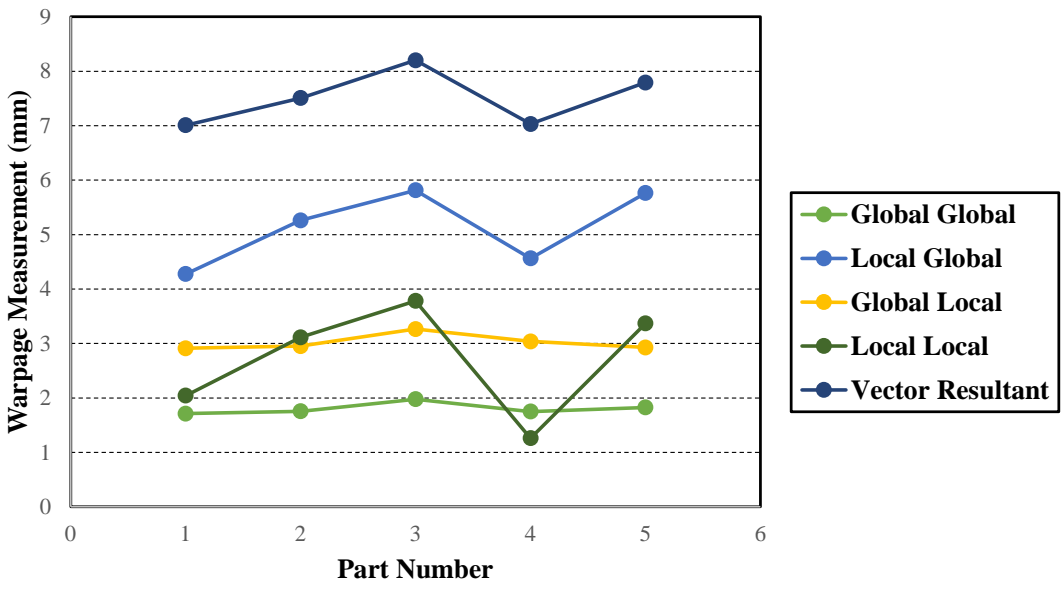


Figure 3.8: Graph of results from several potential warpage metrics. Measurements are made on five SBO parts from series 1.

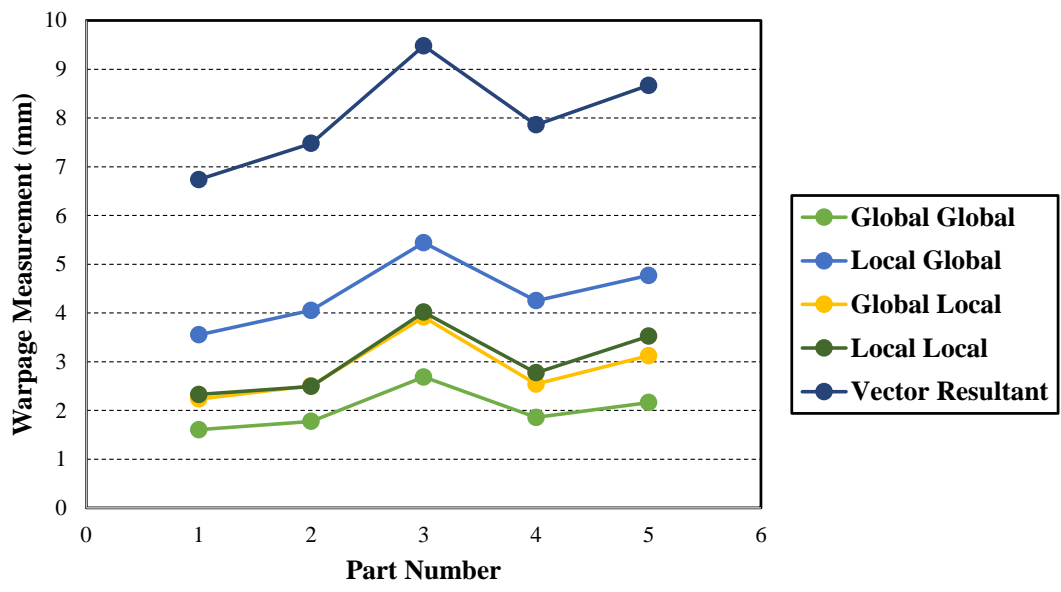


Figure 3.9 Graph of results from several potential warpage metrics. Measurements are made on five SBO parts from series 2.

The differences in magnitudes of warpage for each metric will be explained. It will be shown that these differences are linked directly to how the measurements are acquired. Figure 3.10 shows an averaged deviation colour map for all five parts in series 1, meaning this colour map is an average of five independent colour maps generated for each part. Inspection of the colour map in Figure 3.10 shows that the deviation is relatively low near the center of the part. Both the ‘global global’ and ‘global local’ warpage metrics gather data from the center of the part. Due to the incredible volume of data acquired from this area while using the ‘global global’ warpage metric, the resulting warpage measurement is dominated by this response (low magnitude of warpage), leading to the ‘global global’ metric outputting the lowest measured warpage for each part (in almost all instances). Although the ‘global local’ warpage metric also gathers deviation measurements from the center of the part, it doesn’t gather nearly enough data points to result in these measurements dominating the response.

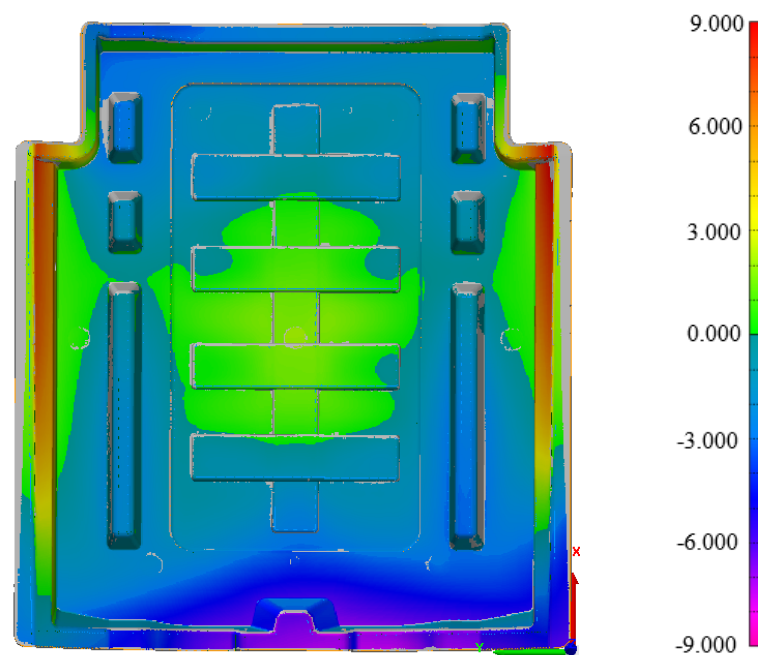


Figure 3.10: Average deviation (mm) colour map for series 1 SBO parts.

Examining the changing magnitude of warpage for the ‘local global’, ‘local local’, and ‘vector resultant’ metrics might initially be confusing, because all three metrics are attempting to represent the warpage at the left and right flanges of each part. These metrics result in varying magnitude because of how the metrics acquire the data. The ‘local local’ measurements report the smallest magnitude in for a number of reasons, the most important being that the measurements are acquired from the CAD model. As discussed before in Section 3.5 (Figure 3.4), the scan is not perfectly mapped to the CAD model by the software. This lead to the inability to collect measurements from the top of the left and right flanges, where warpage is the largest. More importantly because the measurements came from the flanges on the CAD model these measurements will only include the ‘z component’ of the deviation as shown highlighted in Figure 3.11.

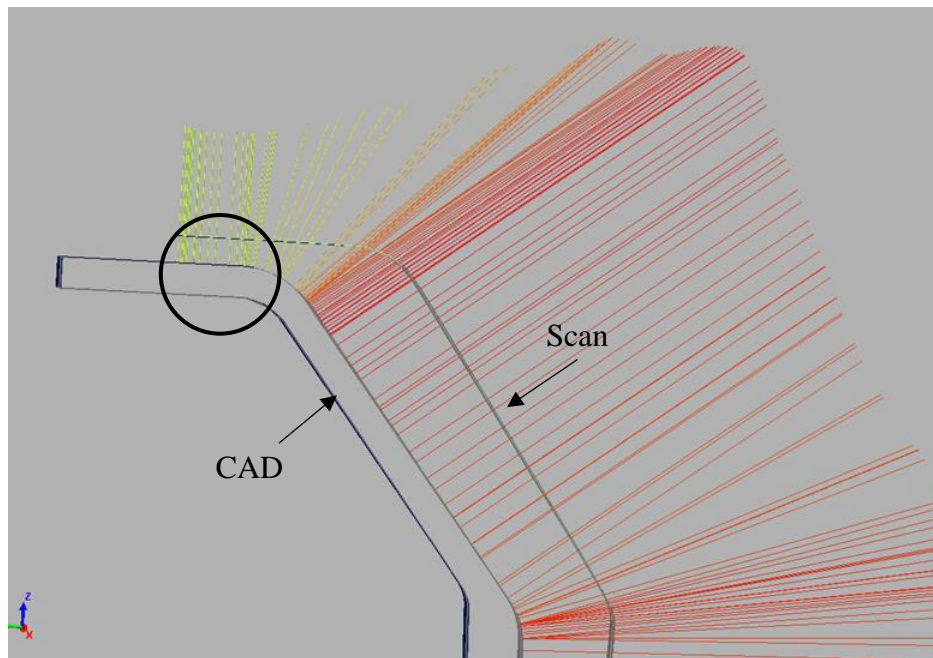


Figure 3.11: Section view of SBO evaluation. Circled area shows where results for ‘local local’ warpage metric are gathered.

For ‘local global’ measurements however, the entire flange of the scan of the SBO part is used to generate the warpage measurement, this is highlighted in Figure 3.12. In Figure 3.12, it’s clear that these measurements include some data points which have not only the ‘z component’, but also a ‘y component’ of the warpage which will intuitively increase the resulting average warpage represented by this metric.

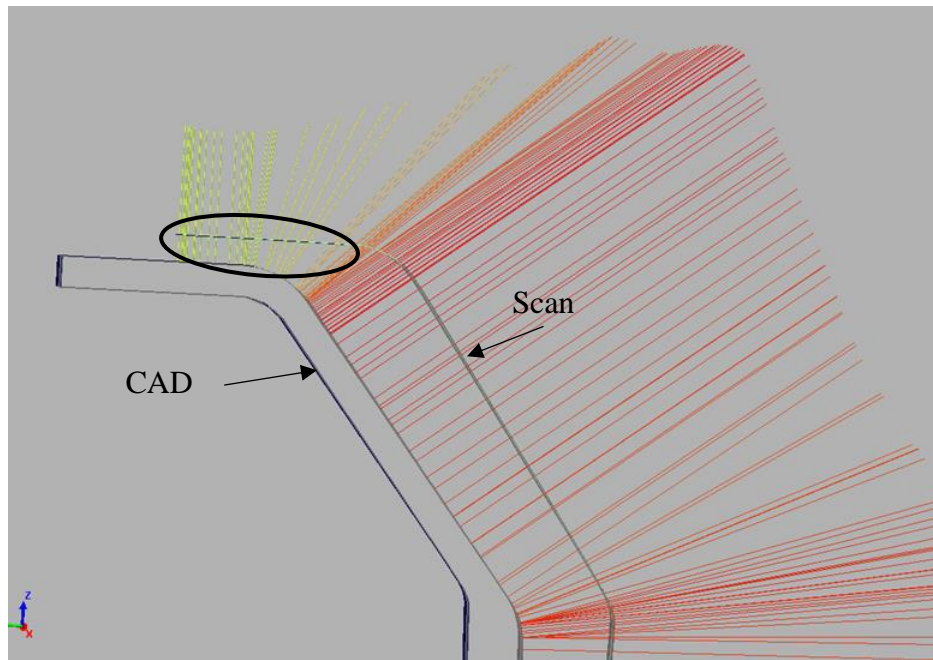


Figure 3.12: Section view of SBO evaluation. Circled area shows where results for ‘local global’ warpage metric are gathered.

Finally, the ‘vector resultant’ metric has the largest reported warpages, Figure 3.13 shows an example of a cross section view for this metric. Figure 3.13 illustrates the large amount of ‘y component’ deviation which is captured by this method. The inclusion of the ‘y-component’ deviation results in the vector resultant method always yielding the highest warpage. All of these cross sectional views also illustrate why the ‘vector resultant’ metric produces the most accurate results. The manual mapping of points will undoubtedly introduce errors; however, the cross

section views demonstrate the even larger errors introduced by poor mapping by the software. The increase in warpage magnitude from the ‘vector resultant’ method and more accurate representation of warpage does not necessarily justify using this metric over others. As mentioned in Section 3.9 the ‘vector resultant’ metric takes significantly more time to produce results. Additionally, examining Figure 3.8 and 3.9 reveals that other warpage metrics will yield the same response in terms of which part has a lower or higher warpage compared to other parts. In this specific case the ‘vector resultant’ method essentially shifts the ‘local global’ results up the y-axis.

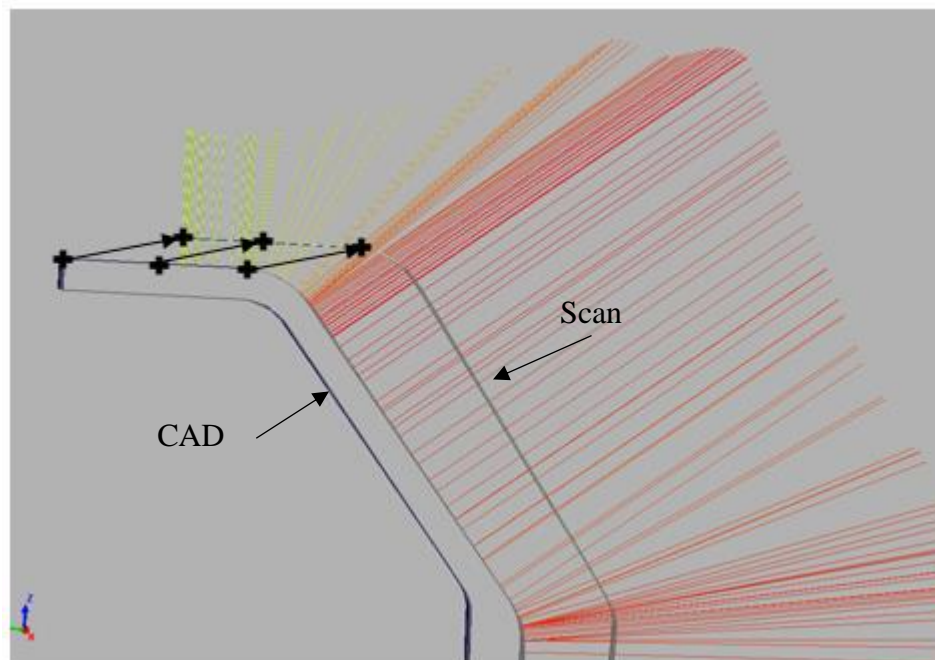


Figure 3.13: Section view of SBO evaluation. Arrows show point to point mapping used for ‘vector resultant’ metric.

Now that there is a better understanding of how the metrics will influence the resulting magnitude of warpage for each part, the differences in part to part variation for the metrics will be explored. In Figure 3.8, the ‘global global’ and ‘global local’ metrics produced results with very little part to part difference. Both of these metrics use measurements acquired from across the entire part

(measurements are not concentrated on specific areas of high warpage). Figure 3.14 shows an averaged standard deviation colour map, which is similar to the colour map in Figure 3.10, however this colour map shows the standard deviation across the entire geometry. From Figure 3.14 it's easy to see that the center of the part has low standard deviation compared to the flanges. It follows that there is little part to part difference at the center of the part and differences between parts are primarily located at the flanges.

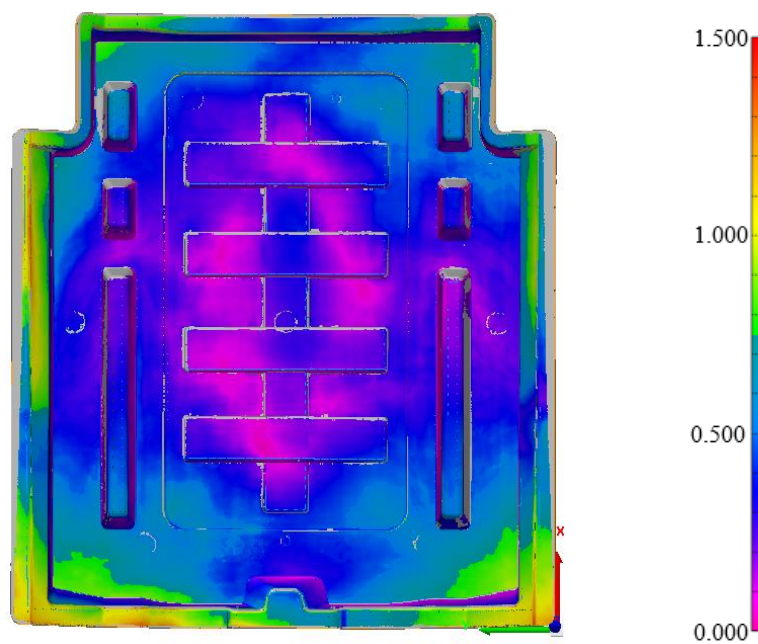


Figure 3.14: Average standard deviation (mm) colour map for series 1 SBO parts.

Both the 'global global' and 'global local' metrics collect measurements from the center of the part where there is low standard deviation. Including many measurements which do not change much from one part to another, will undoubtedly reduce the variation in the warpage measurements. Since many measurements are acquired in low standard deviation areas of the part, this low standard deviation will dominate the response, making it difficult to distinguish one part

from another. For this reason ‘global global’, and ‘global local’ metrics are not particularly useful for comparing two individual parts in a set. Acquiring measurements from across the entire part has muted the considerable part to part variation in warpage seen at the flanges.

For the five parts in series 2 the differences in magnitude of warpage will be explored. In the series 2 average deviation colour map (Figure 3.15) the center of the part typically has much lower deviations than the flanges, leading to lower deviations reported by the ‘global global’ metric (similar to the findings from series 1). The ‘global local’ method does not take as many data points from the low deviation areas. The differences in magnitude of warpage for the metrics ‘local local’, ‘local global’, and ‘vector resultant’ are due to all of the same factors explored in the analysis of the previous series.

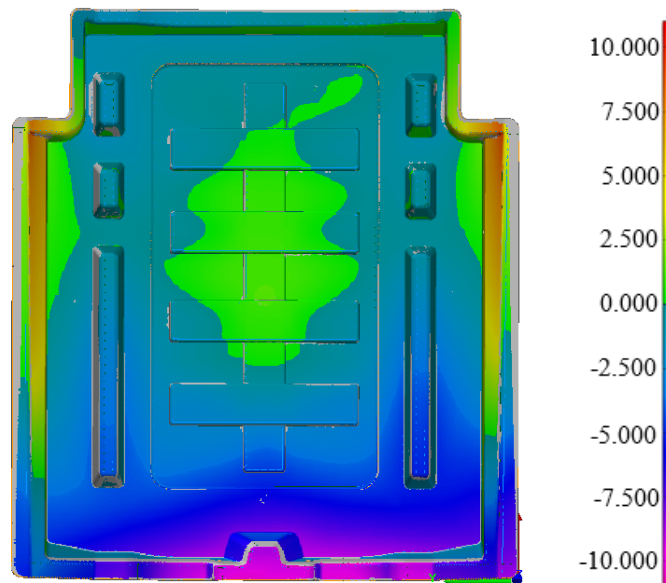


Figure 3.15: Average deviation (mm) colour map for series 2 SBO parts.

Although the relative magnitudes of warpage resulting from different metrics is consistent for both series 1 and series 2, the part to part variability is not. ‘Global global’ and ‘global local’ metrics do not display the same very low part to part deviation. Figure 3.17 shows the average standard

deviation for parts in series 2 and can illustrate why this difference exists between the two sets. An important difference between the standard deviation colour map from the first series (Figure 3.14) and the standard deviation colour map from the second series (Figure 3.17), is the generally larger standard deviation across the entire part (for series 2). Due to this larger standard deviation across the whole part the ‘global global’ metric now yields warpage results which allow easier distinction of parts which are more or less warped. Similarly, the larger standard deviation across the entire part had the same impact on the results of the ‘global local’ metric. Due to the part to part variation being less concentrated at the flanges for series 2, the ‘global global’ and ‘global local’ metrics produced results with greater part to part differences.

Despite the fact that the overall average standard deviation across the part is larger in series 2, the standard deviation located at the flanges is largely unchanged. This is why there isn’t an expansion (to the same degree) in the range of results using the ‘local global’, ‘local local’, and ‘vector resultant’ metrics which focus on the flanges for measurements.

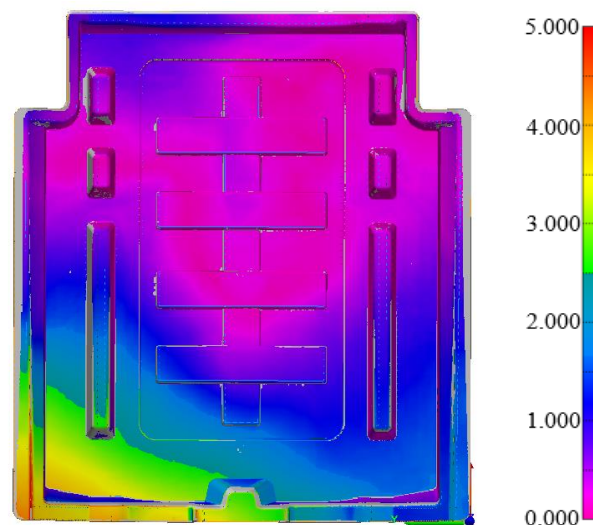


Figure 3.16: Average standard deviation (mm) colour map for series 2 SBO parts.

The initial examinations into the effectiveness of these warpage metrics have revealed many key findings. There are costs and benefits associated with the different methods of measuring warpage. Whether or not the measurements are gathered ‘globally’ (across the entire part) or ‘locally’ (at specific areas of interest) will, without a doubt, influence the results. In series 1 it was revealed that gathering measurements ‘globally’ (across the entire part), would lead to an attenuated response due to the vast quantity of data extracted from areas of the geometry with little part to part differences. The attenuated response is seen in the flattened curves from ‘global global’ and ‘global local’ results in Figure 3.8. When comparing the standard deviation colour maps for series 1 and 2 (Figures 3.14 and 3.17 respectively) they clearly show that there is more part to part variability in series 2. However, since the ‘local local’ and ‘local global’ metrics only collect data from the flanges, the standard deviation of the results of these metrics will not be impacted by the increased part to part variability which is noticed outside the flanges for this set.

In summary, if results are collected from across the entire part (globally) there is a risk of weakening the signal. At the other end, if results are collected at specific locations (locally) there is a risk of missing out on important changes at locations where the data is not collected. For the purposes of this geometry the most important areas to examine are weld locations and upon visual inspection of the part it was very clear to see that the left and right flanges exhibited the most warpage of any other weld area in the entire part. Additionally, large part to part variability at these flanges will result in warpage measurements (concentrated at these locations) to be discernable from one another; that is, the warpage measurements can be useful to determine which part is more or less warped than another. Due to the aforementioned factors it appears that the ‘local’ measurements are best in this specific scenario of comparing parts within sets.

3.10 Chapter Summary

Due to the lack of established warpage metrics five different warpage metrics have been proposed in this chapter. All warpage metrics use the same CAD and scan files, in the same alignment to produce results. To test the effectiveness of the five warpage metrics two series of five parts are analyzed by each metric (total of 10 different parts). The results from this study showed that for most instances the different warpage metrics were able to show the differences in warpage of each part relative to the other parts. The only exception to this were the results collected using the 'global global' and 'global local' metrics on the first set of parts. It is theorized that collecting data from the entire geometry while changes in warpage are mainly concentrated in specific areas of the part reduced the sensitivity of these metrics in that circumstance.

Chapter 4 : Application: Simple Experiments

4.1 Overview

Chapter 4 shows the application of two of the warpage metrics applied to two simple experiments. The first experiment tests the impact of altering the mold temperature from 100°C to 150°C. The results obtained using the two metrics are shown and a t-test is used to determine if altering the mold temperature had a statistically significant impact on the measured warpage. The second experiment tests the impact of charge placement. In this experiment there were three different charge placements tested. Since there are three sets of data (one for each condition) an ANOVA was used to determine if changing the charge placement yielded statistically different warpage for any of the sets.

4.2 Background

The extent of the warpage present in the geometries after manufacturing the LFT SBO parts prompted the investigation into potential processing conditions which could affect the warpage of the part. In the aim of eventually conducting more complex experiments using a ‘design of experiments’ (DoE) framework, simpler experiments were used as a starting point. These simple experiments are essentially ‘1 input DoEs’, meaning that one factor would be altered from one set to another. The purpose is to examine if this alteration would result in an alteration in the output, which in this project, is the warpage. Since the response is the warpage, the application of an effective warpage metric is incredibly important to the analysis of the experiments.

4.3 Mold Temperature Experiment

In this experiment all processing conditions are held constant except for mold temperature which was set at two levels, 100 °C and 150 °C. Under each condition 10 parts are manufactured and then analyzed. The purpose of the experiment is to understand the impact of mold temperature on

the warpage of SBO parts. Mold temperature is thought to have an impact on warpage because temperature plays an important role in the warpage of plastic and FRP parts [15]. The expectation being that reducing the mold temperature could potentially reduce warpage; however, reducing the mold temperature has a negative impact on the flowability of the material in the mold. If the flowability is reduced too much then the material could fail to fill the mold. Therefore even if it is found reduction in mold temperature corresponds to a reduction in warpage, there are still operating limits for the process to consider.

To determine if the alteration of inputs (mold temperature) generated different outputs, a two sample t-test is used. A t-test is a statistical tool which is used to determine if two sets of data are statistically different. The null hypothesis of the t-test is that the means of two groups are statistically equal. It is standard for a 95% confidence interval (CI) to be applied while performing a t-test, and so this is the confidence interval selected for these experiments. A 95% CI sets $\alpha = 0.05$, a p-value less than α is required to reject the null hypothesis. If the null hypothesis is rejected then the t-test suggests the alternative hypothesis is true, which is that the two sets are statistically different from one another (and therefore claim that the changing of inputs resulted in a change in measured warpage).

4.3.1 Selection of Warpage Metric

From the results acquired in Chapter 3, the following warpage metrics were selected for this analysis: ‘global global’, and ‘local local’. ‘Global global’ was selected to test if this metric could produce results which were distinguishable between sets. In section 3.9 it was discovered that the ‘global global’ metric had attenuated the differences between parts within a set, so it was possible that the metric was not sensitive enough to compare two different sets of parts. ‘Local local’ was selected because it produced results which could be used to determine the relative warpings of

parts within a set, and so the metric should be sensitive enough to highlight any differences that exist between sets. Selecting metrics which collect results both ‘globally’ (across the whole part) and ‘locally’ (at the left and right flanges) could illustrate trends in the warpage. If for example both sets were statistically different according to the ‘local local’ metric, but not the ‘global global’ metric, it could mean that the change in mold temperature impacts warpage specifically at the flanges but does not have a profound impact on other areas of the geometry.

Although the ‘vector resultant’ fixes the poor point to point mapping problem discussed in Chapter 3 it was not selected for use in this experiment. The ‘vector resultant’ method is extraordinarily time consuming and did not offer any real benefit to metric evaluations in Chapter 3. The main benefit of the ‘vector resultant’ method is the inclusion of the lateral warpage at the flanges. Since an increase in lateral warpage results in an increase in vertical warpage (see Figure 3.13), metrics like ‘local local’ and ‘local global’ (which measure vertical warpage primarily) are also impacted by differences in lateral warpage, and therefore lateral warpage differences are accounted for in the resulting warpage measurement. As stated before, results from both ‘local local’ and ‘local global’ metrics follow similar trends as the ‘vector resultant’ results (see Figure 3.8 & 3.9), confirming that differences in lateral warpage also directly impact vertical warpage measured by the simpler methods.

4.3.2 Data and Analysis

First the ‘global global’ metric will be used for analysis (review Section 3.4 for more details). The ‘global global’ metric uses data across the entire part. The ‘global global’ results (see Figure 4.1) show that most of the data points for both sets are clustered together except for a few outliers. Although upon visual inspection of the results it becomes clear that these two sets do not seem different from one another, a t-test will be conducted to confirm these suspicions.

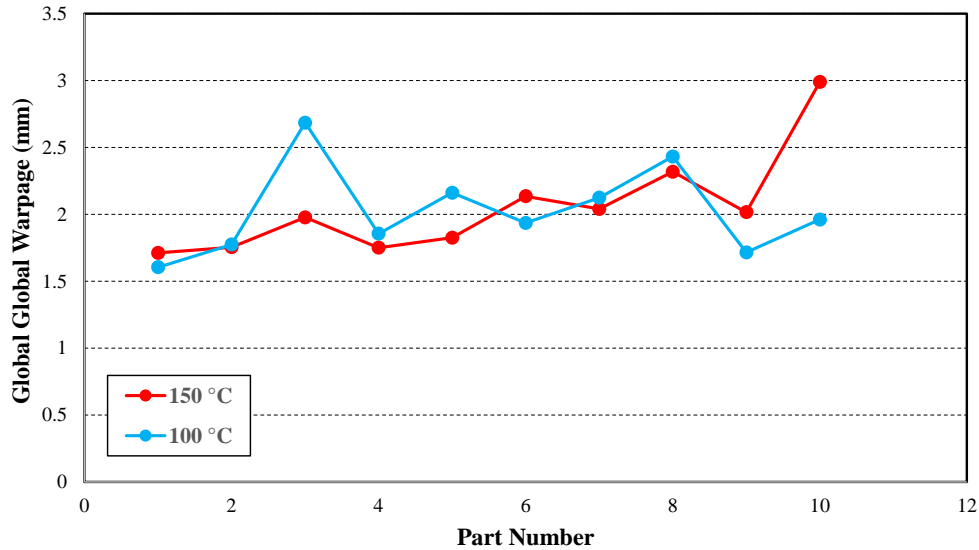


Figure 4.1: Measured warpage (mm) of each part in ‘Mold Temperature Experiment’ using ‘global global’ metric.

Accompanying the t-test is a bar chart (see Figure 4.2) which shows the average deviation from each set and error bars representing one standard deviation for that set.

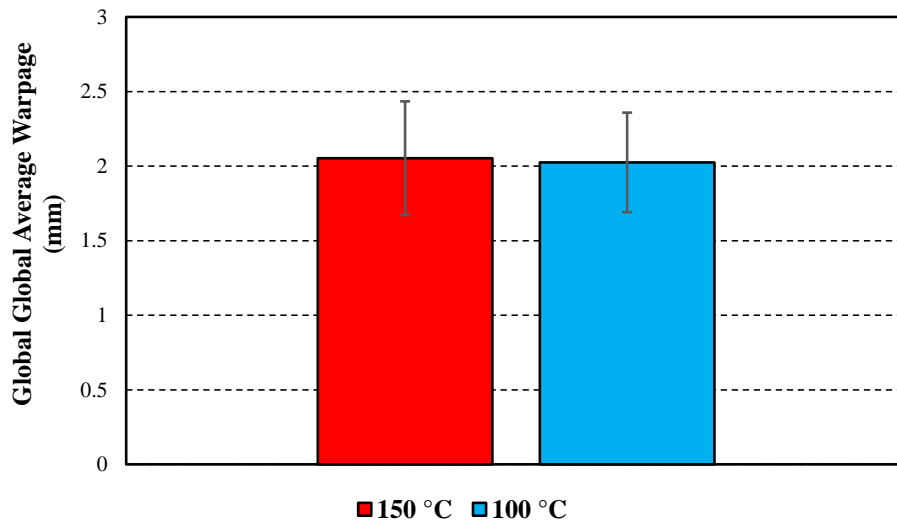


Figure 4.2: Bar chart shows average deviation for each mold temperature and error bars show one standard deviation for that series. Data is gathered using ‘global global’ metric.

Interestingly, Figure 4.2 shows that not only are the averages for each set incredibly similar, but the standard deviation for each set was as well. Upon quick visual inspection of Figure 4.2 the

results once again suggest that there is no difference between the measured warpage of the two sets. The calculated p-value from the t-test is 0.87 and therefore the null hypothesis is not rejected.

Next the ‘local local’ metric will be utilized for analysis. For this metric the data is collected specifically at the left and right flanges (review Section 3.7 for more details). Results gathered using the ‘local local’ metric once again show the clustering of data points for both sets (Figure 4.3).

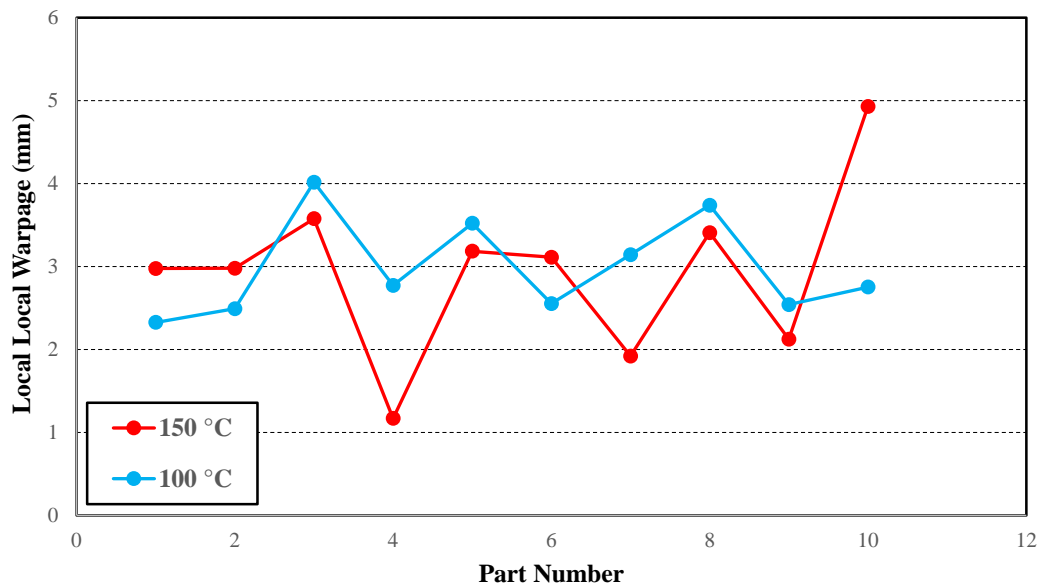


Figure 4.3: Measured warpage of each part in ‘Mold Temperature Experiment’ using ‘local local’ metric.

The clustering of data points is a good indication that the results will once again show no statistical difference between the two series. Next in Figure 4.4 the bar chart also shows that the two series had similar warpage results. However, the standard deviations are marginally different; the standard deviation for 150 °C and 100 °C being 1.03 and 0.59 respectively.

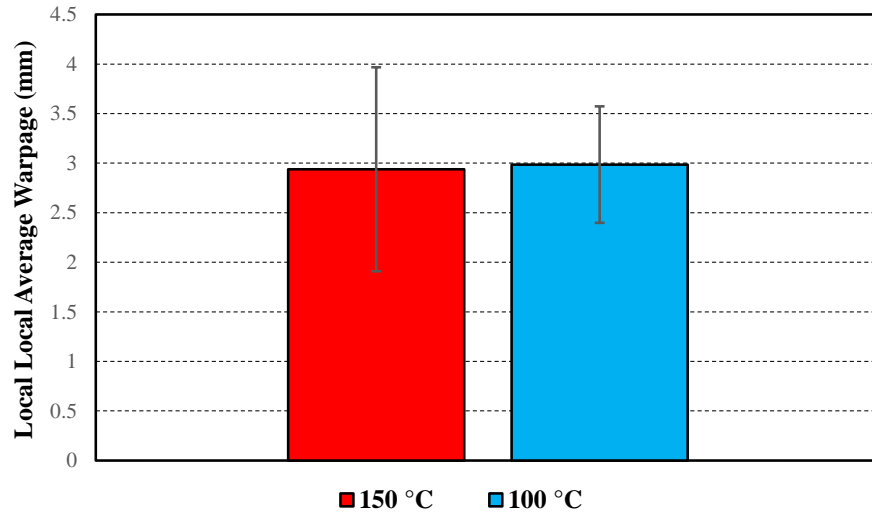


Figure 4.4: Bar chart shows average deviation for each mold temperature and error bars show one standard deviation for that series. Data is gathered using ‘local local’ metric.

Finally the t-test produced a p-value of 0.9 which once again fails to reject the null hypothesis. Therefore, the series are once again determined to have no statistical differences.

4.3.3 Discussion

The results using the ‘global global’ metric implied that altering the mold temperature from 100°C to 150°C does not impact the overall warpage of the seat back outer part. The p-value of 0.87 from the t-test performed on the ‘global global’ results proves the previous statement with some degree of confidence. In practical terms, there is no benefit of selecting one mold temperature over the other, and so these results do not clarify a method to reduce part warpage. However, the ‘global global’ metric collects data from the entire part, and so local improvements will be obscured by data from other areas of the part.

The ‘local local’ metric can be used to understand if altering mold temperature results in different warpage at the left and right flanges. Although the t-test performed using the ‘local local’ results also determined that no statistical difference existed between the two sets, this does not

mean no knowledge was gained from this study. In Figure 4.4 there is a notable difference in standard deviation between the two sets. That difference in standard deviation could mean that the warpage located at the flanges of the parts is more consistent when the mold temperature is 100°C.

In summary the results suggest that no difference in magnitude of warpage resulted from changing the mold temperature from 100°C to 150°C. The local local results suggested that using a mold temperature of 100°C could result in more consistent magnitude of warpage at the left and right flanges.

4.4 Charge Placement Experiment

Since the charge placement is not automated the location of the charge will have a larger degree of random error than some other parameters. To determine if there exists a correlation between where the charge is placed and resulting warpage, three series of LFT SBO parts were manufactured with different charge placements (nine parts per series). All other processing parameters were held constant. If it was discovered that the resulting warpage was impacted by charge placement then it is possible that the natural variation in charge placement would result in an increase in random error of warpage. To make this experiment more efficient one of the sets from the mold temperature experiment was used as the ‘center charge placement’ series for this experiment (both sets had the charges placed in the center of the mold). The other two series were ‘left charge placement’ and ‘right charge placement’. The rough dimensions of the charges were 400 x 100 x 45 mm, and the locations of all of the charge placements can be seen in Figure 4.5.

In the mold temperature experiment a t-test was used to determine if the two series had statistically different warpages; however, this experiment required the use of three different series, and a t-test cannot perform a comparison of three series. Therefore an analysis of variance

(ANOVA) will be performed using the data from all three series. ANOVAs are similar to t-tests, as the null hypothesis states that the means of all populations are equal. The key difference being that ANOVAs can be used when comparing more than two populations.

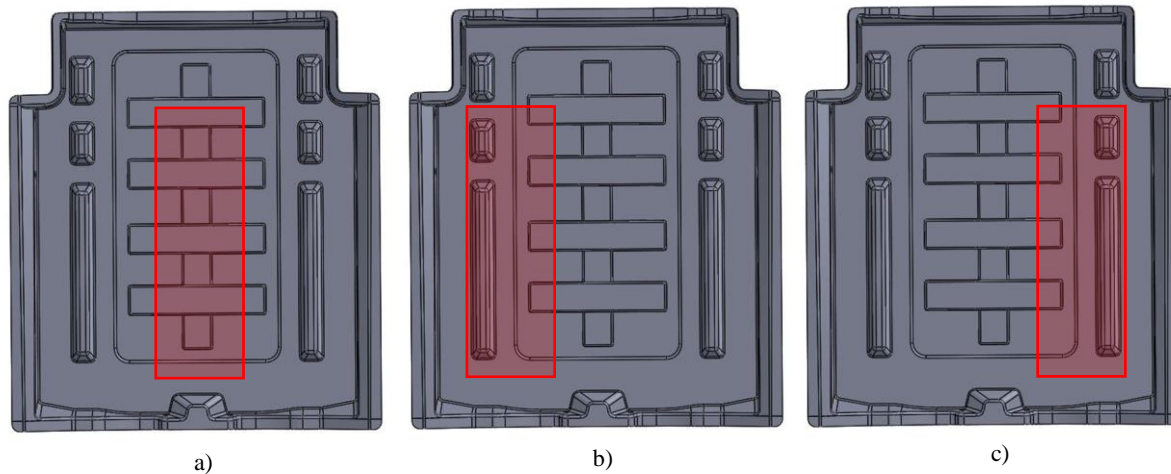


Figure 4.5: Charge placement location visualization: a) Center charge placement, b) Left charge placement, c) Right charge placement.

4.4.1 Selection of Warpage Metric

The same warpage metrics are used for this DoE and they are used for the same reasons as in Section 4.3.1. That is, the ‘global global’ and ‘local local’ metrics are selected for this evaluation.

4.4.2 Data and Analysis

The results gathered using the ‘global global’ metric will be explored first. The ‘global global’ warpage for each individual part in each set is plotted in Figure 4.6 below. The warpages of the three series are fairly intermingled. There is no immediately noticeable differences between the results of the three sets. In Figure 4.6 the bar chart displays the average warpage in each set, with error bars depicting one standard deviation in that set. Once again the averages are extraordinarily similar to one another and the error bars show significant overlap between the three sets.

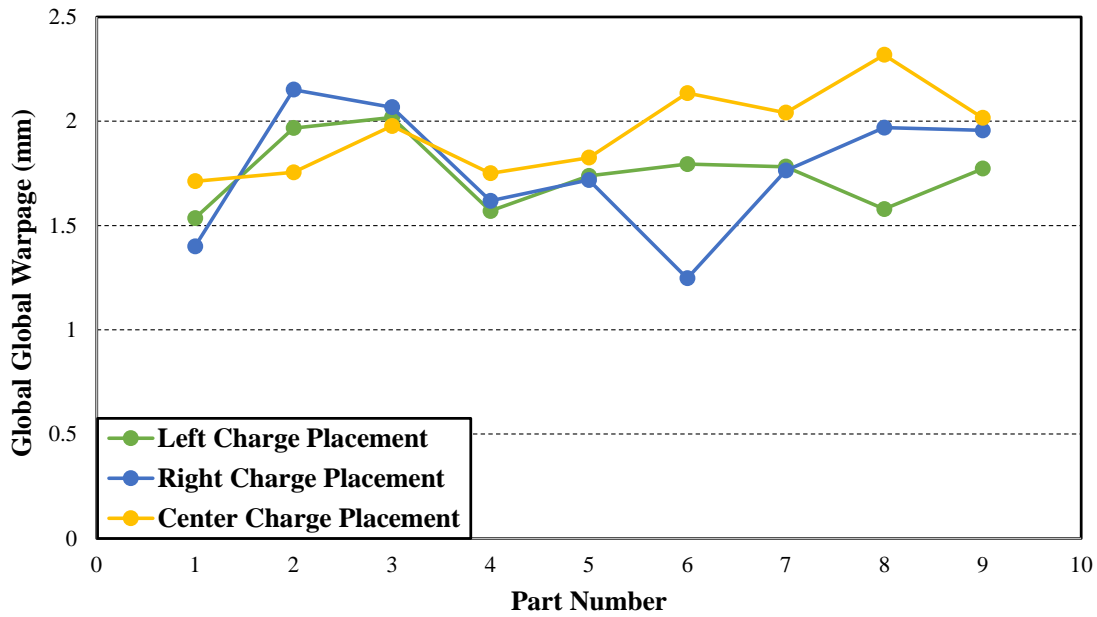


Figure 4.6: Measured warpage of each part in 'Charge Placement Experiment' using 'global global' metric.

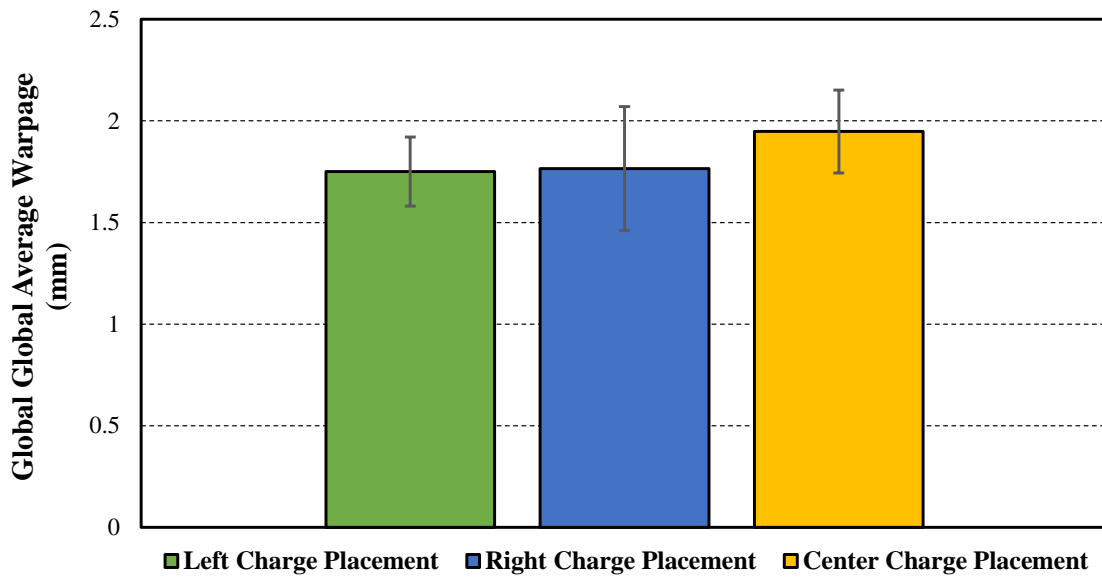


Figure 4.7: Bar chart shows average warpage for each charge placement and error bars show one standard deviation for that series. Data is gathered using 'global global' metric.

In Figure 4.7 the average deviation from the center charge placement is clearly higher than both the left and right charge placements. However, the difference is minimal and appears to be

accounted for by random error. With the overlapping error bars and very similar average warpages (in Figure 4.7) there is no surprise that the p-value of the ANOVA ($p\text{-value} = 0.11$) was greater than 0.05 and therefore failed to reject the null hypothesis.

Now moving on to the ‘local local’ metric. Once again a graph displaying the warpage calculated for the individual parts in each series is generated (see Figure 4.8). Figure 4.8 reveals overlapping responses from different series; meaning there is no clearly distinct response by any individual series.

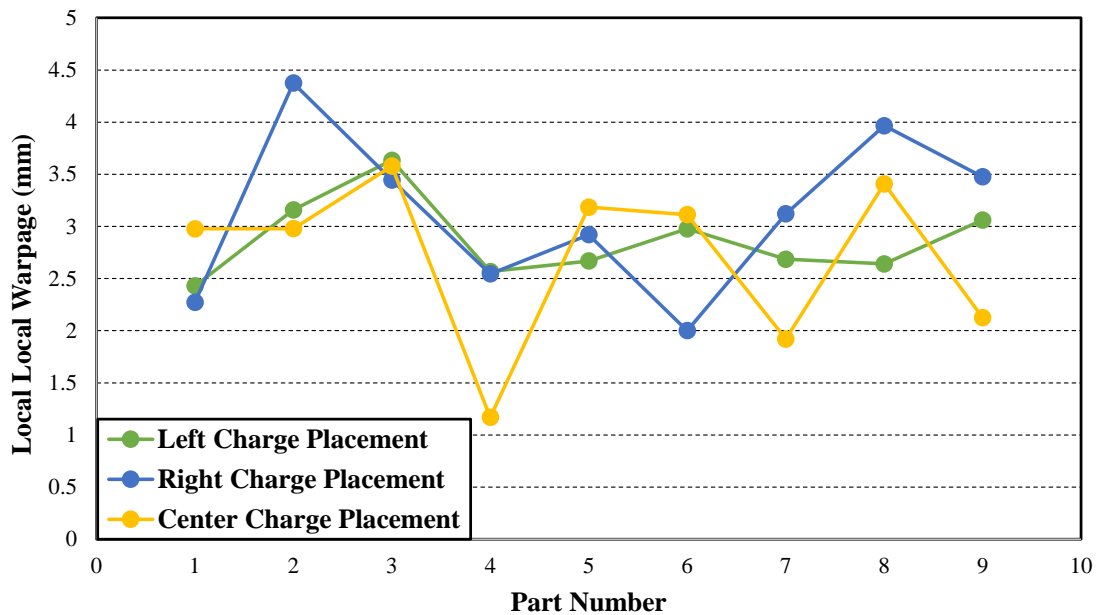


Figure 4.8: Measured warpage of each part in ‘Charge Placement Experiment’ using ‘local local’ metric.

Next the average warpage of each series is calculated and displayed in a bar chart (see Figure 4.9).

Once again the error bars represent one standard deviation for each series.

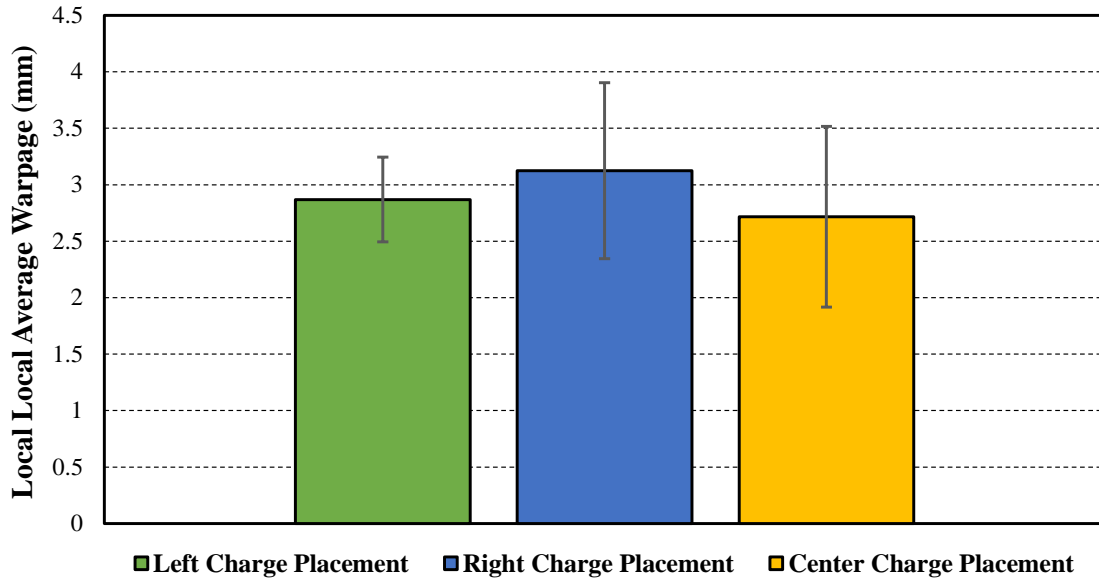


Figure 4.9: Bar chart shows average warpage for each charge placement and error bars show one standard deviation for that series. Data is gathered using ‘local local’ metric.

Figure 4.9 clearly shows the difference in the standard deviation between series. Interestingly the standard deviations for ‘Right Charge Placement’ and ‘Center Charge Placement’ are very similar (0.78 and 0.8 respectively), and the ‘Left Charge Placement’ has a much lower standard deviation (0.38). Larger differences in average warpage also exist between series, however given the standard deviation of each set, these differences are small.

Using ANOVA the different series are evaluated to reveal if the warpage measurements of one series are statistically different from any other series. The p-value from the ANOVA was 0.56 which fails to reject the null hypothesis, therefore no series is statistically different from any other series.

4.4.3 Discussion

Both of the p-values from the ANOVAs conducted using the results from the ‘global global’ and ‘local local’ metrics could not reject the null hypothesis; and thus there is no statistical difference

in the warpages from each series. The results of the ANOVAs for both metrics confirms that small variations in charge placement do not have a large impact on results across the whole part, or locally at the flanges. ‘Local local’ results suggest that ‘Left Charge Placement’ could reduce the part to part variability. The improved part to part variability is suggested by the much lower standard deviation of warpage.

4.5 Chapter Summary

Two simple experiments were carried out to test suspected causes of warpage and increased part to part variation. Useful information about the impact (or lack of impact) of the parameters tested (mold temperature and charge placement) has been gained because of these experiments. Unfortunately, no clear path forward is outlined by the results.

The ‘Mold Temperature Experiment’ did not yield results which could facilitate manufacturing decisions that would reduce part warpage. Warpage measurements from both the high (150°C) and low (100°C) mold temperature were found to be not statistically different using a t-test on two different warpage metrics. These results proved that one mold temperature did not produce parts with a lower warpage than another. The ANOVA results of ‘Charge Placement Experiment’ proved that small variations in charge placement did not have a significant impact on warpage measurements.

**Chapter 5 : Application: Impact of Geometry and Material
on Part Warpage**

5.1 Overview

Chapter 5 details the construction of a DoE used for the purposes of evaluating the factors of material and geometry. The materials used are the LFT material and GMT material discussed in section 1.2.1. The geometries used are the SBO (Figure 5.3 b)) and SBI (Figure 5.3 a)) geometries. For the evaluation of this DoE all five of the warpage metrics proposed in chapter 3 are used to perform their own assessments. Pareto charts generated from analyzing the DoE (using each metric) highlight the impact of the two factors (material and geometry). A discussion about the results obtained using each of the metrics highlights important factors to consider while measuring warpage. Finally the relative impacts of each factor are clarified.

5.2 Background

After many parts had been manufactured with the LFT material, attempts to reduced magnitude of warpage and part to part variation have been unsuccessful. In other experiments a GMT material was used. A visual inspection of the warpages of parts made from the two different materials gave the impression that parts made with the GMT material have a smaller magnitude of warpage and potentially lower part to part variation when compared to parts manufactured with the LFT material.

Additionally the mating part for the seat back assembly had been manufactured with both materials. The mating part is called the ‘Seat Back Inner’ (SBI) part (see Figure 5.1). Upon visual inspection of these parts it was clear that they exhibited warpage in different ways (different locations, patterns, magnitudes, and directions).

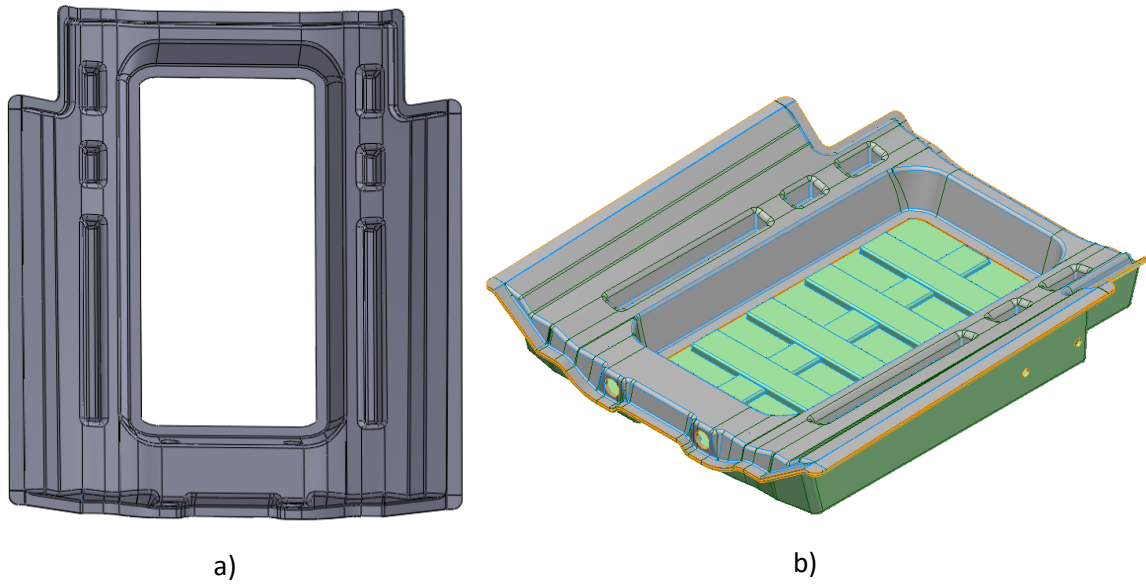


Figure 5.1: a) SBI CAD model b) Assembly of SBI (gray) and SBO (green) CAD models.

To investigate the differences in warpages resulting from the use of the two materials and the differences present in the two geometries a DoE was developed. DoEs are useful statistical tools which allow researchers to investigate the impact of input variables, also known as factors, on an output variable also known as a response. A DoE was selected for this application because of its ability to not only investigate the impact of the input variables, but also if there are interactions between the input variables.

5.3 SBI Mesh Alignment and Warpage Metrics

Since SBI is a different geometry it has its own alignment method. This method was designed to be as similar to the SBO alignment method as possible. This was done to keep a similar frame of reference. The SBO part was aligned using a selected elements best fit alignment, with the selected elements being in the center of the part (see Figure 3.1). The idea behind this selection was to use the relatively flat center portion of the SBO as kind of reference plane. Selecting those elements in the center of the part at that plane made it so that the aligned scanned models would always

attempt to align to that center portion. The same needed to be achieved for the SBI part. However the CAD model does not include the center portion of the SBI because it is to be removed prior to assembly. This means that selecting elements at the center of the scans of the SBI will not work. As a work around, the edges of the of the center portion of the part were selected for the best fit operation (see Figure 5.2). This area was selected because it still exists in the CAD model and allows the best fit to target a similar reference plane as the SBO. Figure 5.3 demonstrates the target reference plane for each geometry, which can be seen as the lowest top facing flat plane on each geometry. It is important to take note, that the reference plane had to be on the top surface because that's the surface which was scanned.

The warpage metrics are replicated for the SBI. This is not very difficult because of the features that both geometries share. Measurements that include specific inspection points like the 'global local', 'local local', and 'vector resultant' are all replicated. All of the exact same XY coordinates are used for the 'global local' and 'local local' metrics. The manual point mapping in the vector resultant method uses the exact same features in the SBI geometry to place the points.

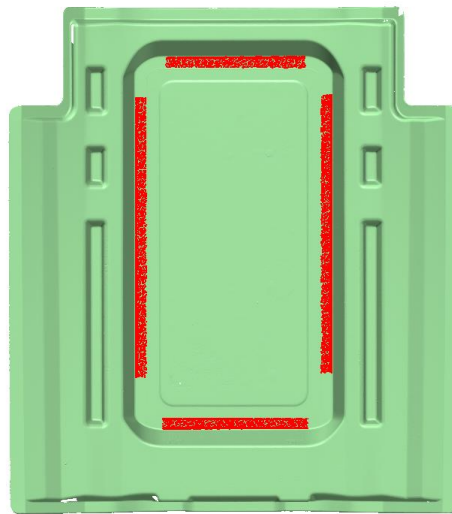


Figure 5.2: SBI scan with selected elements for the purposes of best fit alignment.

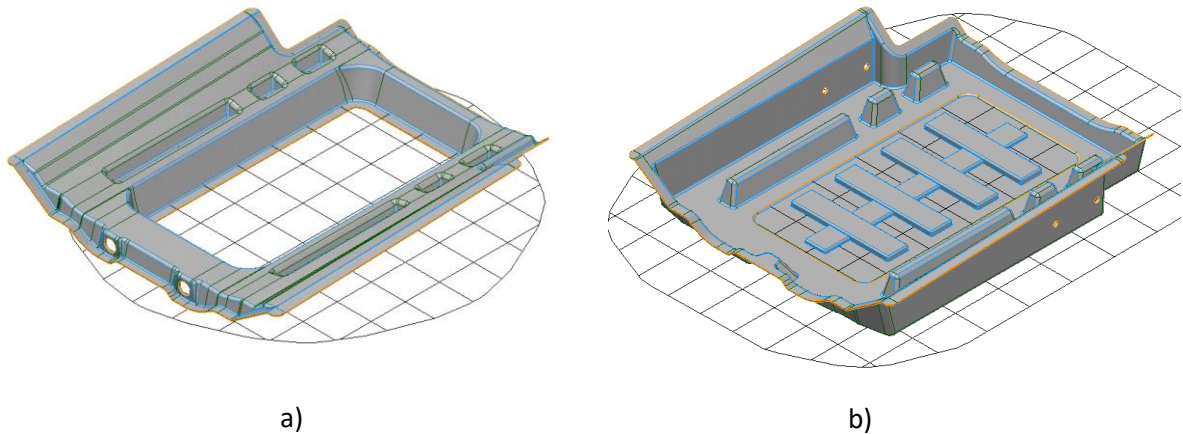


Figure 5.3: CAD geometries with respective reference planes (black grid) a) SBI and b) SBO. Reference plane demonstrates area to be targeted for best-fit alignment.

5.4 Details of DoE

Since the warpage was clearly altered while using different material and different geometry a DoE should be conducted to understand the impact of these variables on the resulting warpage. Therefore this DoE has two input variables, geometry and material. Each variable has two levels, for geometry it is SBO and SBI, and for material it is LFT and GMT. Since this is a simple DoE with only two inputs, a full-factorial design for the DoE is the only option. A full-factorial design uses every combination of inputs. The number of conditions tested in a full factorial design can be calculated by the equation:

$$C = 2^n \quad (5.1)$$

Where C is the number of conditions and n is the number of factors (aka input variables). Therefore four conditions will be tested in this DoE. The structure of the DoE can be represented using a 2 x 2 matrix (see Table 5.1).

SBO & LFT 5 Replicates	SBI & LFT 5 Replicates
SBO & GMT 5 Replicates	SBI & GMT 5 Replicates

Table 5.1: Shows the four conditions of the material and geometry DoE, and the number of replicates for each condition.

Table 5.1 shows that there will be 5 replicates for each condition. This means that there are 5 parts manufactured under each of those conditions, and thus there are 20 parts in total in this experiment. The number of replicates was selected to ensure reliable results for the DoE and also to maximize cost effectiveness.

5.5 Selection of Warpage Metric

For this experiment all warpage metrics are used. This was decided to be the best option because of the different geometries being tested in this DoE. Originally the analysis of different warpage metrics was performed using the SBO. A visual inspection of post-alignment overlays of SBI geometry on the CAD model shows an important difference in warpage between the two geometries which will severely impact results of measurements obtained at the flanges (see Figure 5.4 and 5.5).

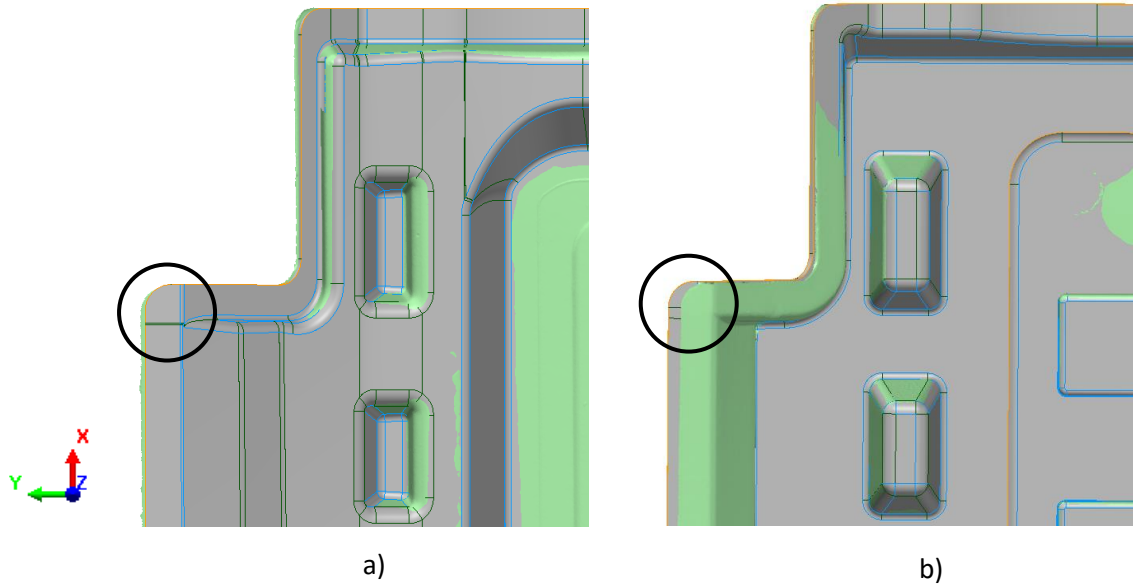


Figure 5.4: GMT a) SBI and b) SBO part scans (green) overlaid on their respective CAD models (gray). View looks down at X Y plane. Circles highlight differences in warpage for SBI and SBO parts (ie: Warpage in y-direction is much larger for SBO parts).

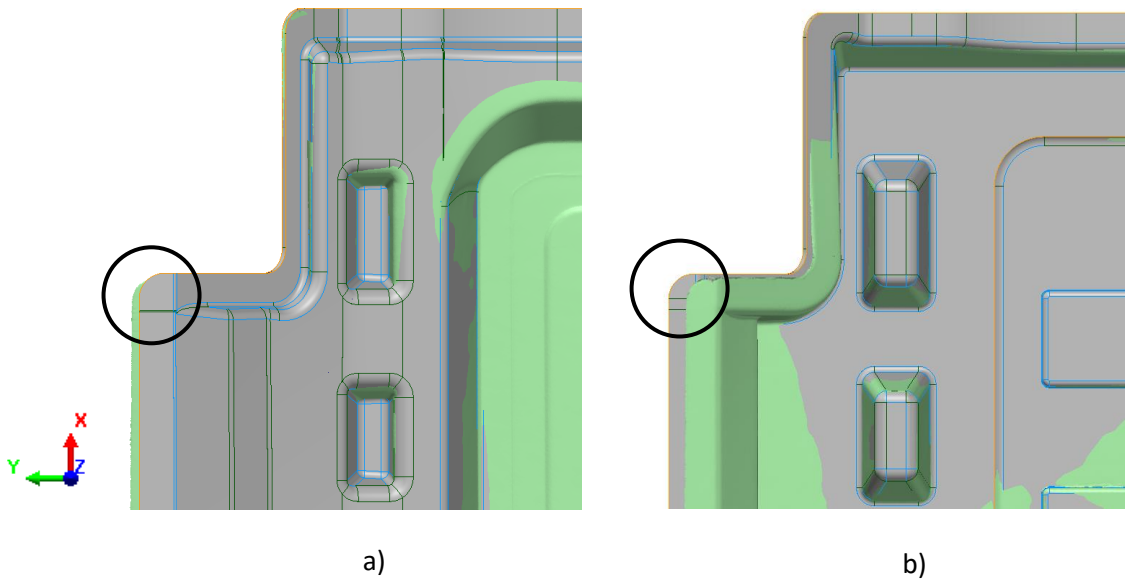


Figure 5.5: LFT a) SBI and b) SBO part scans (green) overlaid on their respective CAD models (gray). View looks down at X Y plane. Circles highlight differences in warpage for SBI and SBO parts (ie: Warpage in y-direction is much larger for SBO parts).

Figure 5.4 and 5.5 highlight the difference in warpage between the SBI and SBO outer parts which is present in both materials. The main difference being the extensive warpage in the 'y' direction

for the SBO parts and the lack of this ‘y’ warpage present in the SBI parts. In Section 3.9 (Figures 3.11 – 3.13) there was a discussion about poor point to point mapping on the flanges of the SBO part due to the extensive ‘y’ warpage. The only warpage metric which properly incorporated the ‘y’ warpage on the SBO parts was the ‘vector resultant’ metric, which used manual point to point mapping. Since this ‘y’ warpage is not present in the SBI geometry the same problems will not be experienced by the other warpage metrics (‘global global’, ‘local local’, ‘local global, and ‘global local’). The better point to point mapping for the SBI geometry can be seen in Figure 5.6.

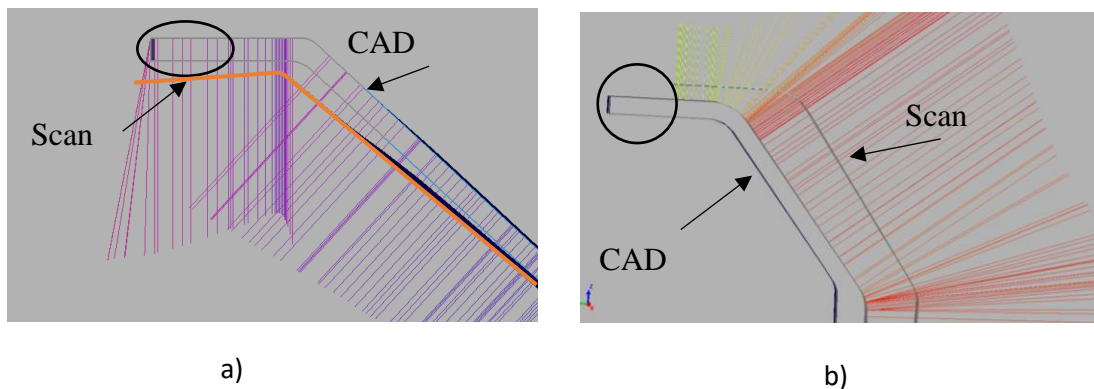


Figure 5.6: Section view of measurements conducted on: a) SBI and b) SBO parts which are aligned to their respective CAD models. Coloured lines show how warpage measurements are acquired. Circled sections show better point to point mapping for SBI scan. In image a) the scan was difficult to see so it was outlined using orange lines.

In Figure 5.6 b) there is clearly a section of the CAD geometry which is not mapped to the scan. However in 5.6 a) that similar section of the flange is indeed mapped to the scan. This discrepancy must be carefully considered while analyzing the results from the different metrics. The discrepancy and the use of a new geometry were the major motivations to use all metrics in this assessment. This DoE can be used to test the metrics once again and help highlight some strengths and weaknesses of each metric.

5.6 Data and Analysis

Since all metrics were used to analyze the DoE, separate evaluations for each metric were created. All of the evaluations use the same scans of the same parts, specific details about scanning can be found in Chapter 2. All of these evaluations also aligned the SBO and SBI geometries using the exact same process. The process being selected elements and best fitting to those selected elements. Details about SBO alignment can be found in Section 3.3 and details about SBI alignment can be found in Section 5.2. Therefore, just as before in Chapter 3 & 4, the only differences between the metrics is the method of extracting the measurement.

5.6.1 Global Global Evaluation of DoE

The ‘global global’ warpage of all 20 parts in the experiment is plotted in Figure 5.7. As a quick reminder, the ‘global global’ metric gathers a warpage measurement by gathering the all of the calculated deviations across the entire part and creates an average from this data (see Section 3.4). In this figure SBO parts are represented by the two blue colours and SBI parts are represented by the two green colours. Parts made using GMT material are represented with a solid line which is lighter in colour, and parts made with LFT are represented using the dotted line in darker colours.

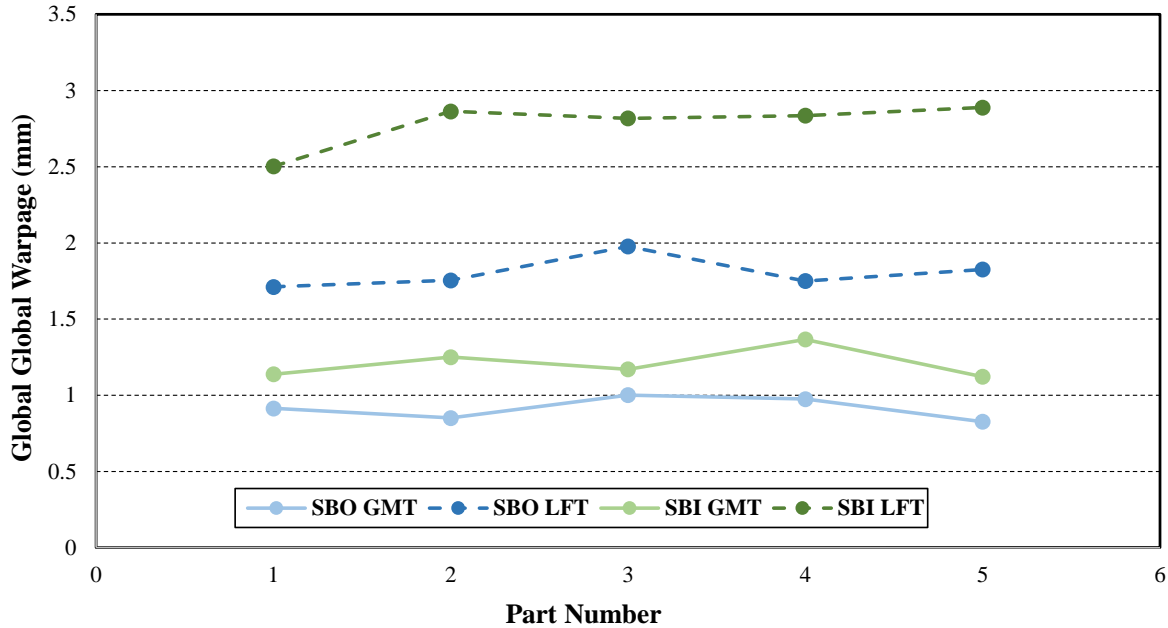


Figure 5.7: Measured warpage for each part in DoE using ‘global global’ metric.

In the Figure 5.7 there is a clear difference in the amount of warpage present in parts made with the LFT material and parts made with the GMT material, the GMT material exhibiting much lower levels of warpage when compared to LFT counterparts. Additionally there seems to be higher warpages for SBI parts when compared to SBO. Looking at the graph more generally it displays four clearly distinct lines. Looking back at the experiments performed in Section 4, altering the mold temperature or charge placement never lead to any results which were so easily distinguishable from one another.

The average warpage of each set in the DoE is calculated using the ‘global global’ metric and shown in Figure 5.8. Based on the results shown in Figure 5.7 there is no surprise that averages from each set are distinct and there is no overlapping of the error bars which are used to represent one standard deviation within that set. The bar chart very clearly illustrates the impact of material on the ‘global global’ warpage results and is especially noticeable in the SBI geometry where the

average warpage is more than doubled when comparing LFT to GMT. Once again altering the mold temperature and altering the charge placement never yielded distinct averages for different sets. Although it might be difficult to notice in Figure 5.8 both GMT sets have a lower standard deviation than their LFT counter parts. With SBO parts having a standard deviation of 0.08 mm and 0.11 mm for GMT and LFT respectively and SBI parts having a standard deviation of 0.10 mm and 0.15 mm for GMT and LFT respectively.

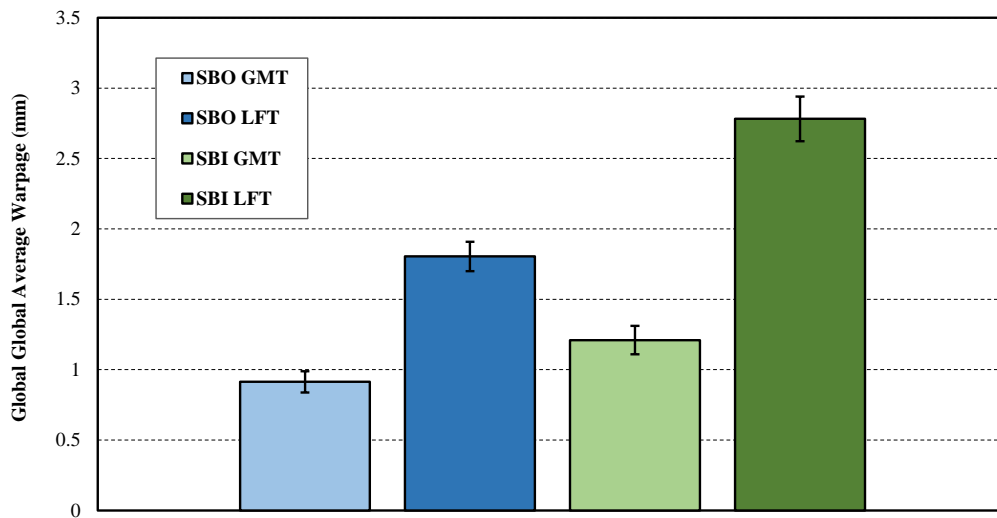


Figure 5.8: Average warpage for each set of parts in DoE using ‘global global’ metric. Error bars represent one standard deviation.

The main goal of performing a DoE is to discover the magnitude of the impact the input variables have on the output variable. One of the best ways of representing this concept is a Pareto chart. Figure 5.9 is a Pareto chart generated from analyzing the DoE using a statistical software. In the figure it shows that material, geometry, and the interaction between material and geometry are important factors which have a statistical impact on the resulting warpage measurement.

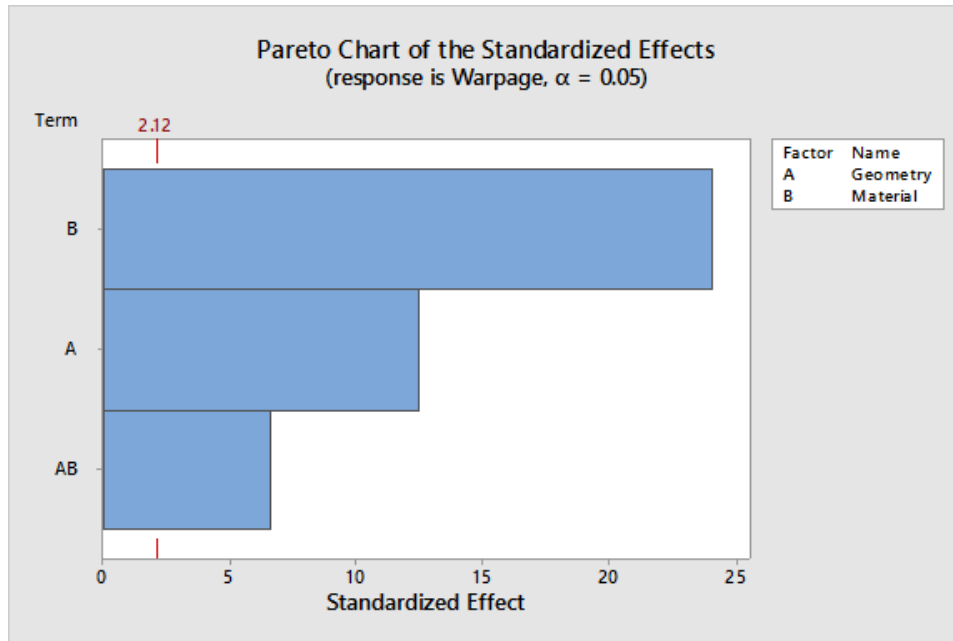


Figure 5.9: Pareto chart showing impact of input variables according to DoE assessment using the ‘global global’ results.

5.6.2 Global Local Evaluation of DoE

The ‘global local’ warpage of all 20 parts in the experiment is plotted in Figure 5.10. The ‘global local’ metric generates a warpage measurement by gathering data from specified measurement locations across the entire geometry (see Section 3.5). The results from ‘global local’ metric are very similar to those from the ‘global global’ metric. The results are similar in the sense that in both Figure 5.7 and Figure 5.10 the different sets appear in the same order of most warped to least warped, additionally there is not overlap of any of the sets. The ‘global global’ and ‘global local’ metrics have yielded similar results in the metric tests which took place in chapter 3.

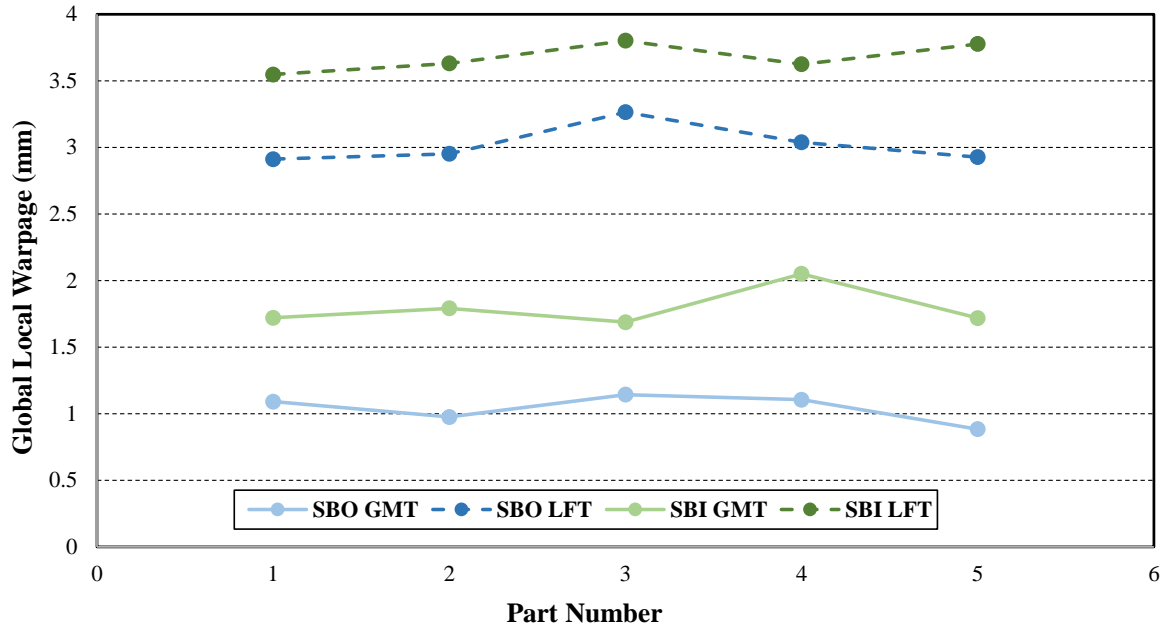


Figure 5.10: Measured warpage for each part in DoE using ‘global local’ metric.

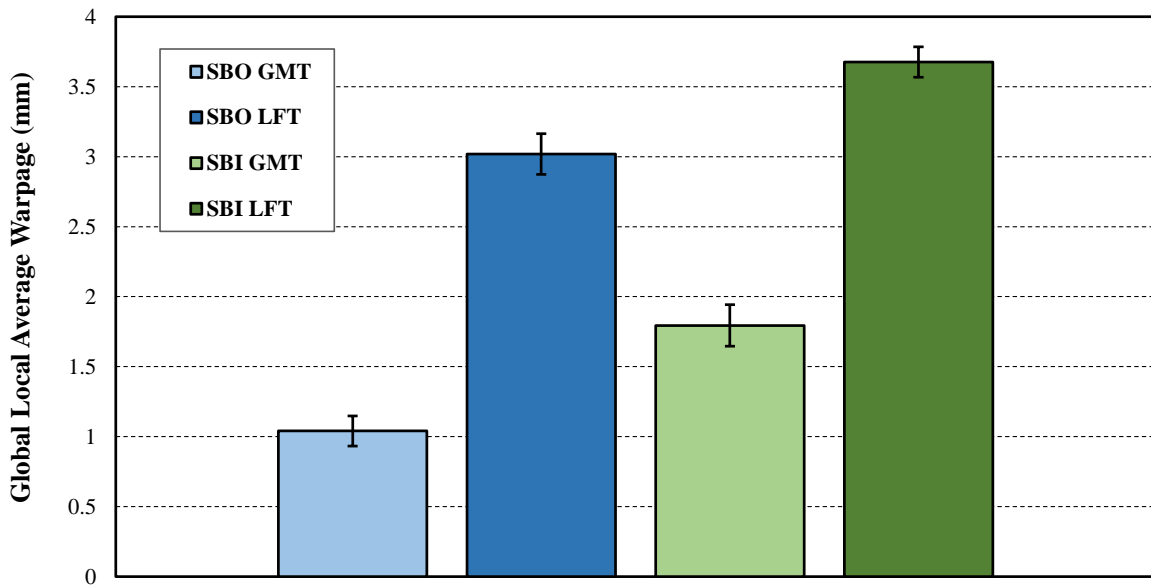


Figure 5.11: Average warpage for each set of parts in DoE using ‘global local’ metric. Error bars represent one standard deviation.

Figure 5.11 shows the average warpage of each set in the DoE calculated using the ‘global local’ metric. Using Figure 5.8 and 5.11 it is much easier to see the differences in results between the

two metrics. The main difference being the increase in measured warpage for the SBO LFT set relative to the other sets.

Analyzing the ‘global local’ DoE results generates the Pareto chart in Figure 5.12. As expected there are once again similarities in the ‘global local’ results and the ‘global global’ results. Both Pareto charts (Figures 5.9 and 5.12) place material as the most impactful input variable with geometry being about half as impactful. The interaction between geometry and material is classified as not significant for the evaluation using the ‘global local’ metric.

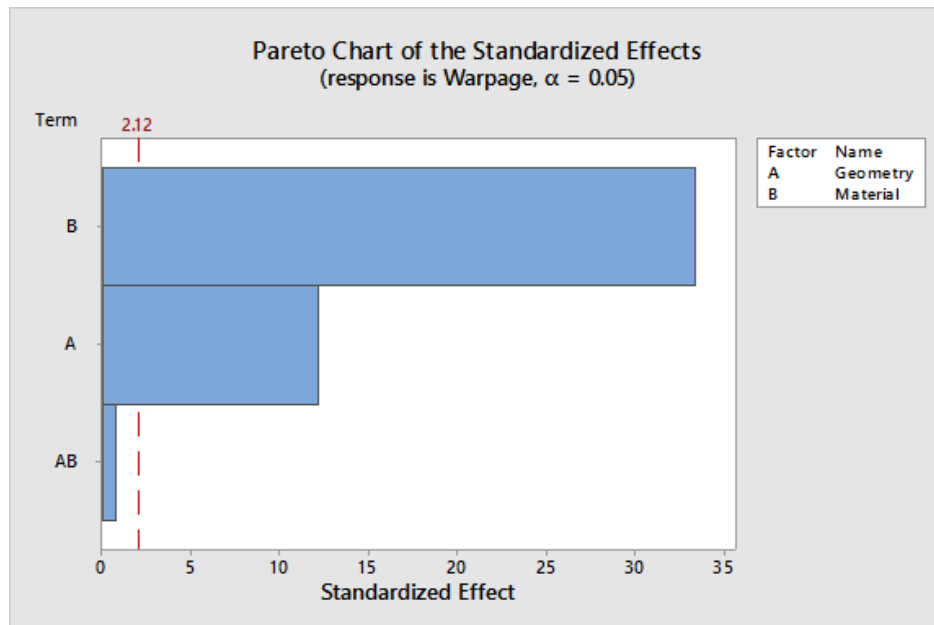


Figure 5.12: Pareto chart showing impact of input variables according to DoE assessment using the ‘global local’ results.

5.6.3 Local Global Evaluation of DoE

The ‘local global’ warpage of all 20 parts in the experiment is plotted in Figure 5.13. The ‘local global’ metric generates a warpage measurement by gathering data at specific locations on the geometry (left and right flanges) and all of the facets at these locations are used to generate an average which becomes the warpage measurement (review Section 3.6). There are some much

clearer differences in Figure 5.13 compared to the other figures. One of the most notable differences is that there is an overlap between two sets. The two sets which overlap are SBO LFT and SBI GMT. This trend would seem to suggest that, the geometry has the most impact on warpage at the flanges. Another large difference is in the magnitude of warpage which is significantly higher than other warpage metrics. This is due to the fact that measurements are exclusively collected on the flanges which typically have higher warpages than other areas of the part. Since the warpage measurement is always an average of several samples, the measurement will undoubtedly be larger for metrics which collect data in high warpage areas exclusively.

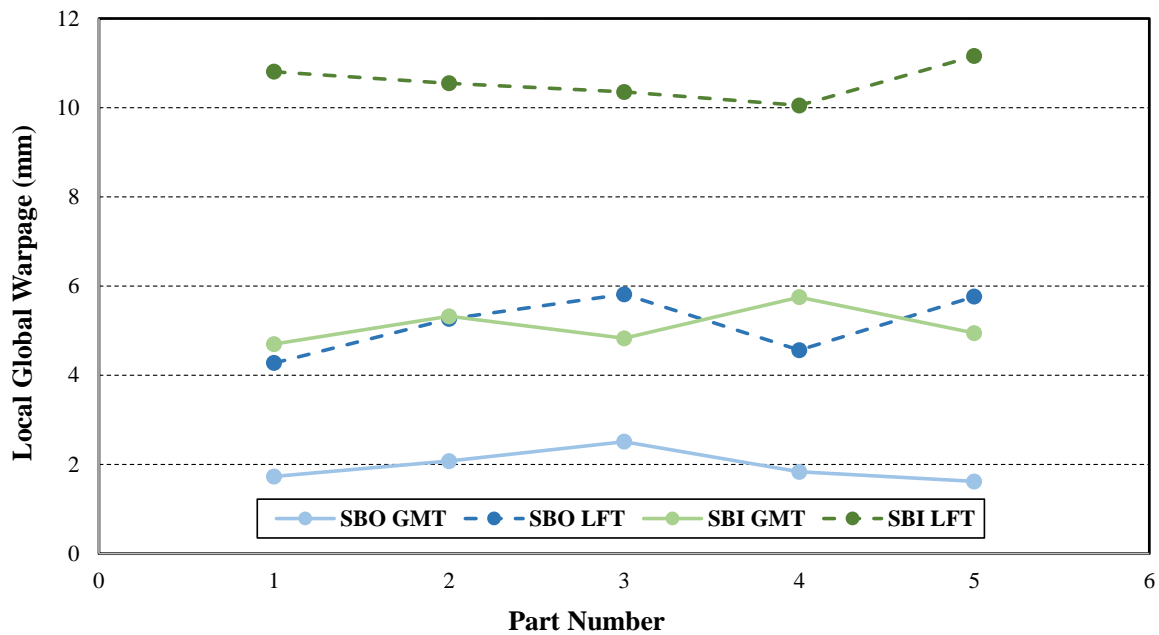


Figure 5.13: Measured warpage for each part in DoE using ‘local global’ results.

The average warpage of each set in the DoE is calculated using the ‘local global’ metric and shown in Figure 5.14. Figure 5.14 helps illustrate another important difference between the ‘local global’ and previous results. The standard deviation is higher for results collected using the ‘local global’ metric. It might be challenging to initially notice the extent of the difference because of the change in scale.

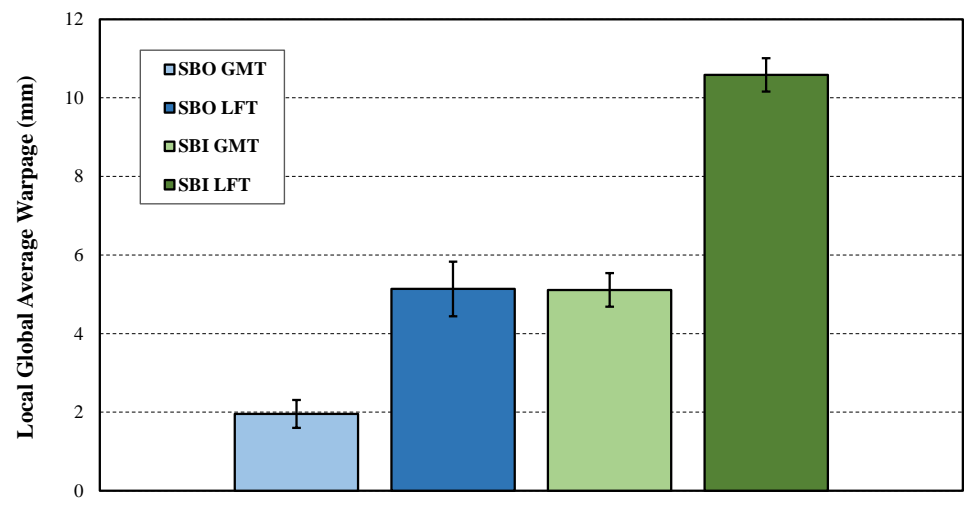


Figure 5.14: Average warpage for each set of parts in DoE using ‘local global’ metric. Error bars represent one standard deviation.

The Pareto chart generated from analyzing the ‘local global’ metric has some notable differences as well. One very clear difference is that material is not the clearly dominant factor, geometry also has a very similar magnitude of impact. According to these results geometry and material are about equal in their impact on the warpage at the flanges. The interaction between geometry and material has no significant impact.

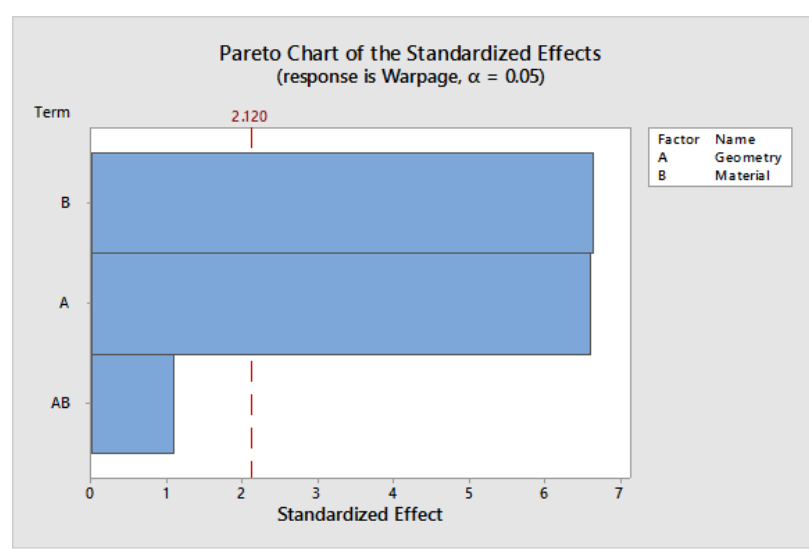


Figure 5.15: Pareto chart showing impact of input variables according to DoE assessment using the ‘local global’ results.

5.6.4 Local Local Evaluation of DoE

The ‘local local’ warpage of all 20 parts in the experiment is plotted in Figure 5.16. The ‘local local’ metric generates a warpage measurement by gathering data at specific locations on the geometry (left and right flanges) and at specified measurement points at these locations, those measurements are used to generate an average which becomes the warpage measurement (see Section 3.7). Similar to the ‘local global’ results in Figure 5.13, SBI GMT and SBO LFT are close in warpage. In Figure 5.16 however, there is a clearer division occurring from geometry, in the sense that the highest warpages are from the two SBI parts. The results from the ‘global global’ and ‘global local’ methods where the highest warpage parts were made with LFT material.

The average warpage of each set in the DoE is calculated using the ‘local local’ metric and shown in Figure 5.17. As with Figure 5.16, Figure 5.17 shows that the SBI parts clearly have a higher warpage than the SBO parts. One difference that stands out is the large standard deviation for the SBO LFT set when compared to the other sets. This is most likely due to the smaller sampling size when comparing ‘local local’ to ‘local global’, essentially the ‘local local’ metric happened to sample areas of low warpage lowered the resulting warpage measurement with that metric. Since the ‘local global’ metric collects from the entire flange the same issue is not present.

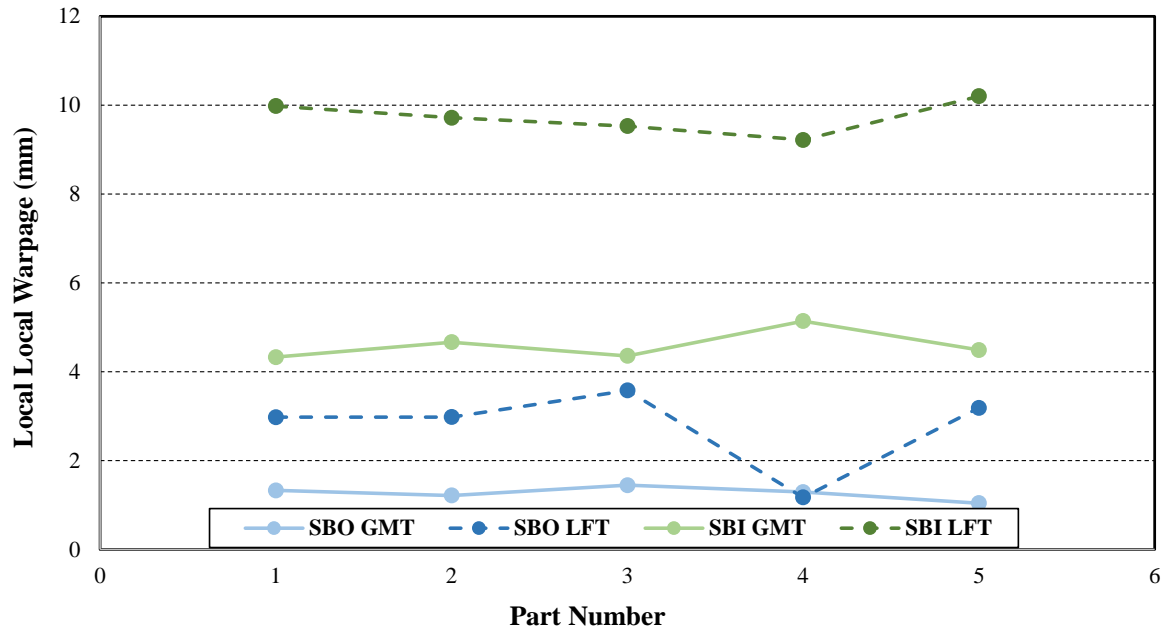


Figure 5.16: Measured warpage for each part in DoE using ‘local local’ results.

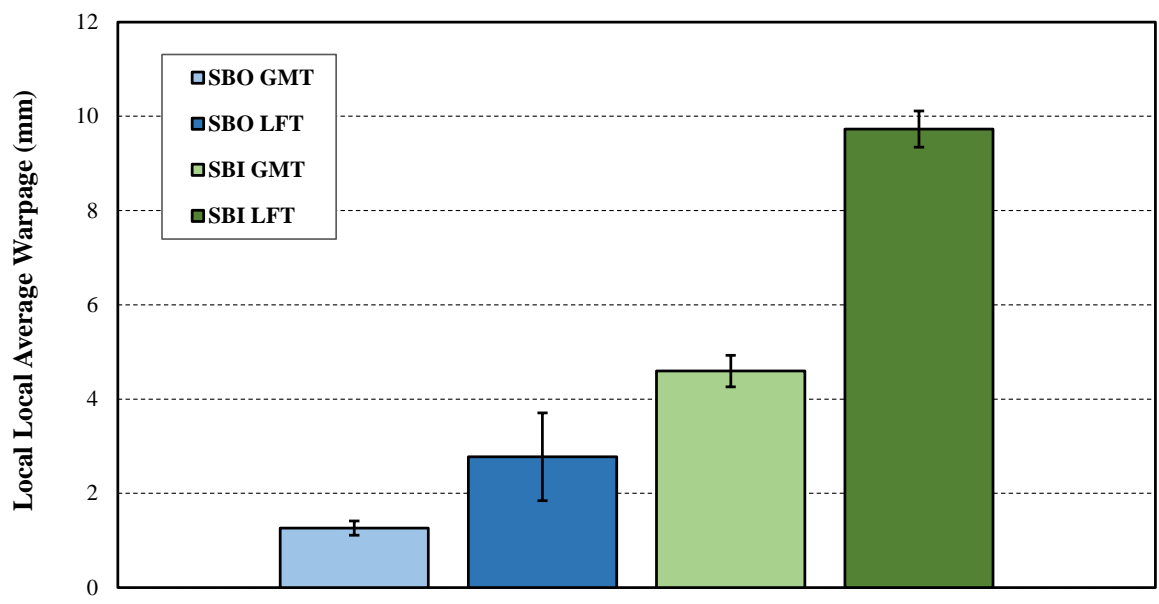


Figure 5.17: Average warpage for each set of parts in DoE using ‘local local’ metric. Error bars represent one standard deviation.

Figure 5.18 is the Pareto chart generated from analyzing the ‘local local’ metric. In the Pareto chart for the ‘local global’ metric (Figure 5.15), the geometry is an equally dominate factor to material,

which had not been seen in results from the other two metrics. In Figure 5.18 geometry is now the dominant factor. In both metrics which collect measurements exclusively from the left and right flanges, geometry impacts the results more than what was seen in the measurements collected across the entire part. Figure 5.18 has the interaction between geometry and material as a significant factor.

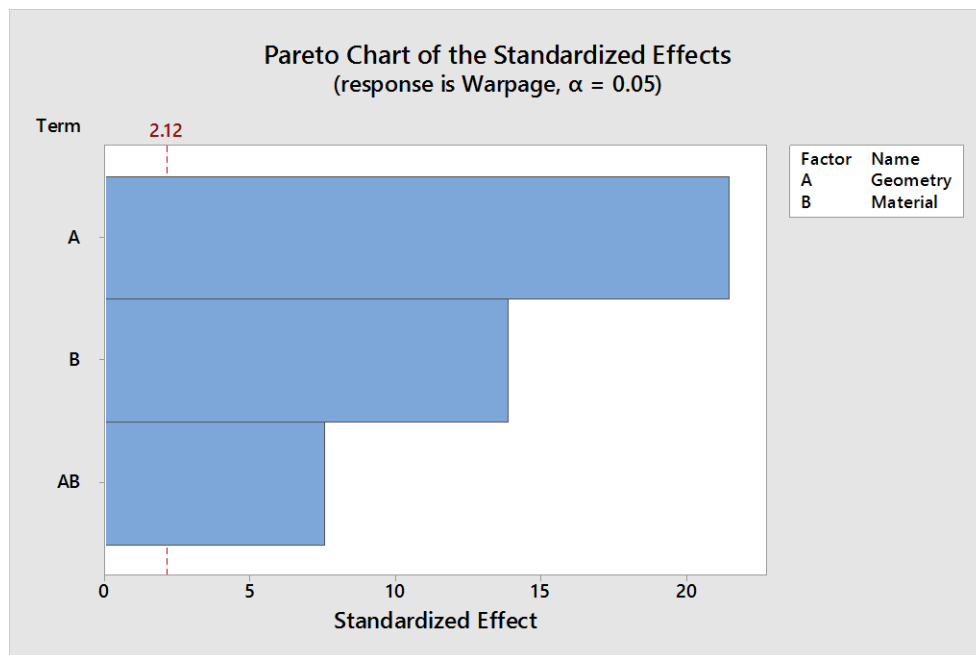


Figure 5.18: Pareto chart showing impact of input variables according to DoE assessment using the ‘local local’ results.

5.6.5 Vector Resultant Evaluation of DoE

The ‘vector resultant’ warpage of all 20 parts in the experiment is plotted in Figure 5.19. The ‘vector resultant’ metric generates a warpage measurement by gathering data at specific locations on the geometry (left and right flanges). Manual point to point mapping on the scan and CAD model is performed at nine locations on each flange. A resultant vector is generated from one of the points on the CAD model, to the complementary point on the scan, all of the resultants are averaged, which becomes the warpage measurement (review Section 3.8). Interestingly in the

‘vector resultant’ results there is significant overlap between the warpages of the two geometries when made with GMT. Overlapping like that has not been seen while using any of the other metrics. Another interesting point, is that the results in Figure 5.19 share more similarities with the results from the ‘global global’ metric and the ‘global local’ metric (Figures 5.7 and 5.10 respectively). Both of these metrics gather data from the entire geometry, while the vector resultant metric gathers data specifically from the flanges (similar to ‘local global’ and ‘local local’ metrics).

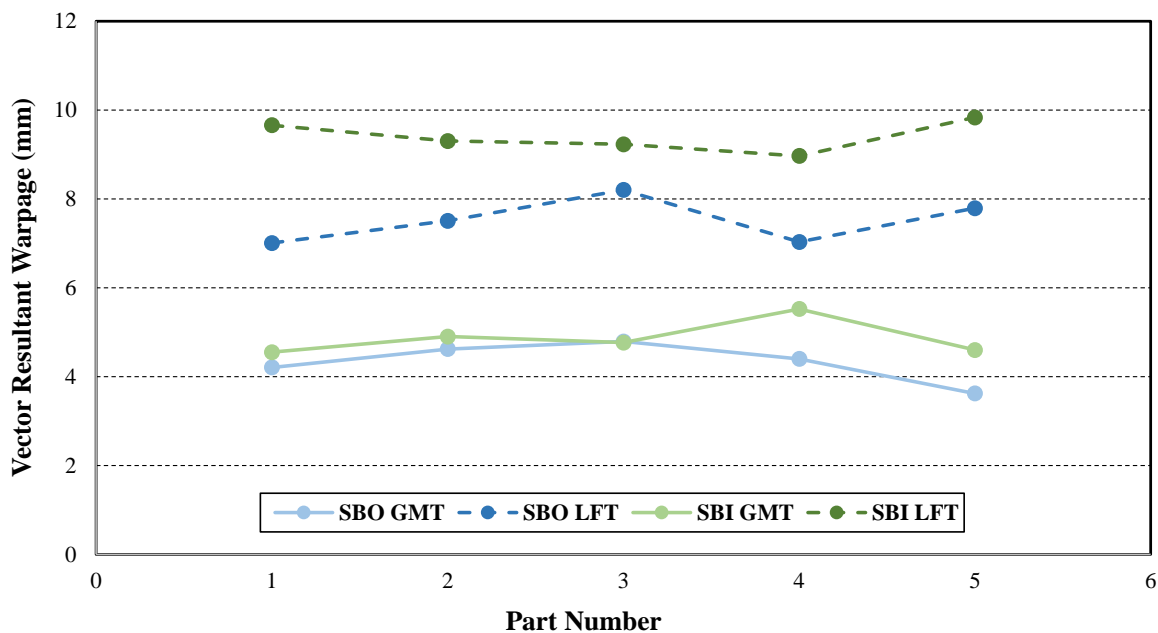


Figure 5.19: Measured warpage for each part in DoE using ‘vector resultant’ metric.

The average warpage of each set in the DoE is calculated using the ‘vector resultant’ metric and shown in Figure 5.20. Comparing Figure 5.20 to the complementary figures from the ‘local global’ and ‘local local’ metrics (Figures 5.14 and 5.17 respectively) clearly outlines the differences in results obtained on the flanges of the part. Both in Figure 5.14 and 5.17, the average warpages for both SBO sets is significantly lower, however SBI sets aren’t impacted to the same degree by the change in metrics.

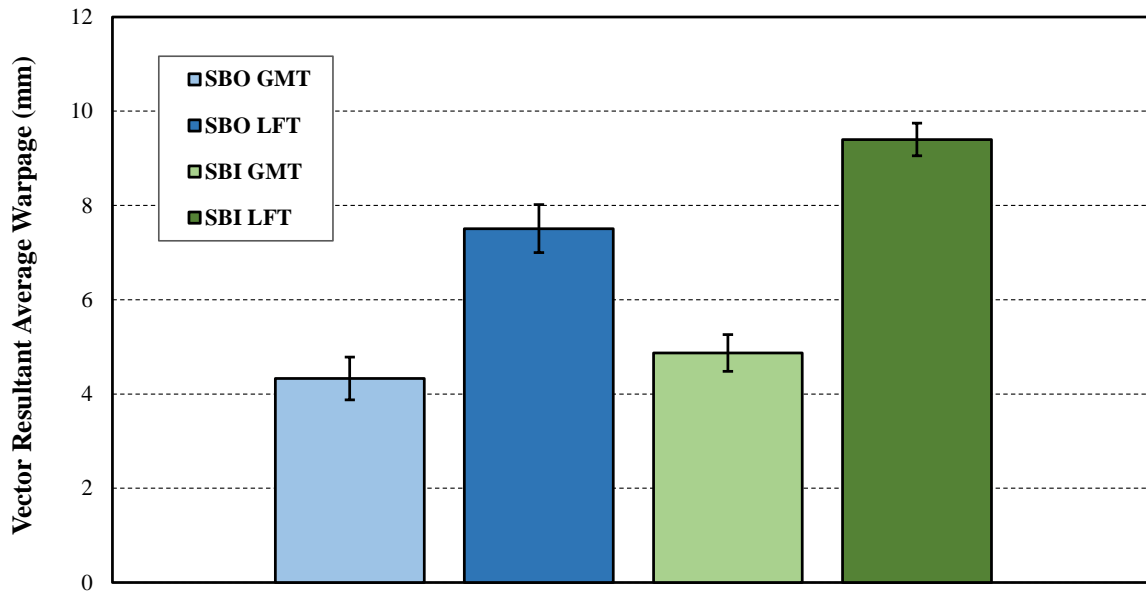


Figure 5.20: Average warpage for each set of parts in DoE using ‘vector resultant’ metric. Error bars represent one standard deviation.

Figure 5.21 is the Pareto chart generated from analyzing the ‘vector resultant’ metric. Once again the results here show more similarities with the ‘global global’ and ‘global local’ Pareto charts (Figures 5.9 & 5.12 respectively), than with the ‘local global’ and ‘local local’ Pareto charts (Figure 5.15 & 5.18 respectively). Material is defined as the most dominate factor, and geometry has roughly a third of the impact material has. The interaction between geometry and material has the least amount of impact, but is still found to be significant.

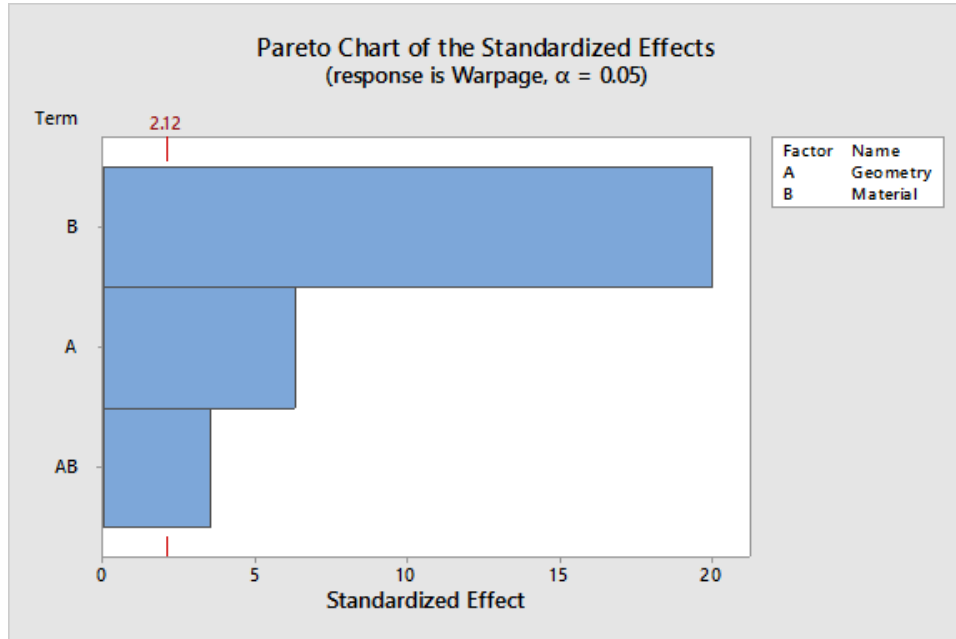


Figure 5.21 Pareto chart showing impact of input variables according to DoE assessment using the ‘vector resultant’ results.

5.7 Discussion

After gathering all of the data in Section 5.6 several of the Pareto charts reveal different conclusions about which factors are more significant relative to each other. Each metric evaluates warpage in a different way, so it is important to take an in depth look into how that has impacted the results.

5.7.1 Warpage Metrics Focused on Data at the Flanges

One large difference was between the ‘local global’/’local local’ results and the ‘vector resultant’ results. These differences are especially interesting because in Section 3 (where the different metrics were tested) these three metrics always shared similar results, typically only varying in magnitude (see Figures 3.7 and 3.8).

In Section 5 it is clear that the results from SBO sets vary in magnitude, however this same pattern is not replicated for the SBI results. In Section 3 the differences in warpage magnitude were discovered to be the result of the majority of the 'y warpage' being ignored in both the 'local global' and 'local local' metrics, but not the 'vector resultant' metric. Essentially the 'local global' and 'local local' methods only incorporate the warpage along the normal direction of the surfaces, because there was poor point to point mapping using these metrics. Figures 5.4 and 5.5 show that the warpage of the SBI parts are primarily along the normal direction (normal to the surface being measured), but not the SBO parts. Figure 5.6 shows that the automatic point to point mapping used for those metrics works much better for the SBI parts. For this reason there is very little difference between the results from the three metrics on the SBI parts, essentially they all measure the same warpage. Since the good point to point mapping on the SBI parts essentially measures the full magnitude of warpage and the poor point to point mapping on the SBO part only measures the part of the warpage in the normal direction while ignoring significant warpage in the 'y direction', the differences in geometry will undoubtedly impact the resulting magnitude of the warpage.

However, this does not mean that according to the 'local global' and 'local local' metrics the magnitude of warpage is much lower for SBO parts and therefore geometry is has the largest impact on warpage. A more accurate statement from the results would be, that the magnitude of warpage along the normal direction of the flanges is much larger for SBI parts when compared to SBO parts (this information is not particularly desirable for the purposes of the DoE). Alternatively from the 'vector resultant' metric the results would be interpreted as, the SBI parts generally have slightly larger magnitude of warpage when compared to SBO parts, however there is a much larger difference in warpage between LFT and GMT parts, LFT parts having a significantly higher warpage at the flanges. Therefore material has the dominant impact on the warpage.

5.7.2 Data at the Flanges ('local') vs Data across the Entire Part ('global')

The differences in results between metrics which gather data 'globally' (across the entire part) and locally (specifically at the left and right flanges) have been discussed in Section 3.9. The main concern outlined in Section 3.9, regarding gathering data 'globally' was that the similarities in large portions of the geometry muted differences between other areas of the geometry (mainly at the flanges). This meant that although there were differences between parts (primarily at the flanges) within the set, these differences weren't observed in the results because of the massive number of data points which was collected in areas of the part where warpage did not change much from one part to another.

However, the data in Section 5 is completely different from the data used in Section 3. The data in Section 3 was collected from two different sets of SBO parts and was evaluated within that set of parts. Although the 'global global' and 'global local' metrics were not great at highlighting the differences between parts manufactured under the same conditions, it doesn't mean that they cannot be useful metrics for evaluating parts manufactured under different conditions. Section 4 was a more similar situation to Section 5, in which multiple sets of parts manufactured using different conditions were being compared. All of the results from Section 4 showed that the differences in manufacturing parameters did not yield statistically different parts. Therefore, in the case of Section 4 there just didn't appear to be any significant differences between the two sets of parts, so the metric was not the issue.

In Section 5 there are four different sets of parts with very large differences between each other. Since the differences between part sets were large enough, the 'global global' and 'global local' metrics showed distinguishable results for each population. This is shown clearly in the results in Figures 5.7 and 5.10.

Understanding the metrics and how the data was sampled from the scan is incredibly important for properly interpreting the results. Since the results are gathered ‘globally’ it must be understood that these metrics report an averaged deviation across the entire part. As explained in the previous section there are differences in how well point to point mapping occurs at the flanges for the two geometries. This difference will be included in the results from the ‘global global’ and ‘global local’ metrics, however due to the massive amounts of data acquired from other areas of the part, these differences will not dominate the response as it does for the metrics in which data is only gathered from the flanges (‘local global’ and ‘local local’).

Since this difference in point to point mapping between the two geometries does not dominate the response, the ‘global global’ and ‘global local’ results can be said to describe the warpage across the entire geometry. Meaning that the parts with a lower ‘global global’ and ‘global local’ warpage are generally closer to the target geometry (CAD model) than parts with a higher warpage according to that metric. According to both of these metrics changing the material has the most impact on warpage measurement, and the geometry has some impact on the warpage as well, but it is not as large as material (see Figures 5.9 & 5.12).

At the other end the ‘vector resultant’ metric can be used to discover which factors impact the magnitude of warpage at the flanges specifically. From the ‘vector resultant’ metric results the same factors are highlighted, material being the most significant and geometry having a less significant impact (see Figure 5.21). If ‘local’ and ‘global’ results differ, it does not mean one metric is evaluating the geometry incorrectly. These measurements are just used to determine different things about the geometry. The ‘global’ measurements can be used to see if one part is generally ‘better’ than another part, and the ‘local’ measurements are used for evaluating at a specific location (or locations).

5.7.3 Interaction Effects

In the Pareto charts from Section 5.6 three charts show that the analysis of the DoE concluded that there were significant interaction effects between the two factors. From the ‘global global’ results in Figure 5.7 there is a larger separation between the two geometries using the LFT material compared to the GMT material. This is why the DoE determined the interaction between the material and geometry to be significant. In this case the materials seem to have a different reaction to changing the geometry. For the LFT material changing the geometry has a larger impact on the magnitude of the warpage; which shows the interaction between the two factors.

The ‘vector resultant’ metric produced similar results (see Figure 5.19), changing the geometry while using the GMT material had a very minimal impact, but changing the geometry while using the LFT material produced a significant change in warpage magnitude. The results from both the ‘global global’ and ‘vector resultant’ metrics suggest the warpage is more stable under geometry changes while using GMT as a material.

The Pareto chart generated from results obtained using the ‘local local’ metric (Figure 5.18) also showed interaction effects to be significant. The interaction effects are deemed to be impactful because in Figure 5.18 the much larger separation between the two SBI parts made with the LFT and GMT materials compared to the two SBO parts made with the LFT and GMT materials. Similar to the larger impact of geometry reported in the ‘local local’ Pareto chart, the interaction effect is due to differences in point to point mapping on the two geometries. A significant portion of the increased warpage on the SBO while changing material is due to increase ‘y direction’ warpage on the flanges. Since this is not included in the ‘local local’ evaluation of the SBO parts the warpage does not change much from one material to the other. However the majority of the warpage is included in the ‘local local’ evaluation of the SBI part. This disparity creates the

perceived importance of the interaction effects. So from these results it cannot be concluded that material change on the SBI geometry has a larger impact than on the SBO geometry generally, or even locally at the flanges. However, it can be concluded that changing the material with the SBI geometry creates larger warpage along the normal direction of the surface.

5.8 Chapter Summary

5.8.1 Measurements at the Flanges ('local global', 'local local', and 'vector resultant')

For this specific application the results from the 'local global' and 'local local' metrics should only be interpreted understanding that the measured warpage is only the 'z-component' warpage. This is due to the differences in the accuracy of the point to point mapping at the flanges. Since the 'local global' and 'local local' metrics exclusively gather data from the flanges, the impact of the discrepancy of point to point mapping between the two geometries (SBI and SBO) has a profound effect on the results. Therefore those results cannot be interpreted as representing the warpage, generally, at those flanges; they can only represent the warpage along the normal vector of the surface of the flanges. The specific measurement of 'warpage along the normal vector of the surface of the flanges' is not particularly useful for the purposes of comparing sets of parts to determine which parts are more or less warped.

Results obtained using the 'vector resultant' metric should be used to determine the impacts of the two factors (material and geometry) on the overall magnitude of warpage at the flanges. The manual point to point mapping of the vector resultant can represent the magnitude of warpage at the flanges for SBO parts much more accurately. Since the warpage from both geometries are being compared directly, it is crucial that measurements from both geometries are representing the same concepts (i.e.: full magnitude of warpage at the left and right flanges).

With the confidence of the accurate measurements from the ‘vector resultant’ metric, the Pareto chart results can be interpreted to suggest that: the material has a very dominant impact on the warpage at the flanges for both geometries, and the two geometries experience different magnitudes of warpage at the flange. Evidence from Figure 5.19 and the significant interaction effect reported in the Pareto chart (Figure 5.21) could suggest that the warpage at the flanges is more stable under geometry changes for the GMT material because the results for both geometries made using GMT were similar, but the results for both geometries made using LFT were different.

5.8.2 Measurements across the Whole Part (‘global global’ and ‘global local’)

The results collected using the ‘global global’ and ‘global local’ metric represent the average warpage of each part. The differences in warpage results due to altering the material and geometry are large enough to produce discernable results for each set in the DoE, while using the ‘global global’ and ‘global local’ metrics. Analyzing the DoE the Pareto charts of both metrics suggest that the material is a dominant factor which impacts the magnitude of warpage across the entire part, and the geometry also impacts the average warpages across the entire part. However, only the results obtained using the ‘global global’ metric suggested that the interaction effects between material and geometry were significant. Any differences in results will naturally be due to the differences in how the data is acquired, mainly ‘global local’ metric is more sensitive to potential errors because it uses fewer data points (see Section 3.4 and 3.5).

5.8.3 Final Comments on Proposed Warpage Metrics

It is difficult to determine if one warpage metric is ‘better’ than the other in a general sense. Each metric has its own strengths and weaknesses. Not only do the metrics have their own strengths and weaknesses but they have their own applications. There are primarily two different types of

warpage measurements explored in this thesis: global warpage measurements (measurements across the entire part), and local warpage measurements (measurements gathered at specific locations). The global warpage measurements are collected using the ‘global global’ and ‘global local’ metrics and the local warpage measurements are collected using the ‘local global’, ‘local local’, and ‘vector resultant’ metrics. Global measurements and local measurements have specific applications. Global measurements should be used when there is a need to understand if the overall warpage of a part is changing. Local measurements should be used when there is a need to understand if the warpage is changing at a specific area of interest. Using both a global and a local warpage metric could help determine if there is an overall warpage change or if the warpage change is exclusive to a specific area(s) of the geometry.

The second major difference in warpage metrics is the method of collecting data from the defined area. The two methods explored being: extraction of all data from all facets of the mesh, and extraction of data from specific inspection points on the mesh. The metrics which gather data from all facets in the inspection area are ‘global global’ and ‘local global’, and the metrics which gather data at predetermined inspection points are ‘global local’ and ‘local local’. There are advantages and disadvantages to each method. One of the major benefits of gathering data from all of the facets being that the vast quantities of data points prevents outlier points from making a large impact on final results. Additionally collecting data this way does not require any additional preparation. One benefit of gathering data at specific inspection points is that the exact same discrete points are inspected each time and additional analysis can be done at individual point locations. Another advantage is that there is significantly less data collected from each part which reduces the computational time and reduces file sizes. Although this method does produce results

faster, time saving is only possible because there is preliminary work done to make the inspection point text files which informs the software where to place the inspection points.

The final difference between metrics is automatic point to point mapping and manual point to point mapping. The warpage metrics which use automatic point to point mapping are ‘global global’, ‘global local’, ‘local global’, and ‘local local’, and the only metric which uses manual point to point mapping is the ‘vector resultant’ metric. Automatic point to point mapping is controlled by the reverse engineering software, typically there are some settings which can be altered to optimize the point to point mapping, however even with attempts to optimize these settings the point to point mapping was poor at the left and right flanges of the SBO parts. Although automatic point to point mapping was unable to perform optimally due the extensive warpage on that geometry it does not mean that the ‘vector resultant’ metric should be used for all cases. The main drawback of the ‘vector resultant’ metric is the immense amount of time it takes to gather results because each measurement point must be mapped manually.

The operator inspecting the parts must use a critical eye (section views showing measurement lines are recommended) to determine if areas of the geometry are properly mapped with the automatic point to point mapping, if not then changing settings in the reverse engineering software to improve point mapping should be the first course of action. If altering the settings fails to improve the mapping, then the ‘vector resultant’ metric should be used to gather results. In any case where automatic point to point mapping is performed correctly then the ‘vector resultant’ metric ought not to be used. In Figure 5.22 a road map was created based on the discussions of the proposed warpage metrics in order to simplify the selection of a useful metric. If other metrics are used instead for future studies, certainly the in depth look and evaluation of these metrics encourages careful and critical gathering and interpretation of warpage measurements.

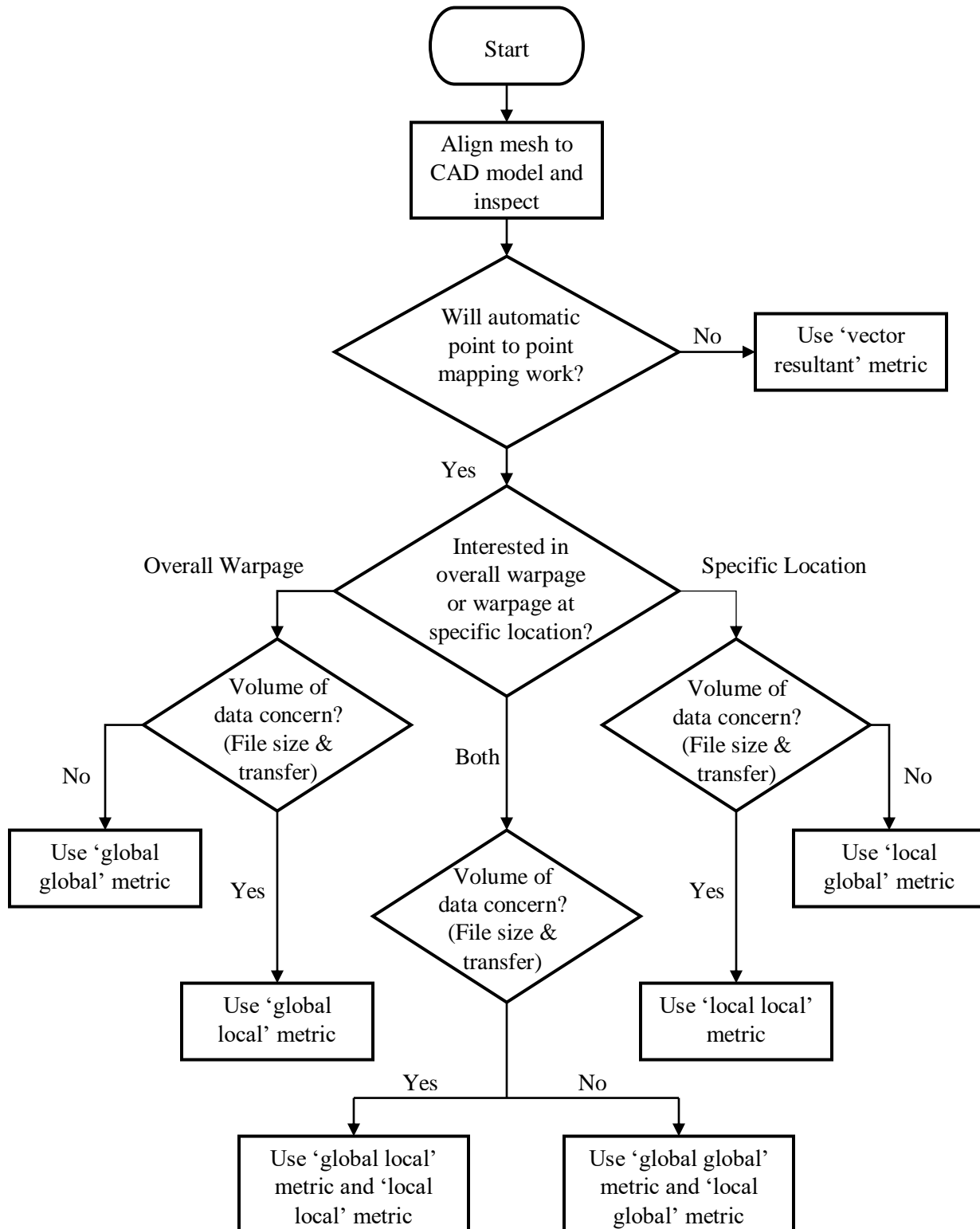


Figure 5.22: Road map to select appropriate warpage metric for a specific application.

5.8.4 Summary

Conclusions from results obtained using the ‘vector resultant’ metric are: 1) warpage at the flanges is significantly impacted by material and also impacted by geometry to a lesser degree; 2) under a geometry change the warpage at the flanges is more likely to be similar using GMT material. Both the ‘global global’ and ‘global local’ metrics determine that the warpage across the entire part is significantly impacted by material (the most dominant factor) and by geometry (to be a lesser degree). Similar to the ‘vector resultant’ metric the ‘global global’ metric also found that when the geometry is changed, the warpage the average warpage is more similar while using GMT material.

Chapter 6 : Conclusion and Future Work

6.1 Conclusions

The work conducted in this thesis has laid the foundation required to tackle the very challenging and important task of the evaluation of warpage for composite components. The many key findings obtained from this will assist future research in this endeavor. To statistically evaluate the impact of processing conditions five quantitative warpage metrics were developed. Investigating the results produced by the warpage metrics illustrated the large differences in the measured warpage of a part depending on how the warpage data is extracted from the scan. ‘Global global’ and ‘global local’ warpage metrics were designed to evaluate the warpage of the entire part. The ‘local global’, ‘local local’, and ‘vector resultant’ metrics were designed to evaluate the warpage at specific areas of interest. These warpage metrics can be applied to any part which is evaluated using a LLP. Through the research conducted in this thesis the metrics have been proven to be able to identify the impact of processing conditions on the measured warpage.

The preliminary scanning work of this project led to many important discoveries. One of the most important discoveries from that area of the project was the large magnitude of warpage induced by applying a fixture to hold the part steady while scanning. The impact of the fixturing was discovered by creating a deviation colour map between two scans of the same part collected while being held in the fixture. The impact of the fixture on the geometry could create differences on the magnitude of several millimeters in some areas. After understanding the issues with fixturing the parts a much more repeatable scanning procedure was outlined, setting a starting point for future work.

The experiments conducted to understand the impact of processing conditions had many important findings as well. The mold temperature experiment was conducted by manufacturing ten parts with two different mold temperatures 100 °C and 150 °C. The warpage was measured

using the ‘global global’ and ‘local local’ warpage metrics. The warpage of the parts manufactured at the two different mold temperatures were compared by conducting a t-test on the results from the two warpage metrics. The results from the t-test proved that for the LFT material altering the mold temperature between 100 °C and 150 °C did not have any significant impact on the warpage. Similarly, the charge placement experiment was conducted by manufacturing nine parts for each charge placement: left, right, and center. The ‘global global’ and ‘local local’ warpage metrics were used to measure the warpage. The warpage of the parts manufactured at the three different charge placements were compared using an ANOVA. The results of the ANOVA proved that changing the charge placement (left, right, and center) had no significant impact on the warpage. The results from the charge placement experiment showed that the random errors associated with the manual nature of charge placement would not yield significant impacts on the warpage.

The DoE conducted to understand the impact of material and geometry successfully identified the differences in warpage under each set of conditions. The warpage was measured using all five proposed warpage metrics. The results from the application of the warpage metrics led to many key findings. From the DoE it was established that the GMT material used in the experiment always produced parts with a lower warpage than the LFT material used in the experiment. Additionally it was discovered that the SBO parts had lower warpage compared to SBI parts. The impact due to altering the material between GMT and LFT resulted in the largest impact on the measured warpage while the impact of the geometry had a secondary impact to that.

The aforementioned findings bare extra significance because many previous works in which the impact of processing conditions are investigated, the experiments were conducted virtually (using molding simulation); while all experiments in this thesis were conducted

physically. Additional significance stems from the compression molding manufacturing method which is less often studied compared to injection molding.

As previously mentioned the work completed in this thesis has laid the foundation to the evaluation of warpage on composite parts. The many contributions provided by the thesis such as: understanding the extent of warpage induced by a fixture, the outline of a scanning procedure, five proposed metrics for measuring warpage, understanding the large differences in measured warpage based on how the data was extracted, and the results from all of the experiments conducted to understand the impact of specific processing conditions on warpage. Although all of these great strides have been made, further developments in the warpage metrics is still critically needed.

6.2 Future Work

Since laser scanning is a relatively new technology there are many potential avenues for researchers to make further contributions. The previous statement is especially true for the application of warpage measurements on highly warped composite components. One potential future work directly related to this research would be to apply the proposed warpage metrics to other experiments to examine their robustness and ability to properly define warpage under other circumstances. Additional potential work related to the proposed warpage metrics would be to reduce the time required to generate results using the ‘vector resultant’ metric. Currently the ‘vector resultant’ metric requires very time consuming manual point mapping, if this could be partially automated then it could benefit everyone looking to make warpage measurements using reverse engineering software.

Potential improvements could also be made in the repeatability and accuracy study. Specifically designing and applying additional supports on the granite table. This could be an

additional avenue to improve repeatability because it could prevent the part from moving slightly while resting on the table. If these supports are added it must be proven that they do not bend the part while applying the forces necessary to support it.

Future experiments could also be conducted on compression molded composites. Determining the impact of processing conditions could lead to the successful implementation of many compression molded composite parts in the fleets of many car companies around the world. The reduction in weight of the cars could save considerable amounts of oil and therefore reduce global emissions.

References

- [1] Ameen, W.; Al-Ahmari, A.; Hammad Mian, S.: Evaluation of handheld scanners for automotive applications, *Applied Sciences*, 8(2), 2018, 217.
- [2] Ascione, R.; Polini, W.: Measurement of nonrigid freeform surfaces by coordinate measuring machine, *The International Journal of Advanced Manufacturing Technology*, 51(9-12), 2010, 1055-1067.
- [3] Beardmore, P.; Johnson, C. F.: The potential for composites in structural automotive applications, *Composites science and Technology*, 26(4), 1986, 251-281.
- [4] Bešić, I.; Van Gestel, N.; Kruth, J.-P.; Bleys, P.; Hodolič, J.: Accuracy improvement of laser line scanning for feature measurements on CMM, *Optics and Lasers in Engineering*, 49(11), 2011, 1274-1280.
- [5] Bondy, M.; Altenhof, W.: Experimental characterisation of the mechanical properties of a carbon fibre/PA66 LFT automotive seatback under quasi-static and impact loading, *International Journal of Crashworthiness*, 25(4), 2020, 401-420.
- [6] Campanelli, V.; Howell, S. M.; Hull, M. L.: Accuracy evaluation of a lower-cost and four higher-cost laser scanners, *Journal of biomechanics*, 49(1), 2016, 127-131.
- [7] Cuesta, E.; Alvarez, B. J.; Martinez-Pellitero, S.; Barreiro, J.; Patiño, H.: Metrological evaluation of laser scanner integrated with measuring arm using optical feature-based gauge, *Optics and Lasers in Engineering*, 121, 2019, 120-132.
- [8] David, H.: Corporate average fuel economy (cafe) standards, *The sage encyclopedia of business ethics and society*, 1, 2018, 677.
- [9] Gardiner, G.: Welding thermoplastic composites, *CompositesWorld*, 4(9), 2018, 50-63.
- [10] Gerbino, S.; Del Giudice, D. M.; Staiano, G.; Lanzotti, A.; Martorelli, M.: On the influence of scanning factors on the laser scanner-based 3D inspection process, *The International Journal of Advanced Manufacturing Technology*, 84(9-12), 2016, 1787-1799.
- [11] He, L.; Lu, G.; Chen, D.; Li, W.; Chen, L.; Yuan, J.; Lu, C.: Smoothed particle hydrodynamics simulation for injection molding flow of short fiber-reinforced polymer composites, *Journal of Composite Materials*, 52(11), 2018, 1531-1539.
- [12] Iuliano, L.; Minetola, P.; Salmi, A.: Proposal of an innovative benchmark for comparison of the performance of contactless digitizers, *Measurement Science and Technology*, 21(10), 2010,
- [13] Kim, B.-S.; Bernet, N.; Sunderland, P.; Manson, J.-A.: Numerical analysis of the dimensional stability of thermoplastic composites using a thermoviscoelastic approach, *Journal of Composite Materials*, 36(20), 2002, 2389-2403.
- [14] Kim, H. K.; Sohn, J. S.; Ryu, Y.; Kim, S. W.; Cha, S. W.: Warpage reduction of glass fiber reinforced plastic using microcellular foaming process applied injection molding, *Polymers*, 11(2), 2019, 360.
- [15] Kitayama, S.; Miyakawa, H.; Takano, M.; Aiba, S.: Multi-objective optimization of injection molding process parameters for short cycle time and warpage reduction using conformal cooling channel, *The International Journal of Advanced Manufacturing Technology*, 88(5-8), 2017, 1735-1744.
- [16] Kitayama, S.; Onuki, R.; Yamazaki, K.: Warpage reduction with variable pressure profile in plastic injection molding via sequential approximate optimization, *The International Journal of Advanced Manufacturing Technology*, 72(5-8), 2014, 827-838.
- [17] Kovacs, L.; Zimmermann, A.; Brockmann, G.; Gühring, M.; Baurecht, H.; Papadopoulos, N. A.; Schwenzler-Zimmerer, K.; Sader, R.; Biemer, E.; Zeilhofer, H. F.: Three-dimensional recording of the human face with a 3D laser scanner, *Journal of plastic, reconstructive & aesthetic surgery*, 59(11), 2006, 1193-1202.

- [18] Krause, W.; Henning, F.; Tröster, S.; Geiger, O.; Eyerer, P.: LFT-D: A process technology for large scale production of fiber reinforced thermoplastic components, *Journal of Thermoplastic Composite Materials*, 16(4), 2003, 289-302.
- [19] Kuş, A.: Implementation of 3D optical scanning technology for automotive applications, *Sensors*, 9(3), 2009, 1967-1979.
- [20] Lee, H.; Huh, M.; Kang, S.; Yun, S. I.: Compressive behavior of automotive side impact beam with continuous glass fiber reinforced thermoplastics incorporating long fiber thermoplastics ribs, *Fibers and Polymers*, 18(8), 2017, 1609-1613.
- [21] Lewis, G. M.; Buchanan, C. A.; Jhaveri, K. D.; Sullivan, J. L.; Kelly, J. C.; Das, S.; Taub, A. I.; Keoleian, G. A.: Green Principles for Vehicle Lightweighting, *Environmental science & technology*, 53(8), 2019, 4063-4077.
- [22] Li, Y.; Gu, P.: Free-form surface inspection techniques state of the art review, *Computer-Aided Design*, 36(13), 2004, 1395-1417.
- [23] Liu, C.; Greene, D. L.: Vehicle Manufacturer Technology Adoption and Pricing Strategies under Fuel Economy/Emissions Standards and Feebates, *The Energy Journal*, 35(3), 2014,
- [24] Mahmud, M.; Joannic, D.; Roy, M.; Isheil, A.; Fontaine, J.-F.: 3D part inspection path planning of a laser scanner with control on the uncertainty, *Computer-Aided Design*, 43(4), 2011, 345-355.
- [25] Martínez, S.; Cuesta, E.; Barreiro, J.; Álvarez, B.: Analysis of laser scanning and strategies for dimensional and geometrical control, *The International Journal of Advanced Manufacturing Technology*, 46(5-8), 2010, 621-629.
- [26] Martínez, S.; Cuesta, E.; Barreiro, J.; Álvarez, B.: Methodology for comparison of laser digitizing versus contact systems in dimensional control, *Optics and Lasers in Engineering*, 48(12), 2010, 1238-1246.
- [27] Michaeli, J. G.; DeGross, M. C.; Roxas, R. C.: Error aggregation in the reengineering process from 3D scanning to printing, *Scanning*, 2017, 2017,
- [28] Polini, W.; Corrado, A.; Sorrentino, L.; Speranza, D.: Measurement of high flexibility components in composite material: critical issues and possible solutions, *The International Journal of Advanced Manufacturing Technology*, 103(1-4), 2019, 1529-1542.
- [29] Rogerio Machado Pereira, J.; de Lima e Silva Penz, I.; da Silva, F. P.: Effects of different coating materials on three-dimensional optical scanning accuracy, *Advances in Mechanical Engineering*, 11(4), 2019, 1687-8140.
- [30] Segreto, T.; Bottillo, A.; Teti, R.; Galantucci, L. M.; Lavecchia, F.; Galantucci, M. B.: Non-contact reverse engineering modeling for additive manufacturing of down scaled cultural artefacts, *Procedia CIRP*, 62, 2017, 481-486.
- [31] Sherman, L. M.: Portable 3D Laser Scanner Slashes Molder's Inspection Time, *Plastics Technology*, 61(11), 2017, 72.
- [32] Song, Y.; Gandhi, U.; Sekito, T.; Vaidya, U. K.; Vallury, S.; Yang, A.; Osswald, T.: CAE method for compression molding of carbon fiber-reinforced thermoplastic composite using bulk materials, *Composites Part A: Applied Science and Manufacturing*, 114(2018), 388-397.
- [33] Vellequette, L. P.: Double duty for 2 VW crossovers: Atlas and Tiguan to help meet consumer demand, stiffer CAFE regulations, *Automotive News*, 91(6784), 2017, 8.
- [34] Walsh, D.: CAFE serves suppliers a large role in pump-passing cars, *Crain's Detroit Business*, 27(33), 2011, 1.
- [35] Wang, Y.; Feng, H.-Y.: Effects of scanning orientation on outlier formation in 3D laser scanning of reflective surfaces, *Optics and Lasers in Engineering*, 81, 2016, 35-45.
- [36] Ward, J.; Gohlke, D.; Nealer, R.: The Importance of Powertrain Downsizing in a Benefit - Cost Analysis of Vehicle Lightweighting, *JOM*, 69(6), 2017, 1065-1070.

Curriculum Vitae

Name: Eric Martin

Post-secondary Education and Degrees: Western University
London, Ontario, Canada
2014-2018 B. E. Sc.

Western University
London, Ontario, Canada
2018-2020 M. E. Sc.

Related Work Experience: Summer Research Assistant
Western University
Summer 2017

Teaching Assistant
Western University
2018-2020

Research Assistant
Western University
2018-2020

Publications:

Martin, E., Tutunea-Fatan, O.R., Gergely, R., Okonski, D.A., 2020, "Repeatability and Accuracy of Laser Scanning-Based Reverse Engineering for Warped Composite Components," accepted for publication in *Computer-Aided Design and Applications*.